แรงเฉือนจากแผ่นดินไหวในอาคารสูงปานกลางซึ่งถูกออกแบบโดยวิธีสเปกตรัมการตอบสนอง

นาย กี เล็ง

วิทยานิพนธ์นี้เป็นส่วนหนึ่งของการศึกษาตามหลักสูตรปริญญาวิศวกรรมศาสตรมหาบัณฑิต

สาขาวิชาวิศวกรรมโยธา ภาควิชาวิศวกรรมโยธา

คณะวิศวกรรมศาสตร์ จุฬาลงกรณ์มหาวิทยาลัย

ปีการศึกษา 2555

SEISMIC SHEAR DEMAND OF A MEDIUM-RISE BUILDING DESIGNED BY RESPONSE SPECTRUM ANALYSIS

Mr. Ky Leng

A Thesis Submitted in Partial Fulfillment of the Requirements
for the Degree of Master of Engineering Program in Civil Engineering
Department of Civil Engineering
Faculty of Engineering
Chulalongkorn University
Academic Year 2012

Thesis Title	SEISMIC SHEAR DEMAND OF A MEDIUM-RISE BUILDING DESIGNED BY RESPONSE SPECTRUM ANALYSIS
By	Mr. Ky Leng
Field of Study	Civil Engineering
Thesis Advisor	Assistant Professor Chatpan Chintanapakdee, Ph.D.

Accepted by the Faculty of Engineering, Chulalongkorn University in Partial Fulfillment of the Requirements for the Master's Degree

……Dean of the Faculty of Engineering
(Associate Professor Boonsom Lerdhirunwong, Dr.Ing.)

THESIS COMMITTEE

……Chairman
(Professor Panitan Lukkunaprasit, Ph.D.)

……... Thesis Advisor

(Assistant Professor Chatpan Chintanapakdee, Ph.D.)

……External Examiner
(Assistant Professor Sutat Leelataviwat, Ph.D.)

กี เล็ง: แรงเฉือนจากแผ่นดินไหวในอาคารสูงปานกลางซึ่งถูกออกแบบโดยวิธีสเปกตรัมการตอบสนอง. (SEISMIC SHEAR DEMAND OF A MEDIUM-RISE BUILDING DESIGNED BY RESPONSE SPECTRUM ANALYSIS) อ.ที่ปรึกษาวิทยานิพนธ์หลัก: ผศ. ดร. ฉัตรพันธ์ จินตนาภักดี, 156 หน้า.

ตามมาตรฐาน ASCE7-05 การวิเคราะห์ด้วยวิธีสเปกตรัมการตอบสนอง (Response Spectrum Analysis, RSA) สามารถถูกนำไปใช้ในการออกแบบโครงสร้างเพื่อต้านทานการสั่นสะเทือนจากแผ่นดินไหวได้กับอาคารทุกความสูง แต่มีงานวิจัยที่พบว่าขั้นตอนการออกแบบนี้ไม่เหมาะสมสำหรับอาคารสูง งานวิจัยนี้จึงมีวัตถุประสงค์ที่จะตรวจสอบการออกแบบด้วยวิธี RSA ที่กำหนดไว้ในมาตรฐานการออกแบบอาคาร มยผ.1302-52 ของประเทศไทย ซึ่งประยุกต์มาจาก ASCE7-05 รวมทั้งเสนอการปรับปรุงเพื่อแก้ไขปัญหาที่พบ การศึกษานี้ใช้อาคารคอนกรีตเสริมเหล็กสูง 16 ชั้นเป็นอาคารตัวอย่าง ซึ่งมีกำแพงรับแรงเฉือนหลักอยู่ตรงกลางและริมอาคาร อาคารดังกล่าวถูกออกแบบโดยใช้การวิธี RSA จากนั้นจะถูกวิเคราะห์ด้วยวิธีแบบประวัติเวลาไม่เชิงเส้น (Nonlinear Response History Analysis, NLRHA) เพื่อตรวจสอบความมั่นคงแข็งแรงและการเคลื่อนตัวของอาคารว่ามีความปลอดภัยตามที่มาตรฐานกำหนดหรือไม่ จากการศึกษาพบว่า แรงเฉือนจากแผ่นดินไหวของกำแพงรับแรงเฉือนที่คำนวณได้จากการวิเคราะห์วิธี NLRHA มีค่าเป็น 2 เท่าของกำลังต้านทานที่ออกแบบไว้ตามค่าที่ได้จากการวิเคราะห์วิธี RSA ผลที่เกิดขึ้นอาจนำไปสู่การวิบัติแบบเฉือนของกำแพงรับแรงเฉือน ถ้าหากอาคารดังกล่าวถูกออกแบบโดยใช้การวิเคราะห์วิธี RSA การศึกษานี้จึงใช้ประยุกต์วิธีการที่เสนอโดย Priestly and Amaris (2002) ในการคำนวณแรงเฉือนเพื่อการออกแบบกำแพงรับแรงเฉือน โดยใช้ค่า R_{eff} (Effective response modification factor) ที่มากกว่าหนึ่งกับแรงเฉือนเฉพาะในโหมดแรกของการสั่นไหวและการแรงบิด และใช้ค่า R_{eff}=1 กับแรงเฉือนในโหมดอื่นๆ สำหรับคำนวณแรงเฉือนเพื่อการออกแบบกำแพงรับแรงเฉือน ผลการศึกษาแสดงให้เห็นว่าวิธีการใหม่นี้จะช่วยหลีกเลี่ยงการวิบัติแบบเฉือนของกำแพงรับแรงเฉือน

ภาควิชา วิศวกรรมโยธา ลายมือชื่อนิสิต .....

สาขาวิชา วิศวกรรมโยธา ลายมือชื่อ อ.ที่ปรึกษาวิทยานิพนธ์หลัก .....

ปีการศึกษา 2555

5370680921: MAJOR CIVIL ENGINEERING
KEYWORDS: SEISMIC SHEAR DEMAND/ MEDIUM-RISE BUILDING/ RESPONSE SPECTRUM ANALYSIS/ NONLINEAR RESPONSE HISTORY ANALYSIS

KY LENG: SEISMIC SHEAR DEMAND OF A MEDIUM-RISE BUILDING DESIGNED BY RESPONSE SPECTRUM ANALYSIS. ADVISOR: ASST. PROF. CHATPAN CHINTANAPAKDEE, Ph.D., 156 pp.

According to ASCE7-05, response spectrum analysis (RSA) procedure can be used to determine the seismic demands of the structures for the seismic design of any type of structures. However, this design procedure has been found to be inappropriate for medium-rise and high-rise buildings. This paper is aimed at verifying the RSA procedure prescribed in the current Thai seismic design code which is based on ASCE7-05 and proposing an appropriate improvement to the RSA procedure if needed. A 16-story medium-rise reinforced-concrete core-wall case-study building is first designed based on RSA procedure and then the non-linear response history analysis (NLRHA) is performed to determine the more accurate seismic demands of the structure. The results show that seismic shear demand of the shear wall from non-linear analysis is about 2 times the shear capacity of the wall designed by RSA procedure. This could lead to shear failure in the shear walls designed by RSA procedure. This study used a modified RSA procedure proposed by Priestly and Amaris (2002) to calculate the design shear force in the walls. In this approach, the R_{eff} (Effective response modification factor) more than 1 is used only for the first mode of translational (E-W direction) and torsional modes, and R_{eff} = 1 is used for other higher modes. The results indicate that this new method could help avoid shear failure in the shear walls.

Department : Civil Engineering Student's Signature .....
Field of Study : Civil Engineering Advisor's Signature .....
Academic Year : 2012

ACKNOWLEDGEMENTS

I would like to acknowledge the financial support provided by JICA through the ASEAN University Network/Southeast Asia Engineering Education Development Network (AUN/SEED-Net) program.

I also would like to express my profound gratitude to Dr.Chatpan Chintanapakdee for his availability and valuable advice.

I am very thankful to Dr. Panitan Lukkunaprasit, Dr. Tospol Pinkaew, Dr. Anat Ruangrassamee and Dr. Chatpan Chintanapakdee for their lectures in dynamic and earthquake engineering courses which give me the motivation and knowledge to conduct this research. My equal thank is given to Dr. Sutat Leelataviwat and Dr. Panitan Lukkunaprasit for their important review of this work.

I sincerely appreciate my friends for their constant discussions and ideas.

Last but not least, I want to thank my beloved parents from the bottom of my heart for their encouragement and mental support. Thank you for always being on my side.

CONTENTS

Page

Page

Page

LIST OF TABLES

Page

Page

LIST OF FIGURES

Page

Page

Page

Page

Page

Page

Page

Page

Page

Page

Page

NOTATION

Greek symbols

Γ_n	*n*th mode modal participant factor
ζ	damping ratio
ζ_n	*n*th-mode damping ratio
$\imath$	influence vector
ν	axial force ratio
ε_y	steel yield strain
ε_c	longitudinal concrete strain
ε_{cc}	strain at maximum concrete stress $f_{cc}^{'}$
θ_u	hinge rotation at ultimate strength
θ_R	hinge rotation at residual strength
$\rho_{sh,eff}$	effective ratio of transverse reinforcement
ρ_{in}	cross-correlation coefficient for modes *i* and *n*
ρ_v	ratio of total web area of longitudinal reinforcement between tension and compression steel to bd
$\rho^{'}$	compression reinforcement ratio
ρ	tension reinforcement ratio
ρ_{sh}	transverse reinforcement ratio
δ'	d'/d
$\delta_{\max}$	maximum displacement at Level *x* computed assuming $A_x = 1$
δ_{avg}	average of the displacements at the extreme points of the structure at Level *x* computed assuming $A_x = 1$
ϕ_y	section curvature at yielding
ϕ_n	*n*th natural vibration mode
ω_n	*n*th natural frequency

Roman symbols

a_{sl}	zero-one variable (effect of pullout of longitudinal bars from anchorage zone)
A	pseudo-acceleration spectrum ordinate
A_n	pseudo-acceleration spectrum ordinate, mode *n*
A_x	amplification factor at level *x*
b	width of compression zone
c_{units}	unit conversion variable
c	classical damping
C_s	seismic response coefficient
d	effective depth of cross section
d'	distance of center of compression reinforcement from extreme compression fiber
d_b	diameter of compression longitudinal reinforcement
D	peak deformation
$D_n(t)$	deformation of *n*th-mode SDF system
E_c	modulus of elasticity of concrete
E_{sec}	secant modulus of confined concrete at peak stress
E_s	elastic modulus of steel
f_s	lateral resisting force vector of the building system
f_c'	compressive strength of unconfined concrete
f_y	yielding strength of tension reinforcement
f_c	longitudinal concrete stress
f_{cc}'	compressive strength (peak stress) of confined concrete
f_{PM}	yield function value (=1 when yield)
f_{MM}	yield function value
H	overall height of the building

I	important factor
k	lateral stiffness
k_y	normalized (to d) compression zone depth at section ultimate
L_n	defined by equation (2.10)
L_s	shear span
m	mass
M_n	generalized mass, mode *n*
M_y	bending moment at yield
M_u	moment at ultimate strength
M_R	moment at residual strength
M	bending moment
M_{YB}	yield moment at $P=P_B$
P	axial force
P_B	axial force at the balance point at each P-M plan
P_{Y0}	yield force at M=0
$P_{eff}(t)$	vector of effective earthquake forces
$q_n(t)$	*n*th modal coordinate
r_n^{st}	*n*th modal static response
r_{n0}	peak modal response
r_o	peak of any response quantities
R	strength reduction factor
s_n	defined by equation (2.11)
s	spacing of transverse reinforcement
S_a	spectra acceleration
T	fundamental period of the structure
T_n	*n*th natural period
u	relative displacement or deformation
$\dot{u}$	velocity
$\ddot{u}$	acceleration

$\ddot{u}_g(t)$	ground acceleration
V	pseudo-velocity spectrum ordinate
V_{static}	seismic base shear calculated from equivalent lateral force procedure
$V_{dynamic}$	seismic base shear obtained from RSA procedure in ETABS
V_p	shear demand at point of flexural yielding
V_n	nominal shear capacity
W	effective weight of the building

CHAPTER I
INTRODUCTION

1.1 Background

High-rise concrete core wall buildings have been used intensively instead of moment frame system used in traditional high-rise construction because of its lower costs, faster construction and more open and flexible architecture. For this kind of system, the lateral-force-resisting system is normally provided by the core wall, since it is much stiffer than the column frame. For economical reason, the building is expected to behave non-linearly and capacity design concept may be applied, then the desired mechanism is that the flexural plastic hinge is formed near the base of the core wall and flexural yielding is anticipated in the coupling beam.

However, arbitrary limitations imposed by the building code on structural systems do not necessarily recognize framing systems which are efficient or consistent with modern high-rise construction. The unique characteristics of tall building are not considered in the current code provision, and this may lead to less-than-desirable result.

In design practice, the equivalent static design procedure, in which the first mode of the structure is assumed to dominate, is generally used due to its simplicity. However, for long-period structure like tall building, the seismic response contributes significantly. The equivalent static procedure is thus found to be inappropriate. Hence, another approach known as response spectrum analysis (RSA), which accounts for multi-mode effects, is employed in the current Thai design code (based on ASCE7-05). In the RSA procedure, to determine the seismic demands of the structure due to earthquake loading, we first compute the elastic responses of each vibration mode from dynamic analysis and the design response spectrum in the code based on 5% damping ratio and then the responses of each mode are combined by either the square root square sum (SRSS) or the complete quadratic combination (CQC) rule, finally the total elastic responses are reduced to the seismic demands for structural design by a response modification factor “R” that accounts for the overstrength and inelastic effects of the structure.

Nevertheless, researchers have found that the RSA procedure described in the current design code can sometimes lead to an unsafe design since it cannot capture the real behavior of tall building under seismic loading, thus the rigorous non-linear response history analysis (NL-RHA) must be used to estimate the true demand of the high-rise building due to earthquake ground motion.

1.2 Literature reviews

The NL-RHA has been introduced numerically in a computer program called IBM 7090 since 1965 by Clough et al. to study the inelastic seismic behavior of tall building due to earthquake excitation. Many other studies on influences of higher vibration mode have been conducted later by means of NL-RHA to evaluate inelastic seismic demands of high-rise buildings and wall structures. In 1984, Keintzel studied the influences of multi-mode on ductility requirement for shear wall and their inelastic shear forces. Nonlinear dynamic analyses were performed for slender cantilever shear wall with 5, 10 and 20 lumped story masses under 10 earthquake ground motions. The research found that the base shear from nonlinear analysis is range from 3 times to 8 times greater than that obtained from the code (German seismic code DIN 4149). On the basis of this research, Eibl and Keintzel (1988) extended it to structure with 2 to 5 stories. A new approximate method called “modal limit forces” (MLF), where shear force demand of each vibration mode is limited by shear force of elastic system and yielding moment of the wall structure in the corresponding mode, was developed to compute inelastic seismic shear forces in RC yielding shear walls more accurately. It should be noted that the MLF procedure was adapted from the RSA procedure to yielding structures by introducing a correction factor.

A 40-story reinforced concrete core wall building had been used as a case study building for a research done by Zekioglu et al. (2007), in the study, for linear elastic analysis, site-specific design response spectrum for design basis earthquake (DBE - 10% probability of being exceeded in 50 years) was used to design the building followed Los Angeles Tall Building Design Council (LATBDC) 2005 guidelines. Seven pairs of time history ground motions for the rare event were employed. NL-RHA was then performed for final seismic evaluation against maximum considered earthquake (MCE - 2% probability of exceedance in 50 years).

The result of NL-RHA showed that the post-tensioned slabs and all gravity columns satisfy the collapse prevention performance limits set by FEMA 356, the measured strains of the wall components which is obtained from flexural response of the wall were lower than the usable strain limits, whereas the shear strength of the core wall segments and coupling beams are controlled by this analysis and base shear corresponded approximately to 18% of the seismic weight of the building is substantially higher than that obtained from DBE hazard which is only 0.059 and 0.054 of the seismic weight in both principal directions. Figure 1.1 (a) and (b) show the distribution of the seismic story shear obtained from RSA and NLRHA procedures respectively. Thus this research identified the non-conservatism of linear elastic approach and non-conservatism with "R" factor for the design of tall building in the current design code.

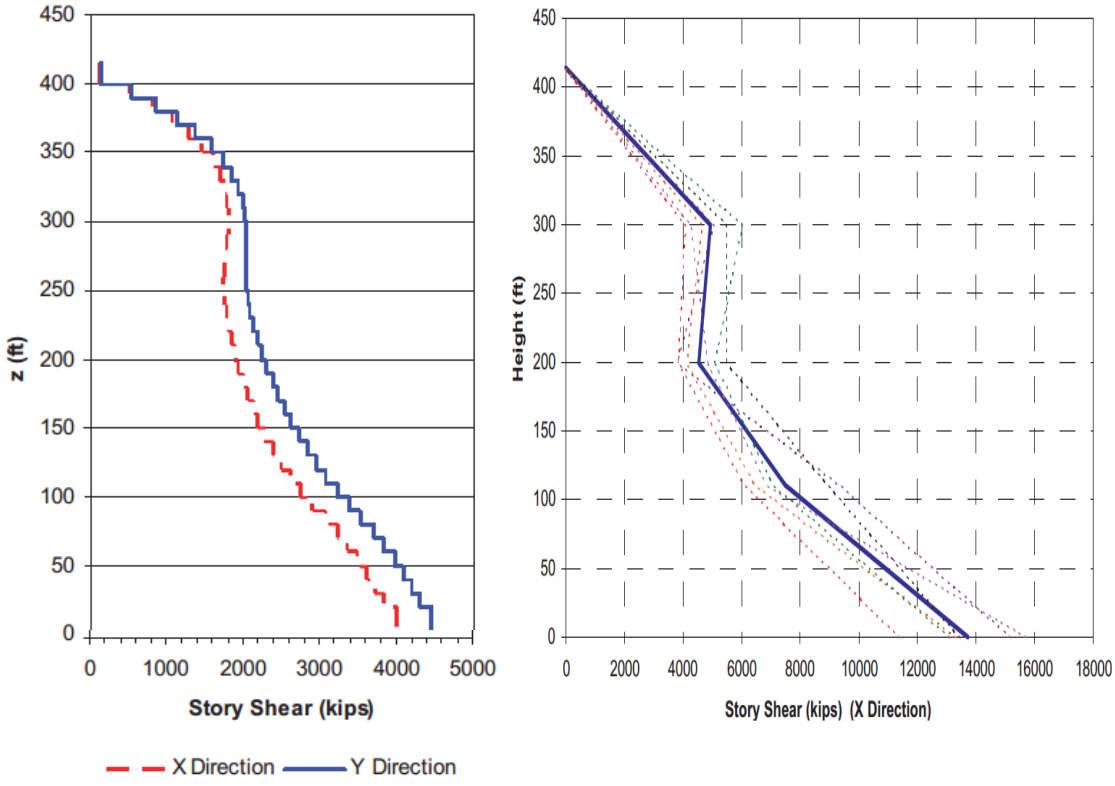

(a) RSA procedure due to DBE (b) NLRHA procedure due to MCE

Figure 1.1 Distribution of seismic story shear (Zekioglu et al., 2007)

A similar study on a 45-storey reinforced concrete frame wall building by Tuan et al. (2008) confirmed the invalidity of RSA procedure by doing similar

process: the building is first design by RSA procedure conforming EC8 (1998) and then verified by NL-RHA procedure during severe earthquake excitations. It should be noted here that the earthquake excitation is only applied to one direction in which the wall action predominate the behavior of the building. The results show that the RSA procedure overestimated the story drift ratios and the drift ratios from both analyses, RSA and NLRHA, are within the allowable limit as shown in Figure 1.2. Moreover, RSA procedure underestimated the force demands (bending moment and shear force) in wall elements as illustrated in Figure 1.3. The seismic moment and shear demand obtained from NLRHA are about 1.5 and 1.25 times, respectively, the corresponding demands from RSA procedure in the wall base. Noted in the figures that EC8 represents responses from RSA procedure conforming Eurocode8 while Ruaumoko represents the responses from NLRHA modeled in Ruaumoko program (2007). Furthermore, the research has also found that unlike the suggestions from the code (EC8, 1998), P-delta effect had found to be negligible for the case study while beam-lengthening can affect the performance of RC structure significantly.

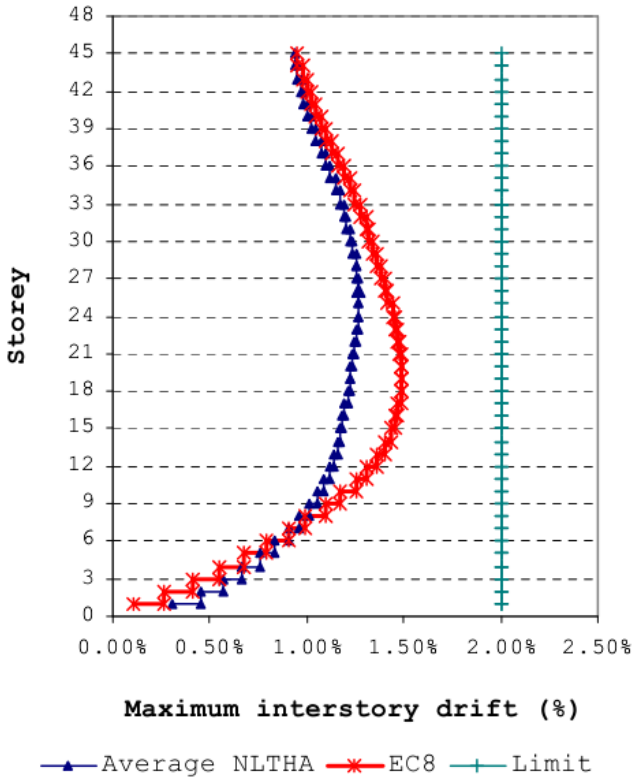

Figure 1.2 Average story drift ratios due to NLRHA and RSA procedure prescribed in Eurocode8 (Tuan et al., 2008)

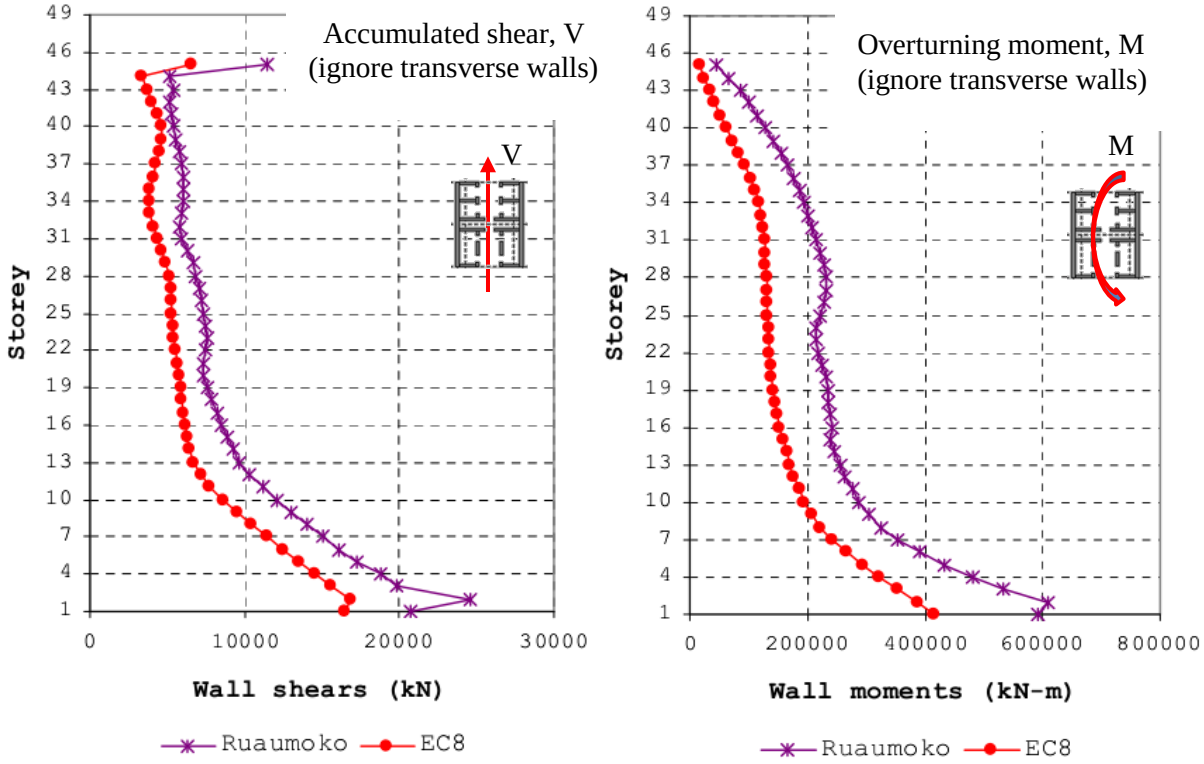

Figure 1.3 Seismic shear and moment demand in wall due to NLRHA in Ruaumoko and RSA in Eurocode8 (Tuan et al. 2008)

Another research by Priestley and Amaris (2002), in which a wide range of cantilever wall buildings: 2, 4, 8, 12, 16 and 20 stories, was used, resulted in the same conclusion which showed that considering the same force reduction factor "R" in all vibration modes will lead to underestimating seismic demands in the structure. Therefore, they proposed a modal combination method called Modified Modal Superposition (MMS). In MMS combination rule, one considers the force reduction factor only in the first mode and elastic seismic demands will be used in the other higher mode. This method works under two assumptions: (1) ductility limits primarily first mode response, and (2) the inelastic higher modes will not differ significantly from elastic mode, which means it is not appropriate to apply a force reduction factor (R) to any mode past the first. The seismic demands from the proposed method are found to agree quite well with NL-RHA procedure. This means that the development of inelasticity does not affect the higher mode responses. However, Priestley (2003) argued that this is not always the case. Priestley conducted a study on frame structure and observed that the higher mode responses are actually influenced by the development of inelasticity. So by adopting the method proposed earlier by Priestley

and Amaris (2002), one obtains generally too conservative story shear forces which is not economic. It can be concluded from these 2 researches that the development of inelasticity influences little in the wall structures while great impact can be expected on the frame structures. A more general and accurate approach to estimate the peak seismic base shear has been proposed by Sullivan et al. (2008). In this approach, the concept of transitory inelastic modes (TIM) of vibration, where TIM is defined as the eigen-value solutions of the structure deforming through its non-linear range, is used. And the seismic base shear is computed from transitory inelastic modal superposition formulation, which is the combination of inelastic first mode demand obtained from plastic mechanism analysis and transitory inelastic higher mode demands. This new approach has been proved to give a better prediction of seismic base shear demands compared with the traditional modal superposition technique and the method proposed by Amaris and Priestley (2002). The method is best suited for the capacity design application since it based on the formation of full mechanism.

Moreover, the influences of higher modes on inelastic seismic demands have also been investigated by Sangarayakul and Warnitchai (2004). In their study, the inelastic seismic responses of tall building ranging from 20 to 40-story were evaluated by NL-RHA procedure, their responses were then approximately decomposed into modal responses. The first mode inelastic seismic demands were found to be much lower than the corresponding elastic seismic demands, which mean the use of "R" factor is reasonable. However, the second and higher mode responses are observed to be close to their corresponding elastic seismic demands, so the same "R" factor used in the current design code is now found to be inappropriate. Similarly, a research by Klemencic et al. (2006) based on their experiences of design of several tall ductile core wall buildings has confirmed the invalidity of response modification factor "R" used in the code provision, so it is recommended that the values of "R" is reassessed to reflect better actual building behavior so that desirable behaviors (flexural yielding) are promoted while undesirable demands (shear forces) are minimized.

Klemencic et al. (2007) conducted another research according to the design experiences of 20 high-rise ductile core wall buildings with a sample design of 40-storey core wall building performed for LATBDC, knowing the fact that it is not conservative to design tall building using linear elastic approach with the same

inelastic modification factor "R" mentioned in the code, Klemencic proposed to anticipate the inelastic behavior of certain elements including shear wall and coupling beams based on linear analysis for DBE hazard to save time since NL-RHA for large, complicated structures consumes many hours of engineering effort. For the case study building, seven pairs of site-specific ground motions are used for NL-RHA based on MCE. An amplification factor of 3 on DBE shear demand was chosen to anticipate the expected nonlinear analysis result while an amplification of 2 on DBE overturning moment demand was selected to anticipate the expected nonlinear analysis result, the result showed that the factor of 3 is good enough to predict the core wall shear demand in the nonlinear analysis result in Y-direction, but this is not sufficient for X-direction, while the factor of 2 is underestimate the overturning moment demand in nonlinear analysis in both directions. Depicted in Figure 1.4 and Figure 1.5 are the seismic demands in core wall along the height of the wall. The solid blue curve represents the DBE demand obtained from RSA procedure, whereas the dash blue curve is the DBE demand scaled by 3 from RSA procedure, and the black curve is the average demand obtained from NLRHA.

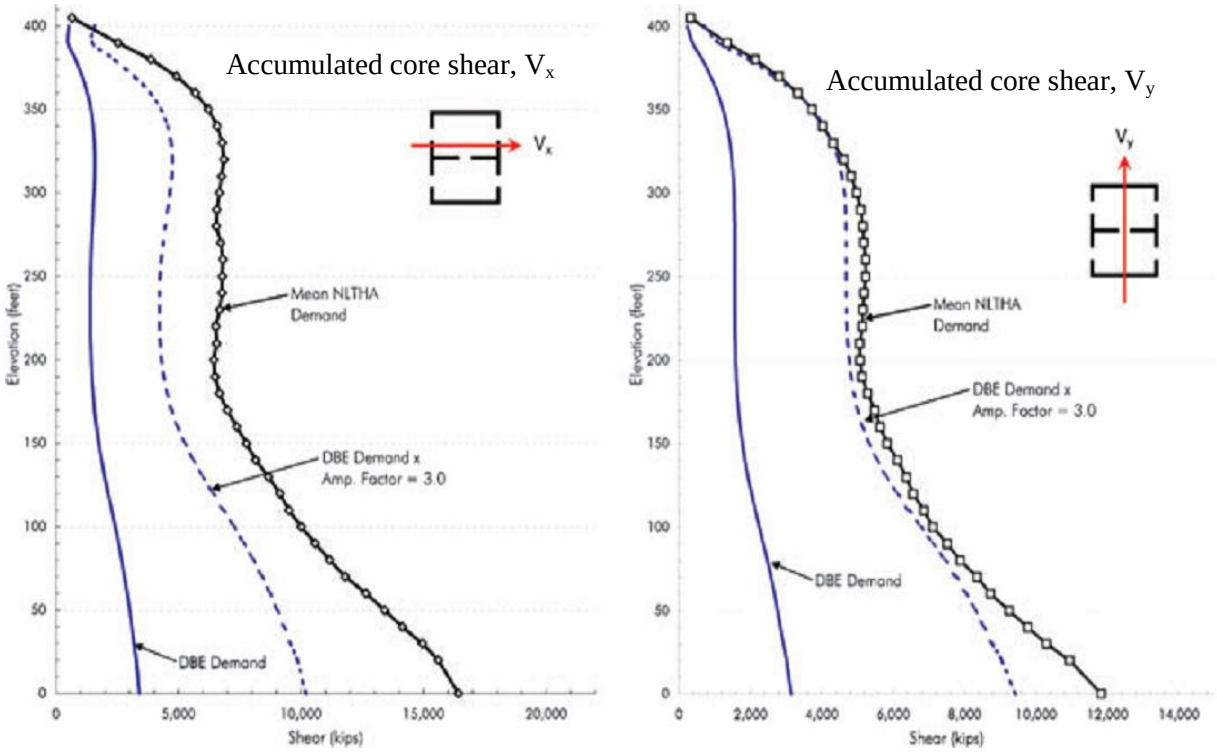

Figure 1.4 Seismic shear demand in core wall due to RSA for DBE and NLRHA for MCE (Klemencic et al., 2007)

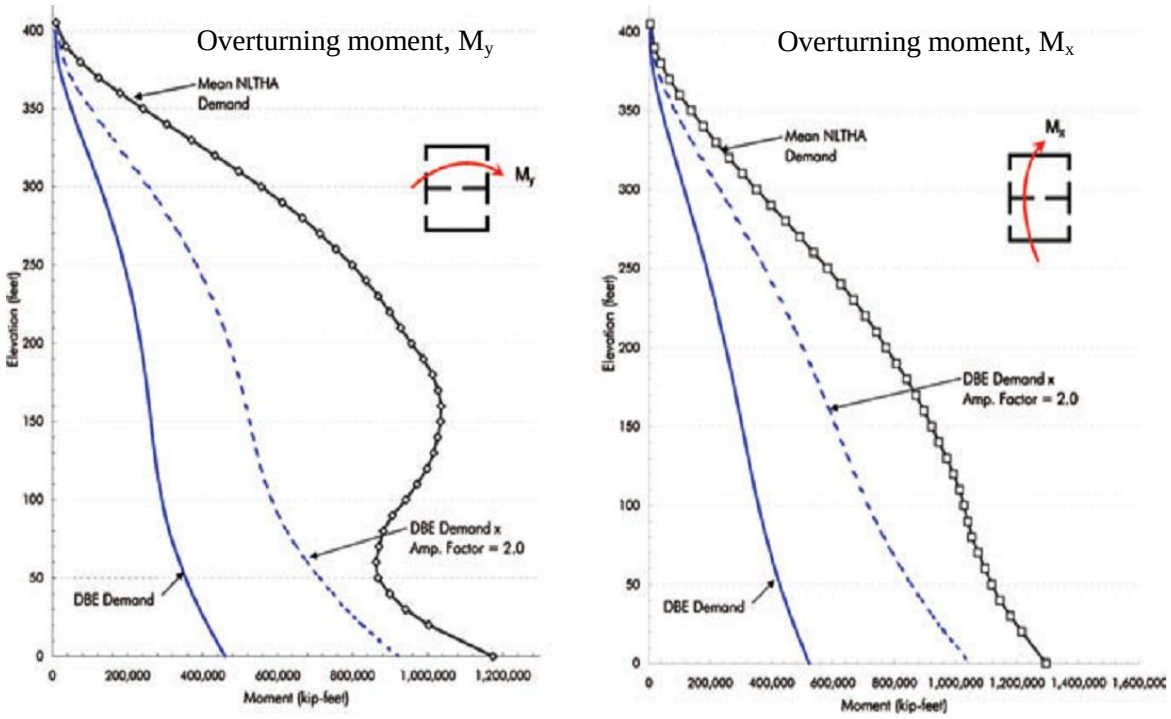

Figure 1.5 Seismic moment in core wall due to RSA for DBE and NLRHA for MCE (Klemencic et al., 2007)

Recently, Munir and Warnitchai (2012) studied the causes of unsafe design by RSA in the current design code through a 40-storey core wall building as a case study. In their study, the case study building is first design by RSA procedure prescribed in UBC97; the NL-RHA is carried out next to verify the seismic demand. After comparing the results from RSA and NL-RHA procedure, differences of seismic demands have been found due to the different ground motions used in both analyses, MCE for NL-RHA procedure and DBE for RSA procedure, different damping ratio used in both analyses, 1% to 5% for NL-RHA and 5% for RSA, and the overstrength effect in plastic hinge zone. Unfortunately, these are not the only reasons. Despite changing the damping to 5% and MCE to DBE in NLRHA, the seismic shear demands from NLRHA is still about 1.5 time the corresponding demand from RSA procedure as shown in Figure 1.6. Similarly, the seismic moment from NLRHA is also greater than the corresponding demand from RSA procedure by about 1.5 time for the upper story.

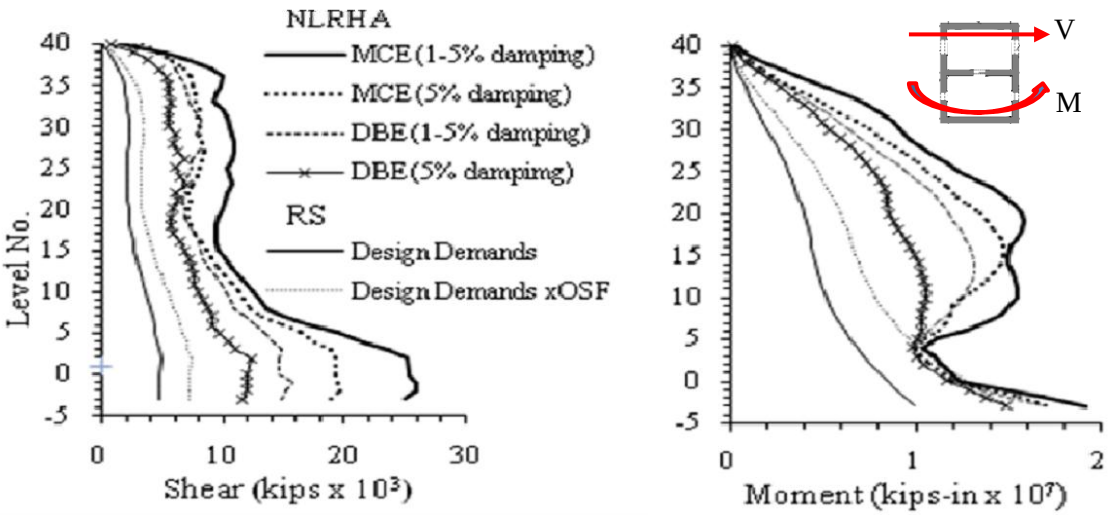

Figure 1.6 Seismic shear and moment in core wall due to RSA and NLRHA (Munir and Warnitchai, 2012)

A modal decomposition of inelastic seismic response called "uncoupled modal response history analysis" (UMRHA) developed by Chopra and Goel (2002) is therefore performed to decompose the response into the contribution of each vibration mode in order to explore the other causes. The modal inelastic responses from UMRHA procedure represent the true seismic demand by MCE ground motion represented by MCE modal demand in Figure 1.7 and are compared with the modal elastic seismic demands due to DBE ground motion represented by DBE elastic modal demand in Figure 1.7 and modal seismic design demands which are obtained from elastic seismic demands divided by R factor represented by modal design demand in Figure 1.7. As illustrated in Figure 1.7, the MCE modal demand is close to the modal design demand only in the first mode, (a) and (e), and much larger than the modal design demand in other higher mode, so these results show that the use of large reduction factor "R" to reduce the seismic demands to the design demand in the RSA procedure is valid only for the first mode and invalid for other higher modes. This is because an effective yielding mechanism to limit seismic demands is either not fully mobilized or not mobilized at all. Based on this findings and understandings, several possible measures have been proposed to effectively reduce the seismic demands to design demands; for instance, the plastic hinges formed in the wall base region only over the entire wall in the conventional design concept are proposed to be developed at several effective locations along the wall height, or some passive energy absorbers

such as viscous damper or buckling restrained braces can be installed into the building to dampen down the targeted modes so that the seismic demands remain within acceptable limits.

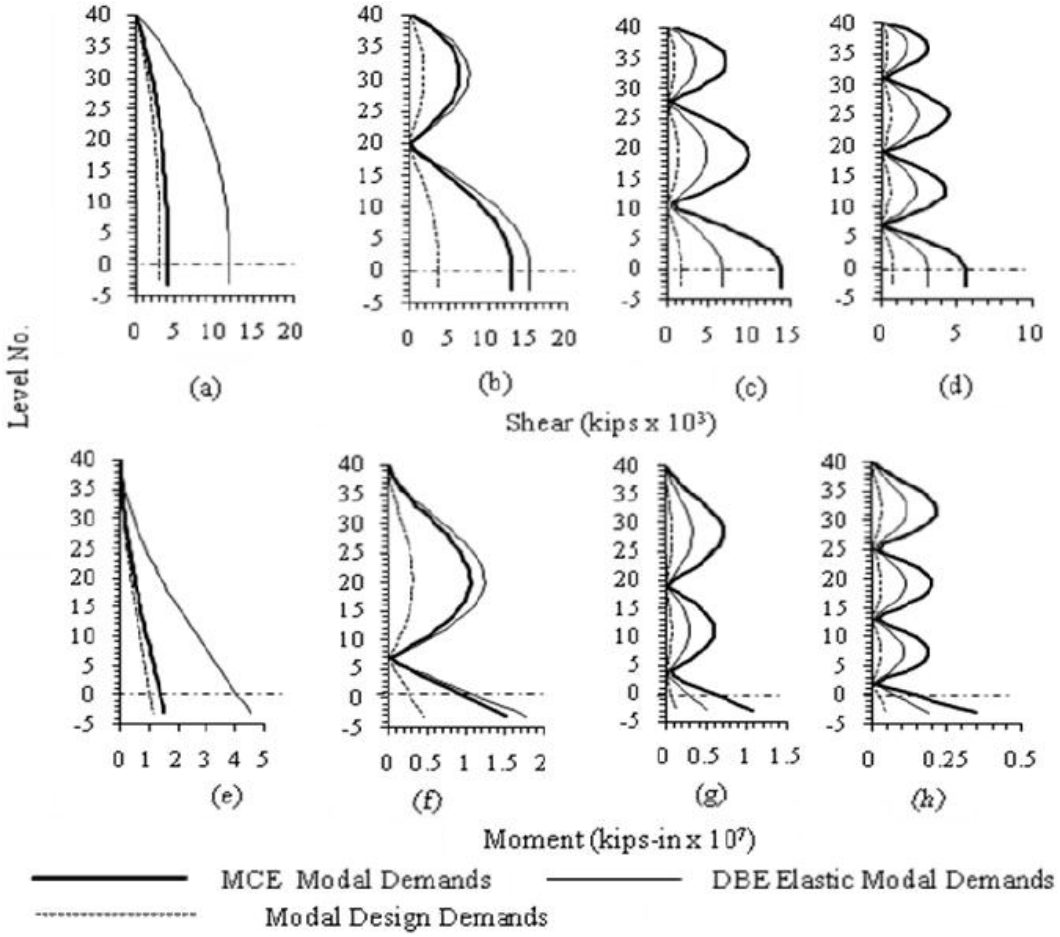

Figure 1.7 Modal seismic shear and moment in core wall due to RSA and UMRHA (Munir and Warnitchai, 2012)

In summary, RSA procedure has underestimated the seismic demands of the wall elements. Seismic shear demand over the entire height of the wall from NLRHA based on MCE level is as high as 5 times the corresponding demand from RSA procedure based on DBE level found by Zekioglu et al. (2007) and Klemencic et al. (2007). And the seismic DBE demands (shear and moment) over the entire height of the wall from NLRHA are about 1.5 times the corresponding demands obtained from RSA procedure based on the findings of Tuan et al. (2008) and Munir and Warnitchai (2012). Keintzel (1984) found that the seismic base shear from NLRHA is ranging from 3 to 8 the base shear from RSA procedure while Sullivan et al. (2007) concluded

in their research that the base shear from NLRHA is about 2 times the corresponding base shear from RSA procedure.

1.3 Objectives

The main objectives of this research are as follow:

1. Verify the response spectrum analysis procedure prescribed in the current Thai seismic design code (based on ASCE7-05) and identify the weak points of structural members (Shear wall, columns)
2. Make appropriate suggestions for improvement of the code to address design of medium-rise building (if necessary).

1.4 Scope of research

The scope of this research is to utilize a 16-story reinforced concrete frame-wall building with 49.2 meters height as case study. The building is assumed to stand on soft soil and fixed at the base. Infill wall is not modeled but its mass is included. P-delta and accidental torsional effects are included in the analysis and seven earthquake ground motions representing extreme earthquake events will be used for nonlinear response history analysis.

1.5 Expected benefit

This study is intended to improve the current design code (ASCE7-05) to address the design of medium-rise building, so upon the completion of the study, we would obtain some benefit as follow:

- Remind the design engineers not to blindly follow the code by showing the insufficient point when dealing with real behavior of the building
- Help the design engineers to be more confident when designing medium-rise building subjected to earthquake loading by using the proposed improvements

CHAPTER II
THEORETICAL BACKGROUND AND METHODOLOGY

2.1 Introduction

Response spectrum analysis (RSA) procedure is used to compute seismic demands for elastic system, while non-linear response history analysis (NL-RHA) procedure is on the other hand used to estimate seismic demands for inelastic system. Both of these methods will be presented here in this chapter. The rigorous theory of RSA procedure will be reviewed followed by the more complicated NL-RHA procedure. Finally, the methodology of this research is proposed.

2.2 Response spectrum analysis procedure

2.2.1 Response spectra

For a linear single degree of free (SDF) system subjected to ground motion excitation $\ddot{u}_g(t)$, the equation of motion of mass *m* is governed by:

$$m\ddot{u} + c\dot{u} + ku = -m\ddot{u}_g(t) \tag{2.1}$$

where *u* is the relative displacement of the SDF system, *m, c* and *k* are the mass, classical damping and lateral stiffness of the SDF system.

Divide equation (2.1) by *m* on both side yields

$$\ddot{u} + 2\zeta\omega_n\dot{u} + \omega_n^2 u = -\ddot{u}_g(t) \tag{2.2}$$

Therefore, for a given ground acceleration $\ddot{u}_g(t)$, the response *u(t)* depends only on the natural frequency ω_n (or period T_n) and damping ratio ζ of the system.

Deformation response spectrum

The peak value of deformation time history response of an SDF system is denoted by:

$$D = u_0 = \max_t \left|u(t)\right| \tag{2.3}$$

If many of such analyses are repeated for many SOF with a fixed damping ratio ζ but different natural period T_n, the deformation response spectra can then be constructed with a range of T_n considered.

Pseudo-velocity response spectrum

Consider a quantity *V* for an SDF system with frequency ω_n which has the peak deformation *D*:

$$V = \omega_n D = \frac{2\pi}{T_n} D \tag{2.4}$$

where *V* is called the peak relative pseudo-velocity or peak pseudo-velocity

Pseudo-velocity response spectrum is obtained from varying the natural period T_n or natural frequency ω_n of the system.

Pseudo-acceleration response spectrum

The quantity *A* has a unit of acceleration and is related to the peak deformation by:

$$A = \omega_n^2 D = \left(\frac{2\pi}{T_n} \right)^2 D \tag{2.5}$$

where *A* is called pseudo-acceleration

A plot of *A* as a function of natural period T_n or natural frequency ω_n of the system is pseudo-acceleration response spectrum.

Elastic design spectrum

The response spectrum to be used for structural design should not be for a particular ground motion but rather represent possible ground motion based on statistics of many grounds motions. The design response spectrum in ASCE7-05 is based on 5% damping ratio.

2.2.2 Modal analysis

Equation of motion

The governing equation of a linear multi-degree of freedom (MDF) system due to earthquake induced ground motion is:

$$\mathbf{m\ddot{u}+c\dot{u}+ku=p_{eff}}(\mathbf{t}) \tag{2.6}$$

where $\mathbf{u}$ is a vector of displacement, $\mathbf{m}$, $\mathbf{c}$ and $\mathbf{k}$ are mass, classical damping and lateral stiffness matrices respectively of the system, $\mathbf{p_{eff}}(\mathbf{t})$ is a vector of effective earthquake forces and can be express as follow:

$$\mathbf{p_{eff}}(\mathbf{t})=\mathbf{-m\iota}\ddot{u}_g(t) \tag{2.7}$$

where $\boldsymbol{\iota}$ is the influence vector in which each element is equal to unity

Modal expansion of displacement and forces

The displacement $\mathbf{u}$ of N-DOF system can be express as the superposition of the modal contributions:

$$\mathbf{u}(\mathbf{t})=\sum_{\mathbf{r=1}}^{\mathbf{N}}\boldsymbol{\phi}_{\mathbf{r}}q_r(t) \tag{2.8}$$

The spatial distribution of the effective earthquake forces can also be express as the summation of modal inertia force distributions:

$$\mathbf{m\iota}=\sum_{\mathbf{r=1}}^{\mathbf{N}}\Gamma_r\mathbf{m}\boldsymbol{\phi}_{\mathbf{r}} \tag{2.9}$$

where

$$\Gamma_r=\frac{L_r}{M_r} \qquad L_r=\boldsymbol{\phi}_{\mathbf{r}}^{\mathbf{T}}\mathbf{m\iota} \qquad M_r=\boldsymbol{\phi}_{\mathbf{r}}^{\mathbf{T}}\mathbf{m}\boldsymbol{\phi}_{\mathbf{r}} \tag{2.10}$$

The contribution of the nth mode to the excitation vector $\mathbf{m\iota}$ is

$$\mathbf{s_n}=\Gamma_n\mathbf{m}\boldsymbol{\phi}_{\mathbf{n}} \tag{2.11}$$

Modal equation

Substituting equations (2.7) & (2.8) into equation (2.6), and multiplying both side by $\boldsymbol{\phi}_n^T$, then using orthogonal properties of mass and damping of mode, finally, dividing the obtained equation by normalize mass M_n gives:

$$\ddot{q}_n + 2\zeta_n \omega_n \dot{q}_n + \omega_n^2 q_n = -\Gamma_n \ddot{u}_g(t) \tag{2.12}$$

substituting $q_n(t) = \Gamma_n D_n(t)$ into equation (2.12) and divide both sides by Γ_n we obtain

$$\ddot{D}_n + 2\zeta_n \omega_n \dot{D}_n + \omega_n^2 D_n = -\ddot{u}_g(t) \tag{2.13}$$

Modal response

The displacement due to the nth mode is therefore:

$$\mathbf{u_n}(t) = \boldsymbol{\phi}_\mathbf{n} q_n(t) = \Gamma_n \boldsymbol{\phi}_\mathbf{n} D_n(t) \tag{2.14}$$

The response quantity contributed from the nth mode is:

$$r_{no} = r_n^{st} A_n \tag{2.15}$$

where r_n^{st} denote the modal static response determined by static analysis due to external forces $\mathbf{s_n}$, and A_n is obtained from pseudo-accelerations response spectrum described above [section 2.2.1]

Modal combination rules

Two approximation rules are introduced to combine the peak modal response r_{n0} determined from earthquake response spectrum, namely: the *square-root-of-sum-of-square (SRSS)* rule and the *complete quadratic combination (CQC)* rule:

SRSS

$$r_o \approx \left(\sum_{n=1}^{N} r_{no}^2 \right)^{0.5} \tag{2.16}$$

CQC
$$r_o \approx \left(\sum_{i=1}^{N} \sum_{n=1}^{N} \rho_{in} r_{io} r_{no} \right)^{0.5} \tag{2.17}$$

where

$$\rho_{in} = \frac{8\sqrt{\zeta_i \zeta_n}\left(\zeta_i + \beta_{in}\zeta_n\right)\beta_{in}^{3/2}}{\left(1-\beta_{in}^2\right)^2 + 4\zeta_i\zeta_n\beta_{in}\left(1+\beta_{in}^2\right) + 4\left(\zeta_i^2 + \zeta_n^2\right)\beta_{in}^2} \tag{2.18}$$

2.2.3 Scaling of design value

For the design of structural members using response spectrum analysis (RSA) procedure, the elastic design spectrum is scaled by I/R (determined from the design code) to account for inelastic behavior and overstrength of the structure. The response quantities are then determined by the RSA procedure mentioned earlier in section 2.2 of this chapter.

In seismic design, the equivalent lateral force (ELF) procedure needs to be operated together with the RSA procedure. Once the seismic base shear ($V_{dynamic}$) obtained from RSA procedure is less than 85% of seismic base shear (V_{static}) from ELF procedure, a scaling factor of $0.85V_{static}/V_{dynamic}$ is used to scale the force response quantities to seismic force demand but not the displacements or drift which should be scaled by the quantity C_d/I (based on seismic Thai design code). It should be noted that the period for RSA procedure is determined from substantiated analysis in ETABS and the period used to calculate the base shear in ELF procedure is either 1.5 time 2% of the overall height of the building or the period obtained from ETABS, whichever is smaller.

2.3 Non-linear response history analysis procedure

The theoretical background of NL-RHA procedure is briefly reviewed here. The governing equation of an inelastic system due to earthquake ground motion $\ddot{u}_g(t)$ is given by:

$$\mathbf{m\ddot{u}+c\dot{u}+f_s}\left(\mathbf{u},\dot{\mathbf{u}}\right)=-\mathbf{m}\ddot{u}_g(t) \tag{2.19}$$

where $\mathbf{u}$ is a vector of displacement, $\mathbf{m}$ and $\mathbf{c}$ are mass and classical damping matrices respectively of the system. $\mathbf{\iota}$ is the influence vector of which each element is equal to unity. $\mathbf{f_s}$ is the lateral resisting force vector of the building system, once the responses are still within linearly elastic range, $\mathbf{f_s = ku}$, when the elastic limit is exceeded, $\mathbf{f_s}$ must be described as a set of non-linear function of $\mathbf{u}$ and $\dot{\mathbf{u}}$.

The classical modal analysis described above in subsection 2.2.2 is no longer applicable to non-linear system. However, even the floor displacement of the non-linear system can be expressed as a combination of natural mode of undamped system vibrating within the range of its linear behavior. So the equation (2.8) is still valid for NL-RHA. Equation (2.9), (2.10) and (2.11) can also be used in this analysis.

Substituting equation (2.8) into equation (2.19), and pre-multiplying both side by $\boldsymbol{\phi}_n^T$, then using orthogonal properties of mass and damping of mode, finally, dividing the obtained equation by normalize mass M_n gives:

$$\ddot{q}_n + 2\zeta_n \omega_n \dot{q}_n + \frac{F_{sn}(q_n, \dot{q}_n)}{M_n} = -\Gamma_n \ddot{u}_g(t) \tag{2.20}$$

Equation (2.20) is standard governing equation of motion for inelastic SDF system. It represents N equations in the modal coordinate q_n. The equation is uncoupled only as long as the structure remains linear, after yielding, the modal equation becomes coupled.

2.4 Research Methodology

To accomplish the objectives raised in the previous chapter, this research will be done step by step as follow:

1. Use RSA procedure mentioned earlier in section 2.2 by means of ETABS Nonlinear version 9.5.0 extended 3D analysis of building system to analyze the case study building, considering both P-delta and accidental torsional effects, the seismic demands (base shear, base overturning moment, element forces etc.) can then be determined by scaling the

responses with appropriate scaling factor described earlier in section 2.2.3 according to current Thai design code.

2. Design shear walls and columns such that the nominal strength of the member time a safety factor is approximately equal to the demand from step 1. Set shear strength of the structural wall equal to the seismic demand from step 1 divided by a safety factor of 0.75.
3. Analyze the building already designed in step 2 using NL-RHA procedure discussed above in section 2.3 by an efficient tool, Perform3D version 5.0. Seven earthquake ground motions representing extreme earthquake events on soft soil will be utilized.
4. The result from Perform-3D will then be compared with the allowable limit in the current design code and guideline for tall building to check the performance of the case study building. Special attention will be provided to shear failure in the walls.
5. Identify the weak points of structural members (shear walls and columns)
6. Recommend appropriate suggestions for improving the current design code to address the design of medium-rise building.
7. Conclusions and recommendations.

CHAPTER III
STRUCTURAL SYSTEM AND GROUND MOTIONS

3.1 Introduction

To accomplish the methodology mentioned in the previous chapter, a 16-story frame-wall building is used as a case study building, and its configuration and structural system is presented in the later subsection.

3.2 Description of the case study building

3.2.1 Building configuration

"Chula Nivas" is an on-campus residential building in Chulalongkorn University located along Chula 9 road. For simplicity, the configuration of the building has been modified to be used here as a case study building. It is 16 stories tall and consisting of core walls together with slab column frames. Figure 3.1 shows its structural configuration in plan view. The typical bays are 5.1m long in east-west (E-W) direction and 5.4m long in the north-south (N-S) direction.

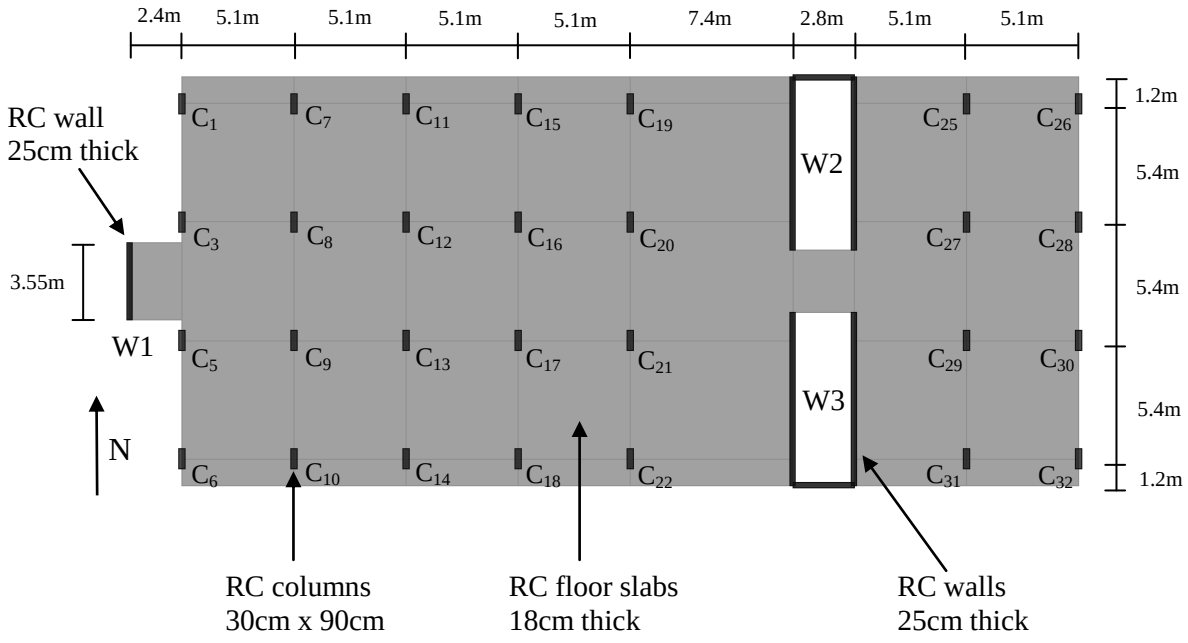

Figure 3.1 Typical floor plan view

The lateral seismic force in the E-W direction is mostly resisted by the four 7-bays moment-resisting frames while the shear walls have small resistance to the seismic force. On the other hand, in the N-S direction, the seismic-force-resisting system is a dual system composed of a combination of frame and frame-wall. In this direction, shear walls will play an important role in resisting seismic loading.

The building configuration and cross-section together with thickness of the structural members are summarized in the Table 3.1 and Table 3.2 respectively.

Table 3.1 Case study building configuration

Structural system		Frame-wall
Plan width in N-S direction, 3bays		18.6m
Plan width in E-W direction, 7bays		43.2m
Building height		49.2m
Number of story		16
Story height	First story	4.2 m
	Other story	3 m

Table 3.2 Members cross-section and thickness

Column cross section (cm×cm)	90×30
Prestress concrete flat slab thickness (cm)	18
Wall thickness (cm)	25

3.2.2 Material properties

The properties of the concrete and rebar used in this study are indicated in the Table 3.3 below:

Table 3.3 Material properties

Concrete strength, $f_c^{'}$ (MPa)	32
Young modulus of concrete, E_c(MPa)	28600
Steel yield strength, f_y (MPa)	400
Young modulus of rebar, E_s (MPa)	200000
Unit weight of reinforced concrete (kN/m^3)	24

3.3 Structural properties of non-linear elements

3.3.1 Plastic hinge-moment/rotation relationship

Trilinear relationship of moment-hinge rotation shown in Figure 3.4 below will be utilized to model the plastic hinge.

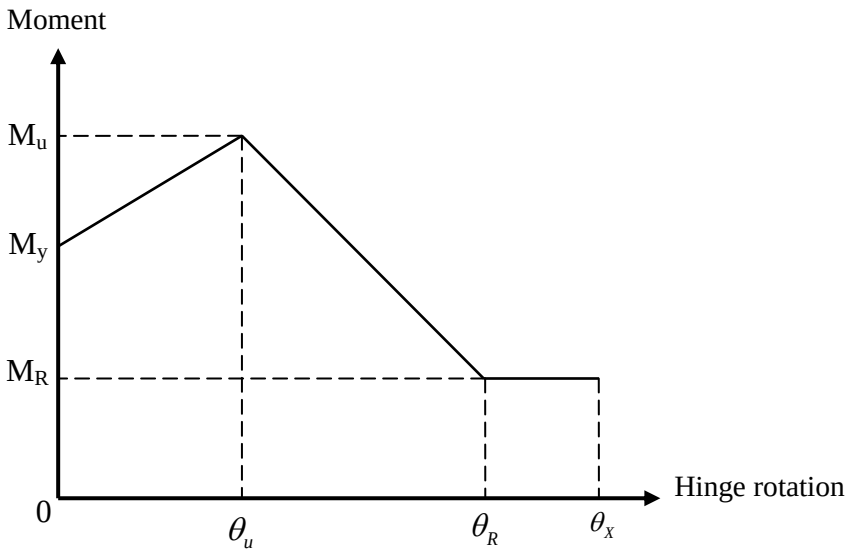

Figure 3.2 Moment-hinge rotation relationship in PERFORM-3D

Haselton et al. (2007) and Panagiotakos and Faris (2001) have proposed expressions to determine some key parameters in Ibarra's model, and these expressions are used here to evaluate the value of the parameters appeared in the above figure, these equations are as follow:

- Moment at yield point

$$\frac{M_y}{bd^3} = \phi_y \begin{Bmatrix} E_c \dfrac{k_y^2}{2}\left(0.5\left(1+\delta'\right)-\dfrac{k_y}{3}\right)+ \\ \dfrac{E_s}{2}\left[\left(1-k_y\right)\rho+\left(k_y-\delta'\right)\rho'+\dfrac{\rho_v}{6}\left(1-\delta'\right)\right]\left(1-\delta'\right) \end{Bmatrix} \tag{3.1}$$

where

M_y = bending moment at yield

b = width of compression zone

d = effective depth of cross section

d' = distance of center of compression reinforcement from extreme compression fiber

ϕ_y = section curvature at yielding

E_c = elastic modulus of concrete

k_y = normalized (to d) compression zone depth at section ultimate

δ' = d'/d

E_s = elastic modulus of steel

ρ_v = ratio of total web area of longitudinal reinforcement between tension and compression steel to bd

- Moment at ultimate strength point

$$\frac{M_u}{M_y} = (1.25)(0.89)^{\nu}(0.91)^{0.01 c_{units} f_c'} \tag{3.2}$$

where

M_u = moment at ultimate strength

ν = axial force ratio

c_{units} = unit conversion variable

f_c' = compressive strength of unconfined concrete

- Moment at residual strength point

$$M_R = \left[(127.2)(0.19)^{\nu}(0.24)^{\frac{s}{d}}(0.595)^{\frac{V_p}{V_n}}(4.25)^{\rho_{sh,eff}} \right] M_y \tag{3.3}$$

where

M_R = moment at residual strength

s = spacing of transverse reinforcement

V_p = shear demand at point of flexural yielding

V_n = nominal shear capacity

$\rho_{sh,eff}$ = effective ratio of transverse reinforcement

- Hinge rotation at ultimate strength point

$$\theta_u = 0.14\left[\frac{\max\left(0.01, \frac{\rho' f_y}{f_c'}\right)}{\max\left(0.01, \frac{\rho f_y}{f_c'}\right)}\right]^{0.175} \quad (1+0.4a_{sl})(0.19)^{\nu}(0.02+40\rho_{sh})^{0.54}(continued...)$$

$$(0.62)^{0.01c_{units} f_c'} - \left[\phi_y \frac{L_s}{3} + 0.0025 + a_{sl}\frac{0.25\varepsilon_y d_b f_y}{(d-d')\sqrt{f_c'}}\right]\frac{M_u}{M_y} \tag{3.4}$$

in which

θ_u = hinge rotation at ultimate strength

ρ' = compression reinforcement ratio

ρ = tension reinforcement ratio

f_y = yielding strength of tension reinforcement

a_{sl} = zero-one variable (effect of pullout of longitudinal bars from anchorage zone)

ρ_{sh} = transverse reinforcement ratio

L_s = shear span

ε_y = steel yield strain

d_b = diameter of compression longitudinal reinforcement

- Hinge rotation at residual strength point

$$\theta_R = \theta_u + (0.76)(0.031)^{\nu}(0.02+40\rho_{sh})^{1.02} \tag{3.5}$$

where

$$(0.76)(0.031)^{\nu}(0.02+40\rho_{sh})^{1.02} \le 0.1 \tag{3.6}$$

in which

θ_R = hinge rotation at residual strength

In M_2-M_3 plan

$$f_{MM} = \left(\frac{M_2}{M_{YP2}} \right)^{\gamma} + \left(\frac{M_3}{M_{YP3}} \right)^{\gamma} \tag{3.8}$$

where

f_{MM} = yield function value

M_{YP2} and M_{YP3} are obtained from equation (3.7) by setting $f_{PM} = 1$ in P-M_2 plan and P-M_3 plan respectively.

Again, El Tawil and Deierlein (2001) suggest value for both exponent α and γ.

3.3.3 Stress/strain models of confined and unconfined concrete

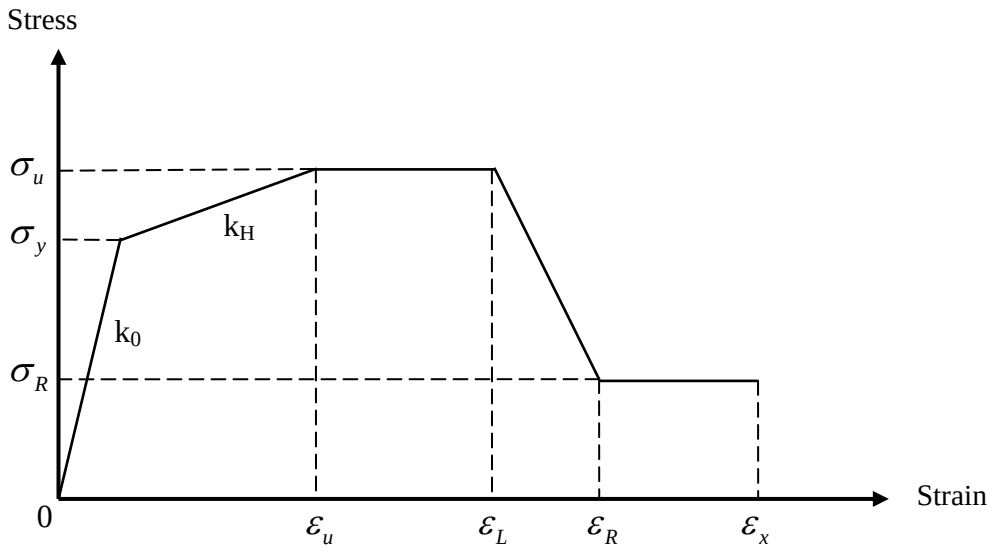

Figure 3.4 Stress-strain model for concrete material in PERFORM-3D

We will employ the stress-strain model proposed by Reddiar (2009), and the stress-strain relation is given by the following expressions:

$$\begin{cases} f_c = K f_c^{'} \left(1 - \left| 1 - x \right|^n \right), & 0 \le x < 1 \\ f_c = K f_c^{'} - \left(f_c^{'} - 12 \right) \left(\dfrac{x-1}{x_u - 1} \right), & 1 \le x < x_u \\ f_c = f_{cu} \left(\dfrac{x - x_f}{x_u - x_f} \right), & x_u \le x < x_f \end{cases} \tag{3.9}$$

where

$$K=1+\frac{\rho_s f_{yh}}{f_c'}\ , \qquad x=\frac{\varepsilon_c}{\varepsilon_{cc}}\ , \qquad x_u=\frac{\varepsilon_{cu}}{\varepsilon_{cc}}=5\ , \qquad x_f=\frac{\varepsilon_f}{\varepsilon_{cc}}$$

$$\varepsilon_{cc}=\varepsilon_{co}\left[1+5(K-1)\right], \qquad \varepsilon_{co}=0.0015+\frac{f_c'(MPa)}{70000}\ , \qquad E_c=5000\sqrt{f_c'(MPa)}$$

$$f_{cu}=12+f_c'(K-1) \text{ in MPa}\ , \qquad n=\frac{E_c\varepsilon_{cc}}{f_{cc}'} \tag{3.10}$$

For unconfined concrete, K=1, $\varepsilon_{cc}=\varepsilon_{co}$, $\varepsilon_{cu}=\varepsilon_{c1}=0.0036$ $n=\frac{E_c\varepsilon_{co}}{f_c'}$

$$\varepsilon_f=\varepsilon_{sp}=0.012-0.0001f_c' \tag{3.11}$$

in which

f_c = longitudinal concrete stress

ε_c = longitudinal concrete strain

K = confinement ratio and for confined concrete (K > 1)

ρ_s = ratio of volume of rectangular steel hoops to volume of concrete core measured to the outside of the peripheral hoop

f_{yh} = yield strength of the hoop reinforcement

f_c' = compressive strength of concrete at 28 days

f_{cu} = post peak stress of confined concrete

ε_{cc} = strain at maximum concrete stress for confined concrete

ε_{cu} = strain at post peak concrete stress for confined concrete

ε_{co} = strain at maximum concrete stress for unconfined concrete

ε_{c1} = strain at post peak concrete stress for unconfined concrete

ε_{sp} = failure strain

E_c = modulus of elasticity of concrete

It should be noted that the equation (3.9) is not linear, which can not accurately capture the trilinear model of concrete material in PERFORM 3D, so we will need to fit the curve given in (3.9) with the trilinear stress-strain relation in Figure 3.4 by setting the strain energy of both models to be approximately equal.

3.3.4 Hysteresis loop of concrete

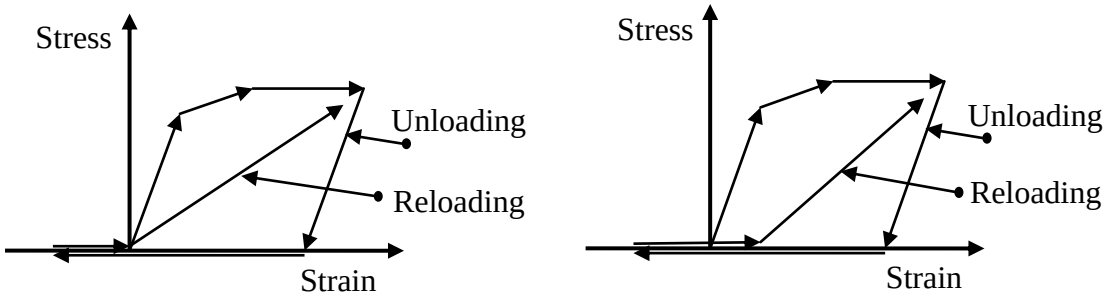

(a) Energy dissipation factor = 1.0 (b) Energy dissipation factor < 1.0

Figure 3.5 Hysteresis model for concrete fiber in compression in PERFORM-3D

The monotonic curve is first input into PERFORM 3D, and then the cyclic behavior of the concrete is determined by specifying the energy factor, different energy dissipation factors will result in different hysteresis loops as shown in the above figure.

3.4 Ground motions

The horizontal ground motion acceleration time histories shall be selected from events having magnitude and fault distances that are consistent with those that control the maximum considered earthquake (MCE). The site-specific MCE spectral response acceleration at any period can be taken as the spectral response acceleration from probabilistic MCE. The probabilistic MCE spectral response accelerations of these ground motions are taken as the spectral accelerations represented by a 5 percent damped acceleration response spectrum having 2 percent probability of exceedance within a 50 years period (ASCE7, 2005). A set of 7 earthquake ground motion data recorded in 7 different locations with magnitude ranging from 6.6 to 7.6is used in this study. The detail information regarding these 7 locations is provided in Table 3.4. The magnitude of these ground motion records are first scaled such that

their spectra approximate the target spectrum (Palasri and Ruangrassamee, 2010) which is obtained from doing probabilistic seismic hazard analysis for bed rock as shown in Figure 3.7. Then they are further scaled and modified so that their spectra matched the target spectrum as illustrated in Figure 3.8. The matched ground motions are shown in Figure 3.6. Finally, these matched ground motion records are simulated in ProShake, in which the soft soil properties shown in Table 3.5 are input, so that the resulted ground motions are usable for soft soil condition of this case study building. These resulted ground motions are scaled by 1.5 so that their average spectrum approaches the design spectrum proposed by Lukkunaprasit et al. (2008) as depicted in Figure 3.10. The obtained ground motions (scaled by 1.5) represent MCE level of seismic excitation having 2 percent probability of exceedance in 50 years corresponding to a 2475 years return period. The ground accelerations of these ground motions (scaled by 1.5) are illustrated in Figure 3.9. The pseudo-acceleration, pseudo-velocity and deformation response spectra against 5% damping ratio of these ground motions (scaled by 1.5) are also presented in the figure 3.10,3.11 and 3.12 respectively.

It should be noted that the set of ground motions in Figure 3.9 will be used for NLRHA.

Table 3.4 List of a set of ground motions (Faculty of Engineering, 2010)

No.	Earthquake	Station	Magnitude	Distance (km)	Vs30 (m/s)	Component	Low Freq (Hz)
1	1999 Kocaeli	Maslak	7.4	64	>750	090	0.03
2	1999 Chi-Chi	TTN 042	7.6	65	845	FP	0.04
3	1994 Northridge	Wrightwood-Jackson Flat	6.7	68	822	180	0.24
4	1989 Loma Prieta	Piedmont Jr High	6.9	73	895	FP	0.25
5	1971 San Fernando	Cedar Springs-Allen Ranch	6.6	90	813	FP	0.25
6	1999 Chi-Chi	TAP 077	7.6	117	1023	FP	0.03
7	1992 Landers	San Gabriel-E Grand Ave	7.3	142	>750	180	0.07

Table 3.5 Average shear velocity and standard deviation along the depth of the soil (Faculty of Engineering, 2010)

Depth (m)	Average shear velocity (m/s)	Standard deviation
0	74	0.15
3.3	79	0.15
4.8	78	0.15
6.3	80	0.15
7.8	79	0.17
9.3	107	0.17
12.3	107	0.17
13.8	301	0.17
15.3	271	0.17
15.8	198	0.17
16.8	307	0.17
18.3	326	0.17
21.3	423	0.17
22.8	234	0.17
24.3	261	0.17
25.8	369	0.17
27.3	280	0.17
28.8	280	0.17
30.3	400	0.17
60	450	0.07
120	550	0.07
300	600	0.07
600	600	0.07

CHAPTER IV
RESPONSE SPECTRUM ANALYSIS PROCEDURE

4.1 Linear modeling

The case study building is modeled in ETABS for the linear analysis. The rigid diaphragm assumption is assigned to the floor slab, assuming that the floor is rigid in plane and flexible out-of-plane, so that all the points within the same floor are constrained to move together. The effective stiffness of the structural members given in the current Thai design code is used to account for the crack sections of the members as shown in Table 4.1. The connection between columns and foundations is assumed to be rigid and modeled as fixed support at the base. Masses are calculated from self-weight of structural members (columns, walls and slabs) plus superimposed dead load divided by gravitational multiplier, g. They are assigned to each joints of the structure on a tributary area basis in all directions (two translational directions – E-W and N-S, and one rotational direction about vertical axis). The building is subjected to the gravity loads (including self-weight of structural members) and response spectrum function shown in Table 4.2 and Figure 4.1, respectively. It should be noted that the superimposed dead load is calculated from the weight of the infill masonry walls and topping of structural members. This response spectrum (solid black curve in Figure 3.10) is used as design spectrum in RSA procedure for design basis earthquake (DBE) level and defined as 2/3 of MCE spectrum. As illustrated in Figure 3.10, it is obtained from multiplying the average spectrum (dash black curve in Figure 3.10) of the 7 MCE ground motions by a factor of 2/3.Appropriate load combination is also considered following the current code provision as illustrated in Table 4.3. The most critical load case will be used for the design of structural members.

The columns are modeled as linear beam-column frame elements while floor slabs and walls are modeled as shell elements, and the 3-dimensional finite element model of the building in ETABS is shown in the Figure 4.2. It should be noted that the infill walls are not modeled in this study, so the period of the model is expected to be longer than the actual building, which has some infill walls.

This linear RSA procedure will be conducted again in PERFORM-3D. The results are compared with those obtained from ETABS and can be found in the APPENDIX F of this report.

Table 4.1 Effective stiffness of cross section of the members (DPT, 2009)

Column	$I_{eff}= 0.70I_g$
Wall	$I_{eff}= 0.70I_g$
Flat slab	$I_{eff}= 0.25I_g$

Table 4.2 Gravity loads

Load case	Value (kN/m^2)
Superimposed dead load (SDL)	2.75
Live load (LL)	2.5

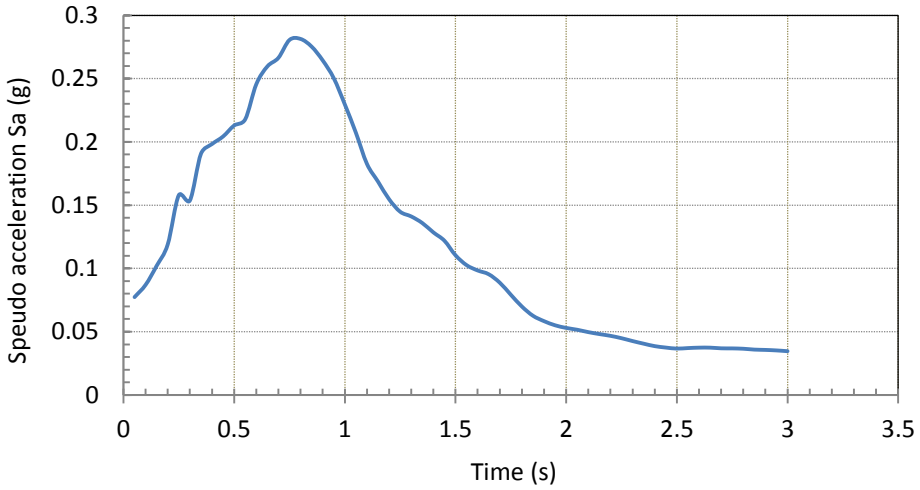

Figure 4.1 Average elastic response spectrum, damping ratio = 5%

Table 4.3 List of load combination considered (ASCE7-05)

No.	Load combination
1	1.4(DL + SDL)
2	1.2(DL + SDL) + 1.6LL
3	1.2(DL + SDL) + 1LL + 1EQx + 0.3EQy
4	1.2(DL + SDL) + 1LL + 0.3EQx + 1EQy
5	0.9(DL + SDL) + 1EQx + 0.3EQy
6	0.9(DL + SDL) + 0.3EQx + 1EQy

Note: DL = dead load, EQx = earthquake loading in x direction (E-W direction), EQy = earthquake loading in y direction (N-S direction).

The maximum and minimum displacements at each story of the building are calculated based on modal analysis conducted in ETABS. The average displacement is then computed as one half of the summation of maximum and minimum displacement. The amplification factors at each story are then computed based on the formula (4.1) and the results are shown in the Table 4.5.

Table 4.5 Amplification factors for accidental torsion

Story	Displacement in E-W direction (m)				Displacement in N-S direction (m)				Amplification factor to be used
	max	min	Avg	A_{xx}	max	min	Avg	A_{yy}	A_x
16	0.050	0.039	0.044	0.930	0.071	0.028	0.049	1.196	1.196
15	0.046	0.037	0.041	0.930	0.066	0.026	0.046	1.199	1.199
14	0.043	0.034	0.038	0.931	0.061	0.024	0.042	1.203	1.203
13	0.039	0.031	0.035	0.932	0.056	0.021	0.039	1.207	1.207
12	0.036	0.028	0.032	0.932	0.051	0.019	0.035	1.212	1.212
11	0.032	0.025	0.029	0.932	0.046	0.017	0.032	1.218	1.218
10	0.029	0.023	0.026	0.932	0.041	0.015	0.028	1.226	1.226
9	0.026	0.020	0.023	0.931	0.037	0.013	0.025	1.235	1.235
8	0.022	0.018	0.020	0.930	0.032	0.011	0.021	1.246	1.246
7	0.019	0.015	0.017	0.927	0.027	0.009	0.018	1.257	1.257
6	0.016	0.013	0.015	0.925	0.022	0.007	0.014	1.270	1.270
5	0.013	0.011	0.012	0.921	0.017	0.005	0.011	1.282	1.282
4	0.010	0.008	0.009	0.917	0.013	0.004	0.008	1.295	1.295
3	0.007	0.006	0.006	0.912	0.009	0.002	0.005	1.306	1.306
2	0.004	0.004	0.004	0.906	0.005	0.001	0.003	1.316	1.316
1	0.002	0.002	0.002	0.897	0.002	0.001	0.001	1.318	**1.318**

Note: max = maximum value, min = minimum value, Avg = average value,
A_{xx} = amplification factor in E-W direction, A_{yy} = amplification factor in N-S direction

So we will use A_x=1.318 as amplification factor for diaphragms in all stories and the total eccentricity ratio is $0.05A_x$=0.0659

4.2.3 Story displacement and drift ratio

Taking into account the natural torsional effect, the new eccentricity of 0.0659 calculated earlier is replacing the accidental eccentricity of 0.05 and the modal analysis of the case-study building is done again through ETABS. To obtain the story displacement and drift ratio, ASCE7-05 required that the results from above modal analysis be scaled up by a deflection amplification factor C_d/I = 3.6, in which C_d of 4.5 is selected corresponding to R = 5.5. Thus the maximum story displacement and story drift ratio are illustrated in Figure 4.4 and Figure 4.5, respectively. The results indicate that the maximum story drift ratios in both E-W and N-S directions are about

0.5% which is just 1/3 of the drift allowable limit imposed by the current code provision (ASCE7-05).

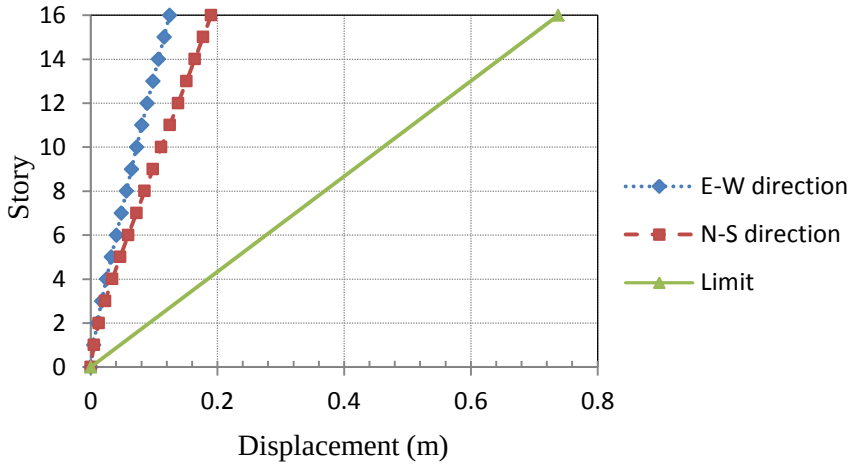

Figure 4.4 Story displacement in both principal directions

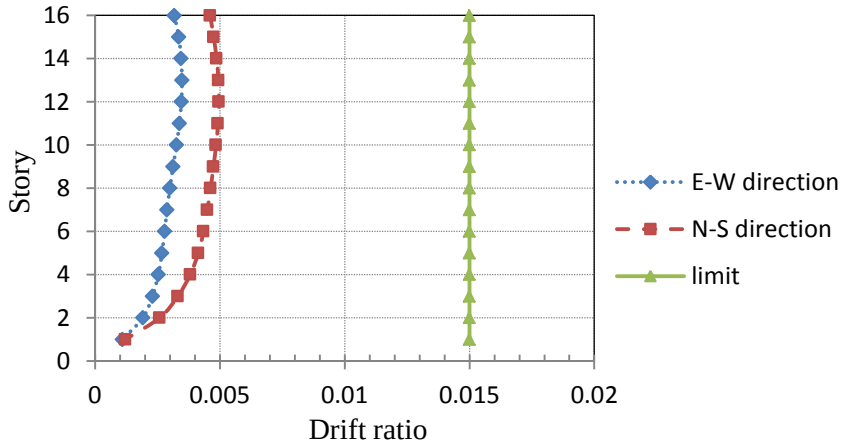

Figure 4.5 Inter-story driftratio in both principal directions

4.2.4 Internal forces

For force quantities, the code do not require the deflection amplification factor to be included, so seismic base shears in both E-W and N-S directions are obtained from modal analysis performed in ETABS considering P-delta and torsional (natural and accidental) effects. The results are presented in Table 4.6.

Table 4.6 Seismic base shears from RSA procedure

Directions	Base shear ($V_{dynamic}$)	
E-W	1310 kN	1.2% *W*
N-S	1570 kN	1.4% *W*

The current Thai seismic design code required that seismic design base shear ($V_{dynamic}$) obtained from linear RSA procedure be not less than 85% of the seismic base shear (V_{static}) evaluated from linear static analysis, which is the equivalent lateral force (ELF) procedure.

4.2.4.1 Equivalent lateral force procedure

The seismic base shear is given by the following equation

$$V_{static} = C_s W \tag{4.2}$$

where W is the effective weight of the building and C_s is seismic response coefficient. C_s can be determined from the following expression:

$$C_s = \frac{S_a I}{R} \tag{4.3}$$

where S_a is spectra acceleration, I is important factor accounting for Category of the building structure and is taking the value of 1.25 for occupancy category III, R is response modification coefficient accounting for inelastic behavior of the structure and is equal to 5.5 for ordinary reinforced concrete shear wall structure.

The fundamental period of the building is computed as:

$$T = \min\left(1.5 \times 0.02H, T_{etabs}\right) = \begin{cases} 1.476 \text{ sec} & \text{E-W direction} \\ 1.3 \text{ sec} & \text{N-S direction} \end{cases} \tag{4.4}$$

where H is the overall height of the building and T_{etabs} is the period of the structure obtained from ETABS. And the corresponding spectra accelerations are as follow:

$$S_a = \begin{cases} 0.113\text{g} & \text{for T = 1.476 sec} \\ 0.14\text{g} & \text{for T = 1.3 sec} \end{cases}$$

Thus

$$C_s = \begin{cases} 0.0257g & \text{E-W direction} \\ 0.0318g & \text{N-S direction} \end{cases}$$

The effective weight of the building is computed as the self-weight of the building plus 100% superimposed dead load and 25% of the live load, W = 10855 ton Therefore the seismic base shear is:

$$V_{static} = \begin{cases} 2.57\%\ W = 2790 \text{ kN} & \text{E-W direction} \\ 3.18\%\ W = 3450 \text{ kN} & \text{N-S direction} \end{cases}$$

The seismic base shears obtained from both ELF and RSA procedures are summarized in Table 4.7.

Table 4.7 Effective seismic modification factor (R_{eff})

Parameters	Value
Equivalent lateral force procedure	
85% of Seismic base shear in E-W direction: $0.85V_{static}$	2371 kN
85% of Seismic base shear in N-S direction: $0.85V_{static}$	2932 kN
Linear dynamic RSA procedure	
Seismic base shear in E-W direction: $V_{dynamic}$	1310 kN
Seismic base shear in N-S direction: $V_{dynamic}$	1570 kN
$R_{eff} = \min\left\{\frac{R}{I} \times \frac{V_{dynamic}}{0.85V_{static}}, \frac{R}{I}\right\}$	
E-W direction	2.43
N-S direction	2.36

4.2.4.2 Shear wall

Since the seismic base shear ($V_{dynamic}$) calculated from RSA procedure is less than 85% of seismic base shear (V_{static}) from ELF procedure as shown in Table 4.7, the force demands of RSA procedure need to be scaled up such that the $V_{dynamic}$ from RSA procedure is equal to $0.85V_{static}$ from ELF procedure. To satisfy this requirement, the RSA procedure has been performed again via ETABS with effective seismic modification factor "R_{eff}" replacing the "R/I" factor, in which R_{eff} is defined as the smaller of R/I multiplied by $V_{dynamic}/0.85V_{static}$ and R/I as illustrated in Table 4.7.With consideration of this effective seismic modification factor, the demands of the structural members can be computed and shear forces, bending moment along the wall height are presented in the following figures:

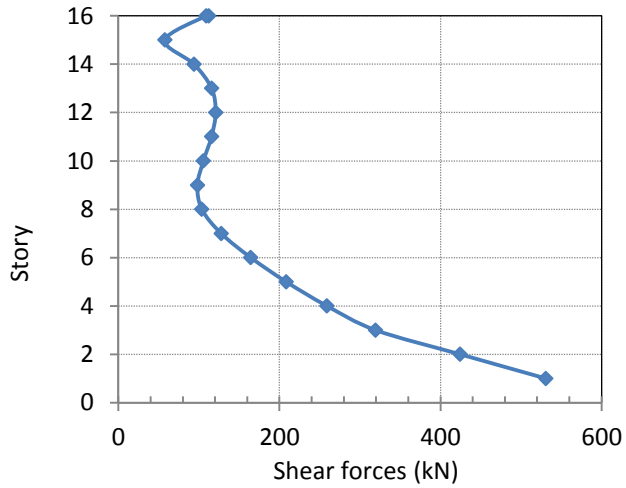

Figure 4.6 Shear force in wall 1 (W1)

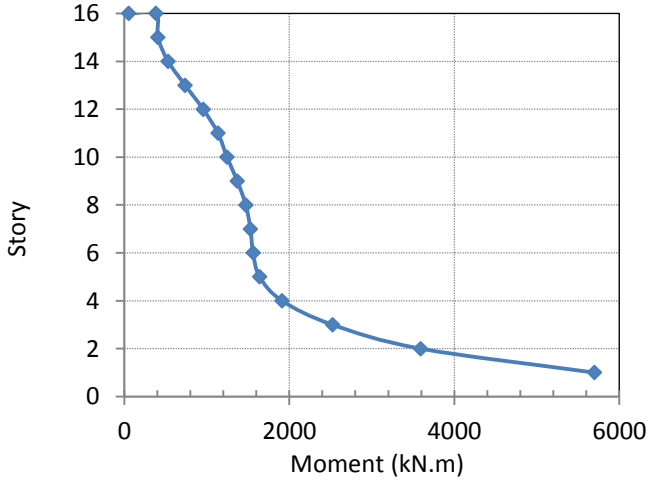

Figure 4.7 Bending moment in wall 1 (W1)

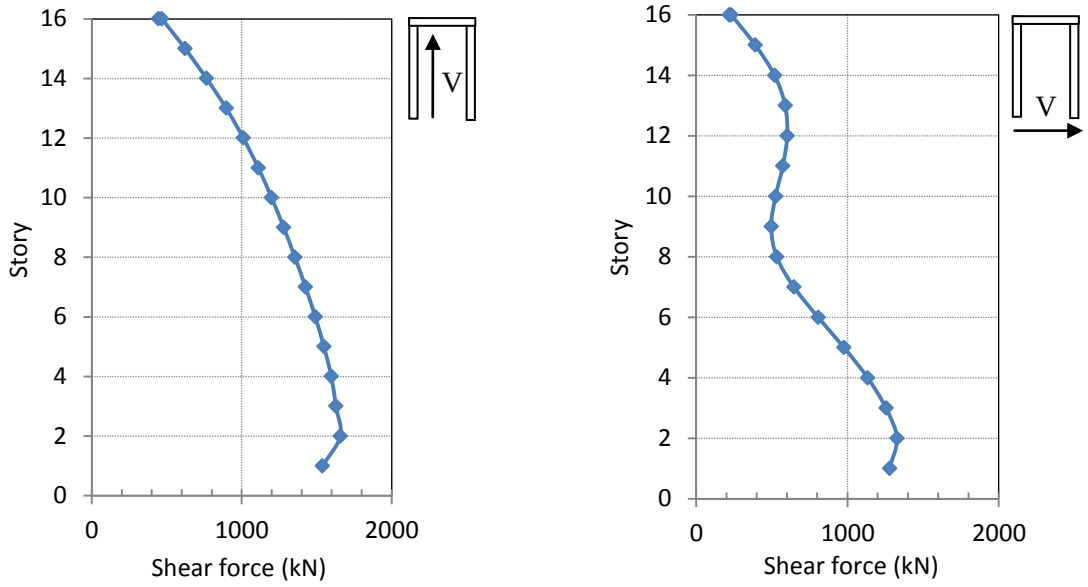

N-S direction E-W direction

Figure 4.8 Shear force in the wall 2 (W2)

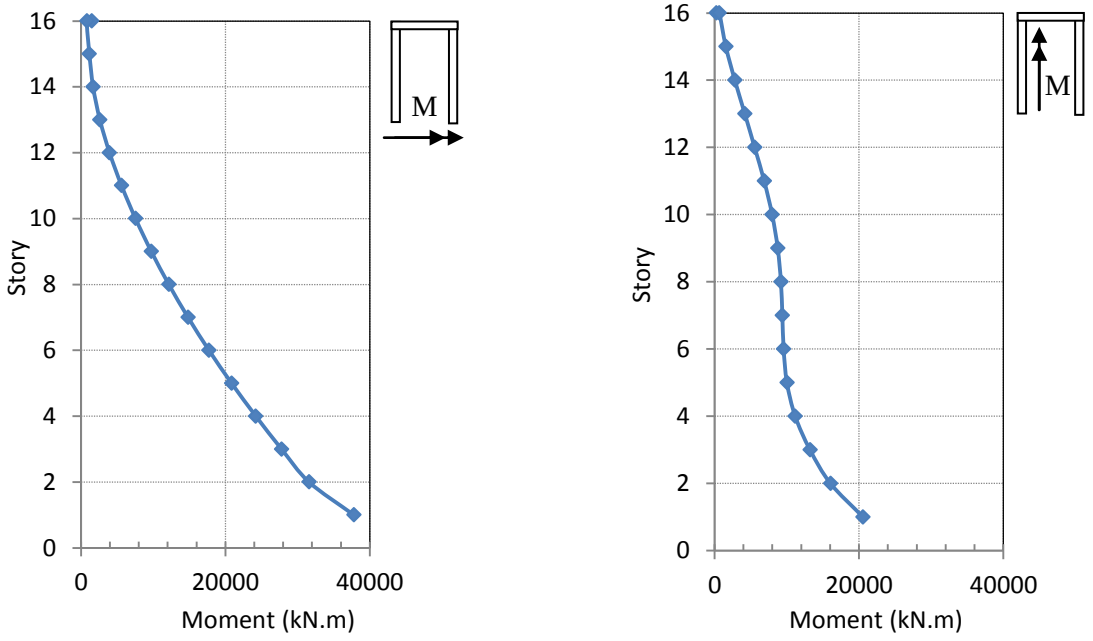

About E-W direction About N-S direction

Figure 4.9 Bending moment in wall 2 (W2)

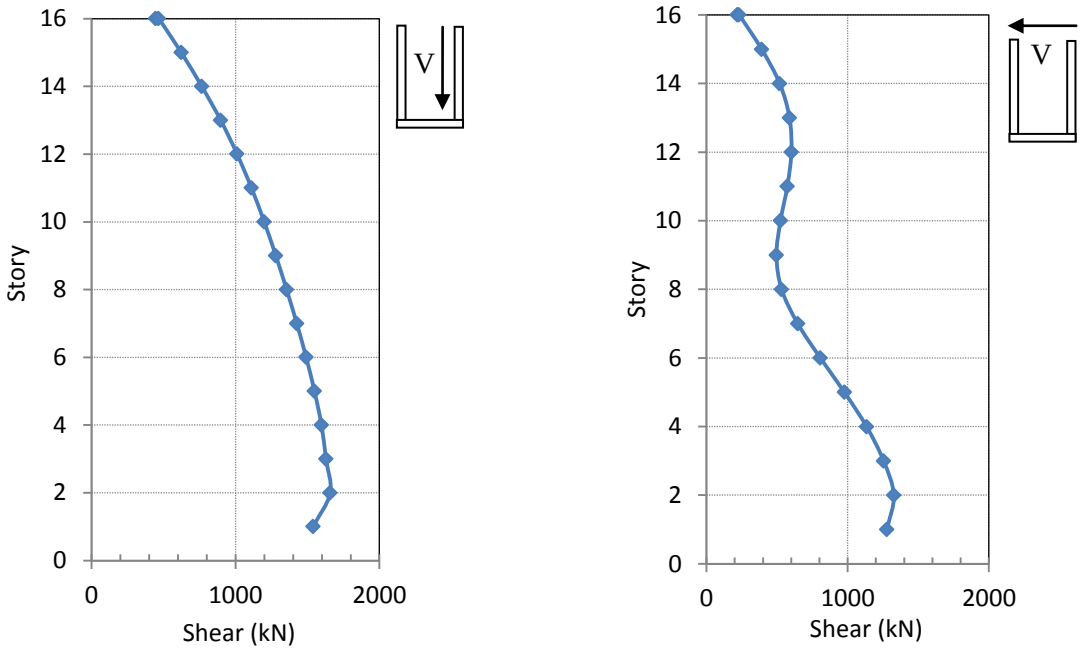

N-S direction E-W direction

Figure 4.10 Shear force in wall 3 (W3)

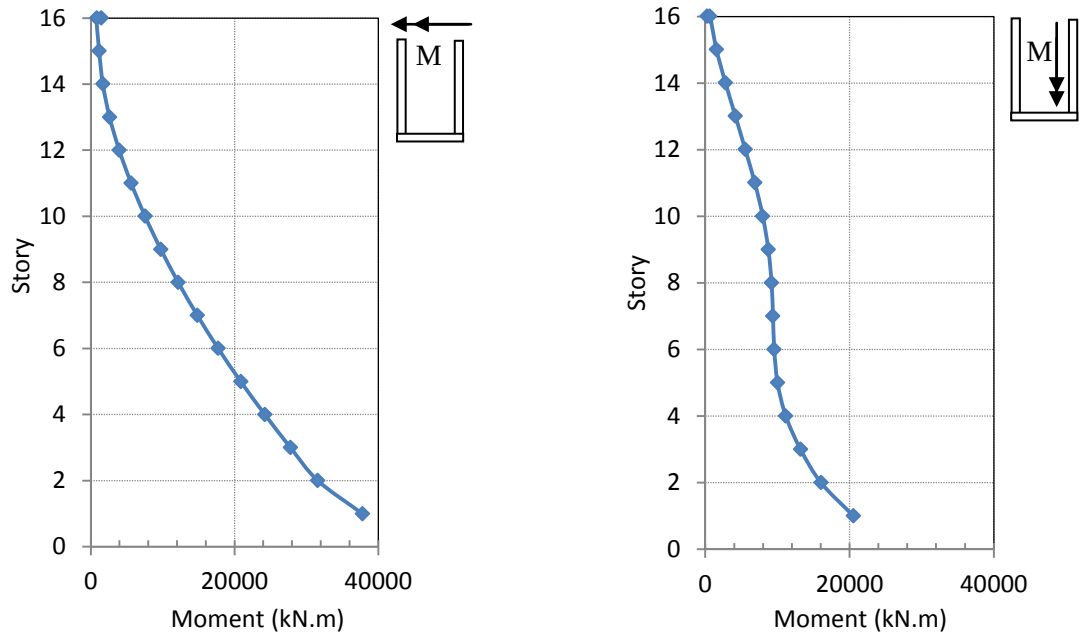

About E-W direction About N-S direction

Figure 4.11 Bending moment in wall 3 (W3)

4.3 Design of the structural members

The lateral forces resisting members, columns and shear walls, are designed such that the demands obtained from RSA procedure are approximately equal to the nominal strength of the elements multiplied by a safety factor mentioned in the ACI318-08. The flexural strength of the members is presented in form of P-M-M interaction diagram, in which the M-M interaction is assumed to be linear. In this study, no attempt is made for shear design.

4.3.1 P-M diagram of the structural members

ACI318-08 limits the amount of reinforcement used in the columns to be 1% (area of reinforcement over area of column cross section) for the lower bound and 8% for the upper bound. The design of vertical reinforcement in the columns must be made such that the area of the rebar lies within the limit in the code. Depicted in Figure 12 through Figure 15 are P-M interaction diagrams of the columns ranging from 1% reinforcement ratio to 8% reinforcement ratio in which the increment is 0.5% in strong axis and weak axis respectively. The columns are designed based on these P-M interaction diagrams. It should be noted that the design safety factor is also included in the P-M diagram of Figure 4.13 and Figure 4.15, while design safety factor is excluded in Figure 4.12 and Figure 4.14.

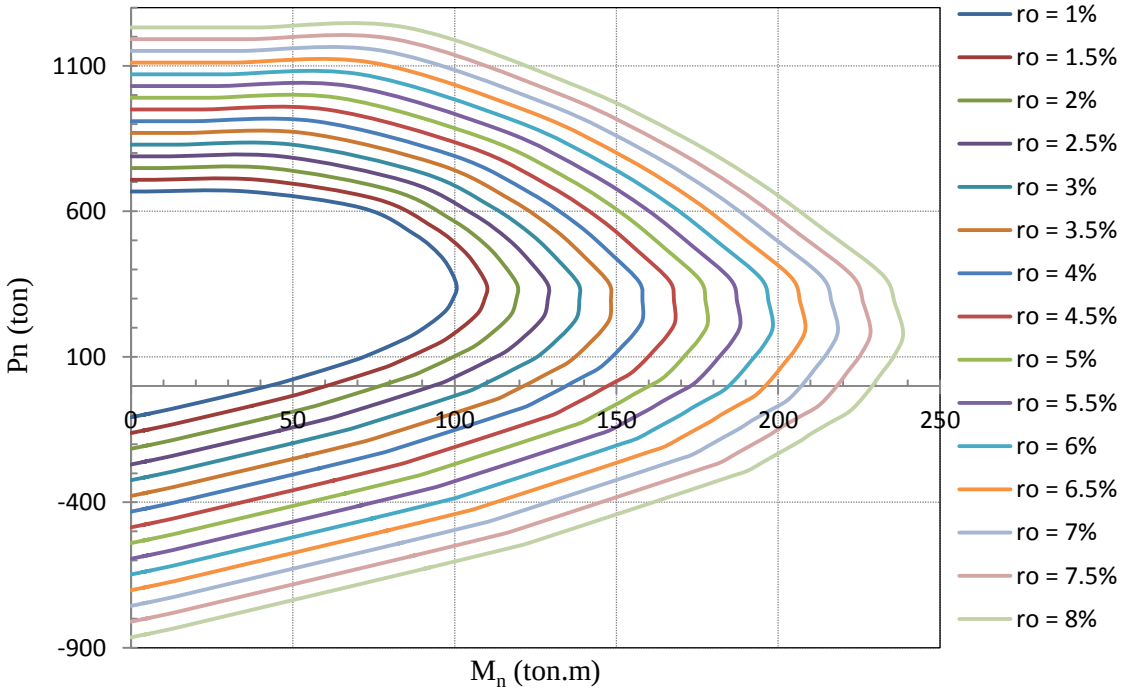

Figure 4.12 P-M interaction diagram of rectangular columns (no phi factor) – strong axis

interaction diagram non-uniform (some increase in just in the tension-controlled branch and remain the same in the compression-controlled branch). Furthermore, for the curves that are crossing each other in Figure 4.21 and Figure 4.23, it is the effect of the safety factor (phi) in the code since this crossing happens only when the interaction includes phi factor. We should also note that this crossing of the interaction curve does not mean increasing reinforcement could decrease the capacity of the cross section since the interaction curve (with phi) does not represent the capacity of the cross-section (it also includes the safety factor set by the code).

4.3.2 Vertical reinforcement of the walls

Based on the P-M diagrams mentioned earlier and the demands from RSA procedure, the amount of vertical reinforcement of shear walls can be determined and illustrated in the table below:

Table 4.8 Vertical reinforcement of the walls in RSA procedure

Story	Wall 1 (W1)	Wall 2 (W2) = Wall 3 (W3)
	ρ (%)	ρ (%)
1	1.05	1.5
2	0.6	0.97
3	0.3	0.835
4	0.3	0.74
5	0.3	0.66
6	0.3	0.55
7	0.3	0.55
8	0.3	0.55
9	0.3	0.4
10	0.3	0.4
11	0.3	0.3
12	0.3	0.26
13	0.15	0.26
14	0.15	0.15
15	0.15	0.15
16	0.15	0.15

Note: ρ = area of vertical reinforcement over the area of the cross section of the wall

4.3.3 Uplift

Attention should be paid to the design of the C-shape structural wall2 (W2) and wall3 (W3). Wall2 (W3) or Wall3 (W3) consists of two flanges (F1 and F2) and one web (W) as shown in Figure 4.24. Large tension forces can be observed when designing the flanges (F1 and F2) and web (W) of the wall separately since the neutral axis of the C-shape cross section is very close to the web resulted in less compressive area in flanges F1 and F2. Moreover, the design of wall with tension is undesirable since it will lead to large amount of reinforcement due to the tension forces. Therefore the C-shape walls must be designed as the whole cross section in order to avoid tension forces in the walls.

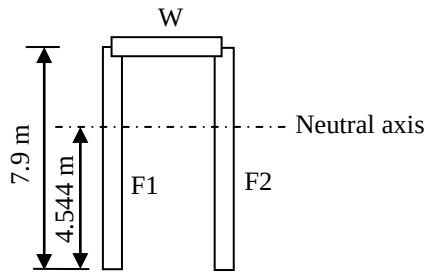

Figure 4.24 W2 or W3 cross section

CHAPTER V
NONLINEAR RESPONSE HISTORY ANALYSIS PROCEDURE

5.1 Nonlinear modeling

For non-linear response history analysis, the case study building is modeled in Perform 3D version 5.0 as shown in Figure 5.1. The horizontal rigid floor slaving constraint is assigned to the floor slab, assuming that the floor is rigid in plane and flexible out-of-plane, so that all the points within the same floor are constrained to move together. Like the linear model, the connection between columns and foundations is assumed to be rigid and modeled as fixed support at the base. The masses are lumped and assigned to the center of mass at each floor and are calculated using the following formula:

$$MMI_{CM} = \frac{M}{A}\left(I_x + I_y\right) \tag{5.1}$$

where MMI_{CM} = Rotational mass moment of inertia of the center of mass

M = Translational mass of the diaphragm obtained from RSA procedure in ETABS

A = Area of the diaphragm

I_x, I_y = Moment of inertia of the diaphragm about x (E-W) and y (N-S) directions

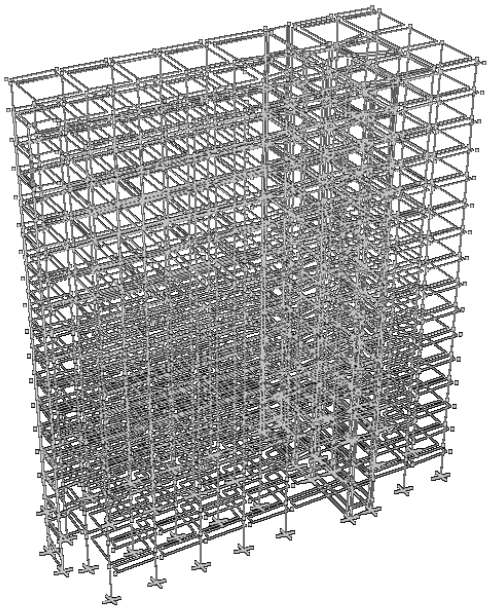

Figure 5.1 Building model in PERFORM-3D

of the plastic hinge is illustrated in Figure 3.2 of Chapter III and its parameters will be used as input in PERFORM-3D. Table 5.1 and Table 5.2 show the properties of the plastic hinges in columns.

Table 5.1 Plastic hinge properties of the columns – strong axis

Columns	Story	Position	Hinge properties					
			M_y (ton.m)	M_u (ton.m)	M_R (ton.m)	θ_u (rad)	θ_R (rad)	θ_x (rad)
C1	1	Top	100	117.53	23.51	0.0089	0.0244	0.0275
		Bottom	100	117.48	23.50	0.0087	0.0241	0.0275
C3	1	Top	100	116.30	23.26	0.0070	0.0184	0.0275
		Bottom	100	116.25	23.25	0.0061	0.0174	0.0275
C5	1	Top	100	116.30	23.26	0.0070	0.0184	0.0275
		Bottom	100	116.25	23.25	0.0061	0.0174	0.0275
C6	1	Top	100	117.53	23.51	0.0089	0.0244	0.0275
		Bottom	100	117.48	23.50	0.0087	0.0241	0.0275
C7	1	Top	100	114.72	22.94	0.0052	0.0128	0.025
		Bottom	100	114.67	22.93	0.0048	0.0123	0.025
C8	1	Top	138.46	156.16	31.23	0.0040	0.0085	0.025
		Bottom	138.46	156.09	31.22	0.0028	0.0074	0.025
	16	Top	100	120.78	24.16	0.0294	0.0643	0.0677
		Bottom	100	120.74	24.15	0.0307	0.0652	0.0686
C9	1	Top	138.46	156.16	31.23	0.0040	0.0085	0.025
		Bottom	138.46	156.09	31.22	0.0028	0.0074	0.025
	16	Top	100	120.78	24.16	0.0294	0.0643	0.0677
		Bottom	100	120.74	24.15	0.0307	0.0652	0.0686
C10	1	Top	100	114.72	22.94	0.0052	0.0128	0.025
		Bottom	100	114.67	22.93	0.0048	0.0123	0.025
C12	16	Top	100	120.76	24.15	0.0357	0.0704	0.0741
		Bottom	100	120.72	24.14	0.0368	0.0712	0.0749
C13	16	Top	100	120.76	24.15	0.0357	0.0704	0.0741
		Bottom	100	120.72	24.14	0.0368	0.0712	0.0749
C16	16	Top	100	120.75	24.15	0.0356	0.0703	0.0740
		Bottom	100	120.71	24.14	0.0367	0.0711	0.0748
C17	16	Top	100	120.75	24.15	0.0356	0.0703	0.0740
		Bottom	100	120.71	24.14	0.0367	0.0711	0.0748
C26	1	Top	100	117.52	23.50	0.0093	0.0248	0.0275
		Bottom	100	117.47	23.49	0.0087	0.0240	0.0275
C28	1	Top	100	116.36	23.27	0.0072	0.0187	0.0275
		Bottom	100	116.31	23.26	0.0062	0.0176	0.0275
C30	1	Top	100	116.36	23.27	0.0072	0.0187	0.0275
		Bottom	100	116.31	23.26	0.0062	0.0176	0.0275
C32	1	Top	100	117.52	23.50	0.0093	0.0248	0.0275
		Bottom	100	117.47	23.49	0.0087	0.0240	0.0275

Table 5.2 Plastic hinge properties of the columns – weak axis

Columns	Story	Position	Hinge properties					
			M_y (ton.m)	M_u (ton.m)	M_R (ton.m)	θ_u (rad)	θ_R (rad)	θ_x (rad)
C1	1	Top	29.23	34.35	0.94	0.0089	0.0244	0.0275
		Bottom	29.23	34.34	0.94	0.0087	0.0241	0.0275
C3	1	Top	29.23	33.99	0.93	0.0070	0.0184	0.0275
		Bottom	29.23	33.98	0.93	0.0061	0.0174	0.0275
C5	1	Top	29.23	33.99	0.93	0.0070	0.0184	0.0275
		Bottom	29.23	33.98	0.93	0.0061	0.0174	0.0275
C6	1	Top	29.23	34.35	0.94	0.0089	0.0244	0.0275
		Bottom	29.23	34.34	0.94	0.0087	0.0241	0.0275
C7	1	Top	29.23	33.53	0.84	0.0052	0.0128	0.025
		Bottom	29.23	33.52	0.84	0.0048	0.0123	0.025
C8	1	Top	38.46	43.38	1.08	0.0040	0.0085	0.025
		Bottom	38.46	43.36	1.08	0.0028	0.0074	0.025
	16	Top	29.23	35.30	2.39	0.0294	0.0643	0.0677
		Bottom	29.23	35.29	2.42	0.0307	0.0652	0.0686
C9	1	Top	38.46	43.38	1.08	0.0040	0.0085	0.025
		Bottom	38.46	43.36	1.08	0.0028	0.0074	0.025
	16	Top	29.23	35.30	2.39	0.0294	0.0643	0.0677
		Bottom	29.23	35.29	2.42	0.0307	0.0652	0.0686
C10	1	Top	29.23	33.53	0.84	0.0052	0.0128	0.025
		Bottom	29.23	33.52	0.84	0.0048	0.0123	0.025
C12	16	Top	29.23	35.30	2.62	0.0357	0.0704	0.0741
		Bottom	29.23	35.29	2.65	0.0368	0.0712	0.0749
C13	16	Top	29.23	35.30	2.62	0.0357	0.0704	0.0741
		Bottom	29.23	35.29	2.65	0.0368	0.0712	0.0749
C16	16	Top	29.23	35.30	2.61	0.0356	0.0703	0.0740
		Bottom	29.23	35.28	2.64	0.0367	0.0711	0.0748
C17	16	Top	29.23	35.30	2.61	0.0356	0.0703	0.0740
		Bottom	29.23	35.28	2.64	0.0367	0.0711	0.0748
C26	1	Top	29.23	34.35	0.94	0.0093	0.0248	0.0275
		Bottom	29.23	34.34	0.94	0.0087	0.0240	0.0275
C28	1	Top	29.23	34.01	0.94	0.0072	0.0187	0.0275
		Bottom	29.23	34.00	0.93	0.0062	0.0176	0.0275
C30	1	Top	29.23	34.01	0.94	0.0072	0.0187	0.0275
		Bottom	29.23	34.00	0.93	0.0062	0.0176	0.0275
C32	1	Top	29.23	34.35	0.94	0.0093	0.0248	0.0275
		Bottom	29.23	34.34	0.94	0.0087	0.0240	0.0275

degradation factor must be included in the component properties. The energy degradation factor is defined as the area of degraded hysteretic loop divided by the area of non-degraded loop. Figure 5.5 and Figure 5.6 show the degraded loop for trilinear behavior of the components. In Figure 5.5, the dash lines represent the first cyclic behavior of the components before the deformations of the components in both positive and negative branches reach U (ultimate) point, whereas the solid lines are the second cyclic behavior of the components in two extreme shapes for the degraded loop; (a) minimum elastic range, this extreme case gives minimum elastic range and maximum strain hardening range. The elastic stiffness remains the same as the first cycle, but the yielding strength of the component reduced and the strain hardening stiffness also degraded. The hardening stiffness is calculated to make the area of the degraded loop equal to the energy degradation factor times the area of the non-degraded loop (first cycle). (b) Maximum elastic range, this extreme case gives maximum elastic range and minimum strain hardening range. The hardening stiffness does not change while the elastic stiffness degraded such that the area of the degraded loop is equal to the energy degradation factor times the area of the non-degraded loop (first cycle). In Figure 5.6, the dash lines represent the first cyclic behavior of the components after the positive and negative deformations of the components attain U point, whereas the solid lines are the second cyclic behavior of the components for the degraded loop. The yield strength of the components degraded, the elastic and strain hardening stiffness degraded and are computed to make the area of the degraded loop equal to the energy degradation factor times the area of the non-degraded loop (first cycle).

5.1.2.1 Material modeling

5.1.2.1.1 Confined and unconfined concrete

The stress-strain curves of unconfined and confined concrete models proposed by Reddiar (2009) are utilized, whereby the tension in concrete is neglected. These models are approximated by a trilinear relationship available in PERFORM-3D. These approximations are made such that the areas under the curves of both Reddiar (2009) and PERFORM-3D models are equal. Figure 5.13 and Figure 5.14 represent the stress-strain relationship of unconfined and confined concrete, respectively.

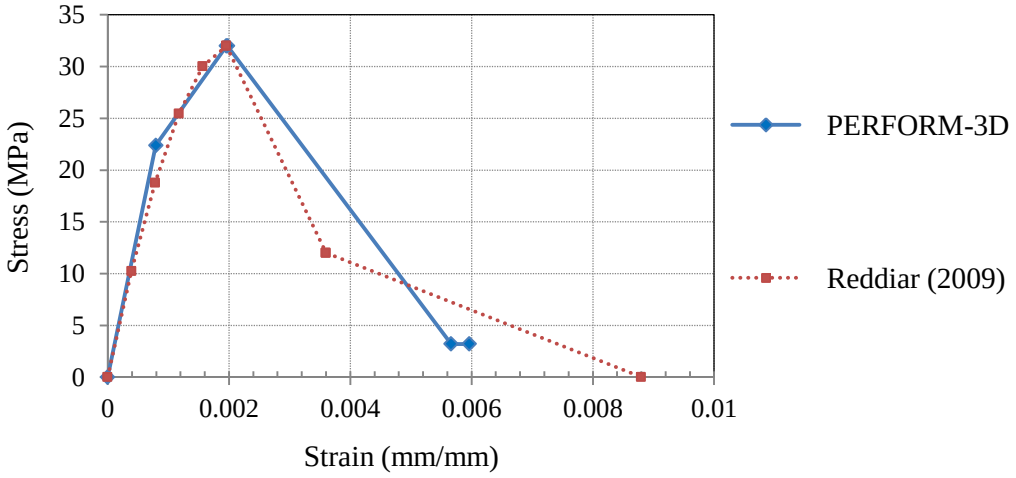

Figure 5.13 Unconfined concrete stress-strain relationship

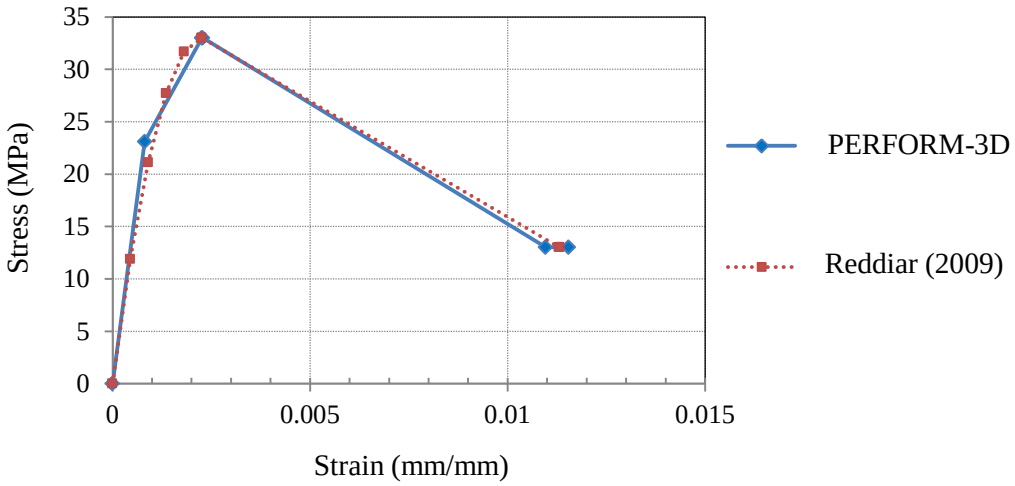

Figure 5.14 Confined concrete stress-strain relationship

The hysteretic model of both confined and unconfined concrete is shown in Figure 3.5(b) of Chapter III. The cyclic behavior of both confined and unconfined concrete is determined by specifying the energy degradation factor as illustrated in Table 5.3.

5.1.2.1.2 Reinforcing steel

The reinforcing steel stress-strain relationship is based on material specification for steel rebar and modeled with nominal yield strength of 400MPa and ultimate strength of 570MPa, as shown in Figure 5.15.

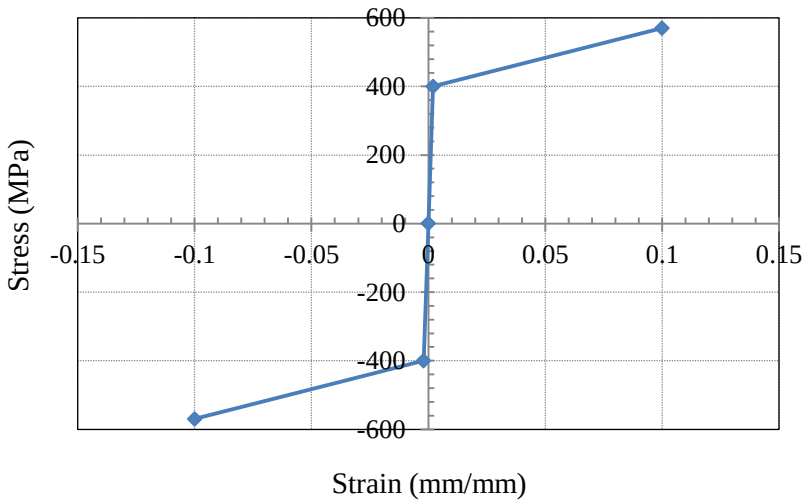

Figure 5.15 Inelastic steel stress-strain relationship

The non-degrading loop for trilinear behavior as shown in Figure 5.4 is used for steel hysteretic model. The energy degradation factor equal to 1 is used in this case so that the hysteretic loop with no energy degradation can be attained.

5.1.3 Post-tension flat slab

Linear elastic shell elements are used to model post-tension flat slab. It should be noted that the effective stiffness found in Table 4.1 of Chapter IV is still used for the linear beam-column elements of the columns and the linear shell elements of the post-tension flat slabs.

5.2 Nonlinear response history analysis procedure

Perform-3D version 5.0 is used for this rigorous nonlinear response history analysis considering P-delta effect. The building is analyzed through two different levels of ground motions to investigate its behavior and performance under earthquake excitation: (1) DBE ground motion and (2) MCE ground motion both consisting of seven records. The seven MCE ground motion records, as mentioned section 3.4 of chapter III, are obtained from site response analysis of Bangkok soft soil using the records shown in Table 3.4 of Chapter III as input ground motion in ProShake program. DBE ground motion records are then obtained from multiplying the MCE records by 2/3. These two levels of ground motions were applied separately in both horizontal directions to the building, namely North-South and East-West directions. It should be noted that the gravity load, which composed on 100% dead load plus superimposed dead load and 25% of live load, is first applied and analyzed in PERFORM-3D then the dynamic earthquake ground motion analyses are followed. The ground motions are applied in one direction at a time. To be consistent with the results from RSA procedure, the results in NLRHA will also include 30% of forces obtained from perpendicular direction of ground motions.

5.2.1 Verification of RSA procedure

In this study, DBE ground motions are used in NLRHA. From the configuration of the building, we can see that the building will displace differently from the edges to the middle of the building, and it is clear that the building displaces more at the edges, particularly at the edge of W1 since the building is more flexible at this side. Figure 5.16 and Figure 5.17 show the maximum story drift ratios of the building, which is in this particular location, in E-W and N-S directions respectively due to the seven DBE ground motions. The mean value obtained from averaging the demand due to these seven ground motions is shown in dash curves.

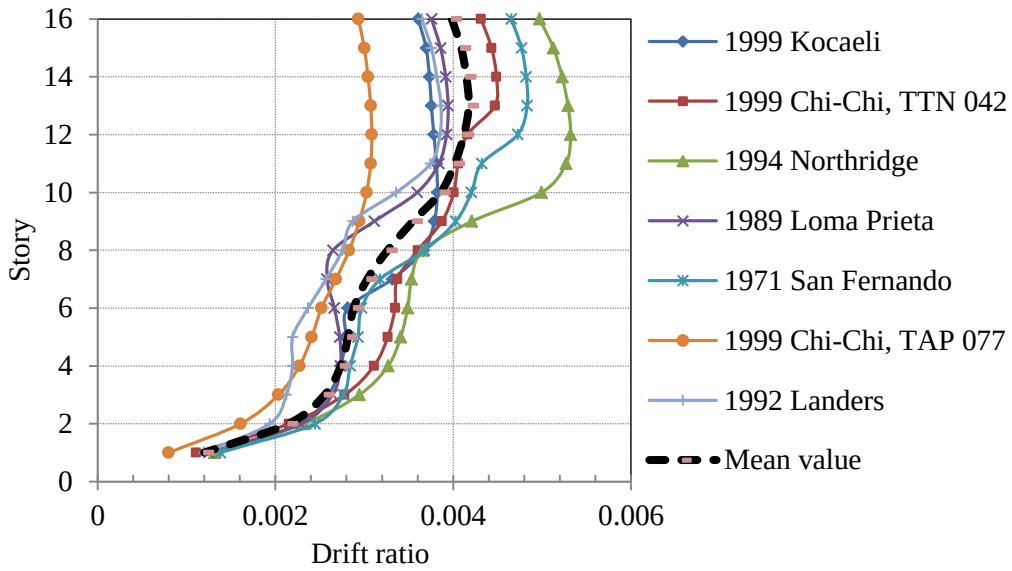

Figure 5.16 Maximum story drift ratios in E-W direction – NLRHA due to DBE

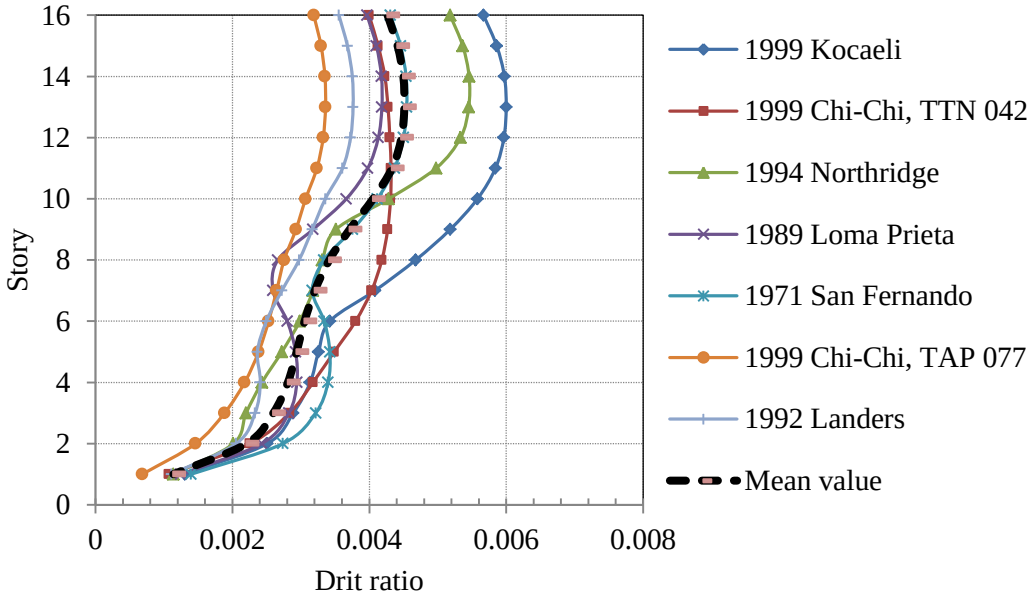

Figure 5.17 Maximum story drift ratios in N-S direction – NLRHA due to DBE

The maximum story drift ratios in both E-W and N-S directions from Figure 5.16 and Figure 5.17 of the seven DBE ground motions are then averaging out to obtain a mean value of response in NLRHA. These average quantities are then compared with the maximum story drift ratios calculated from RSA procedure and shown in Figure 5.18 and Figure 5.19, respectively. The RSA procedure overestimates story drift ratios in N-S direction, which is predominated by the shear wall action. This result agrees well with the work done by Tuan et al. (2008). In

contrast, the RSA procedure underestimates the story drift ratios in the E-W direction which is predominated by the frame action.

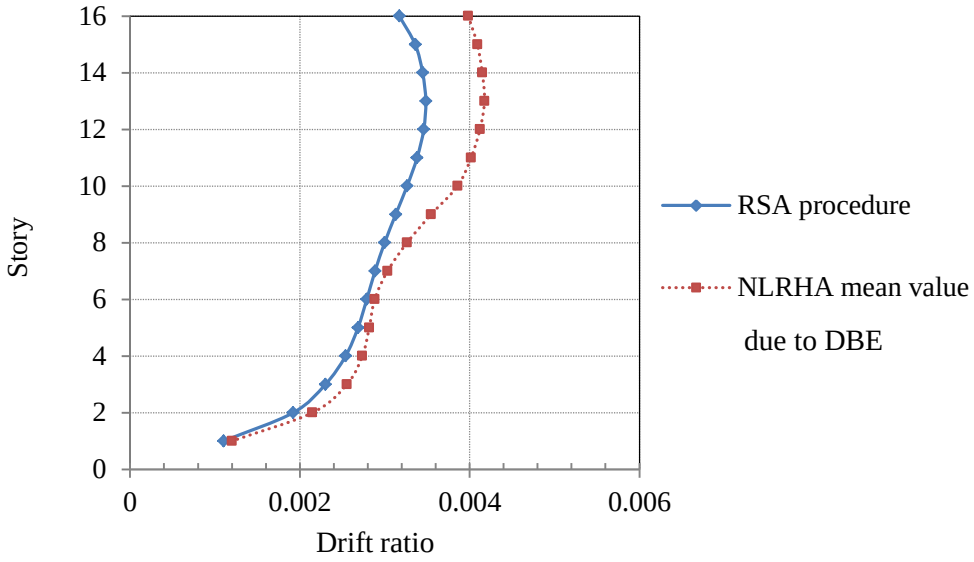

Figure 5.18 Comparison of maximum story drift ratios in E-W direction – RSA versus NLRHA

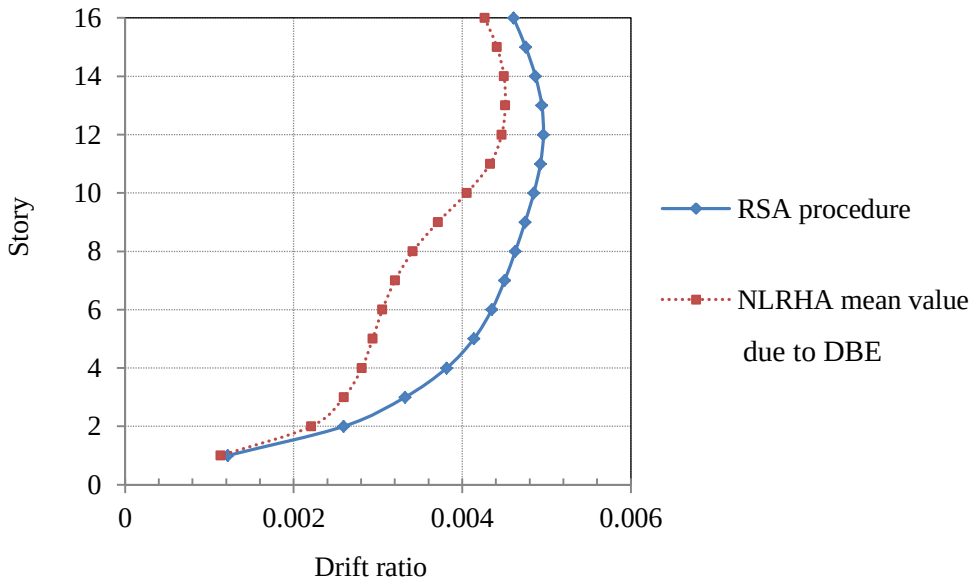

Figure 5.19 Comparison of maximum story drift ratios in N-S direction – RSA versus NLRHA

The seismic demands (shear forces and bending moments) in shear walls (W1, W2 and W3) due to the seven DBE ground motions in NLRHA conducted via PERFORM-3D are shown in Figure 5.20 through Figure 5.29. The mean value

obtained from averaging the demand due to these seven ground motions is shown in dash curves.

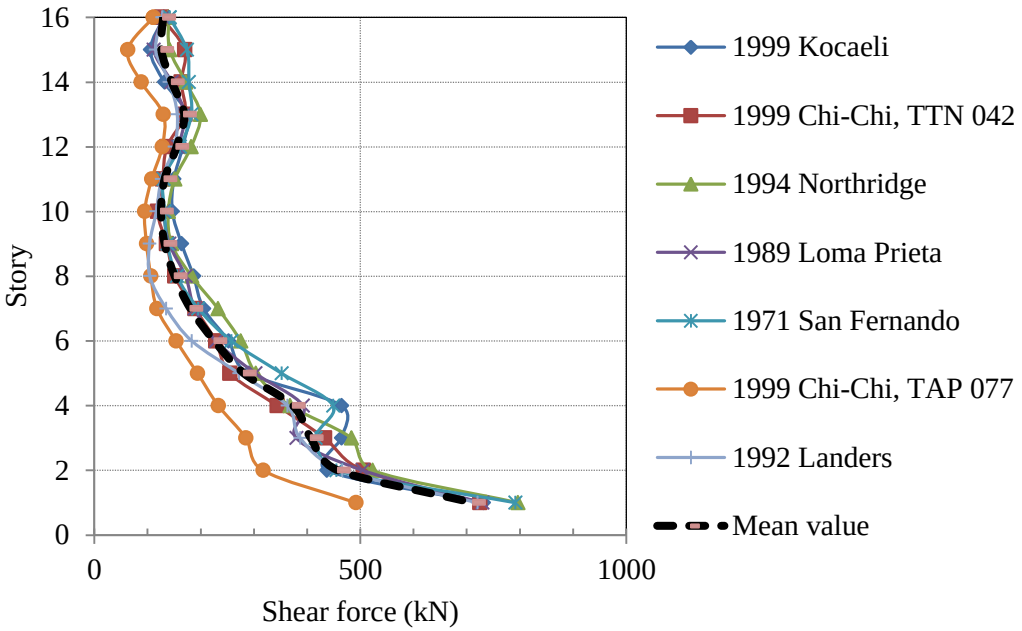

Figure 5.20 Shear force in wall1 (W1) – NLRHA due to DBE

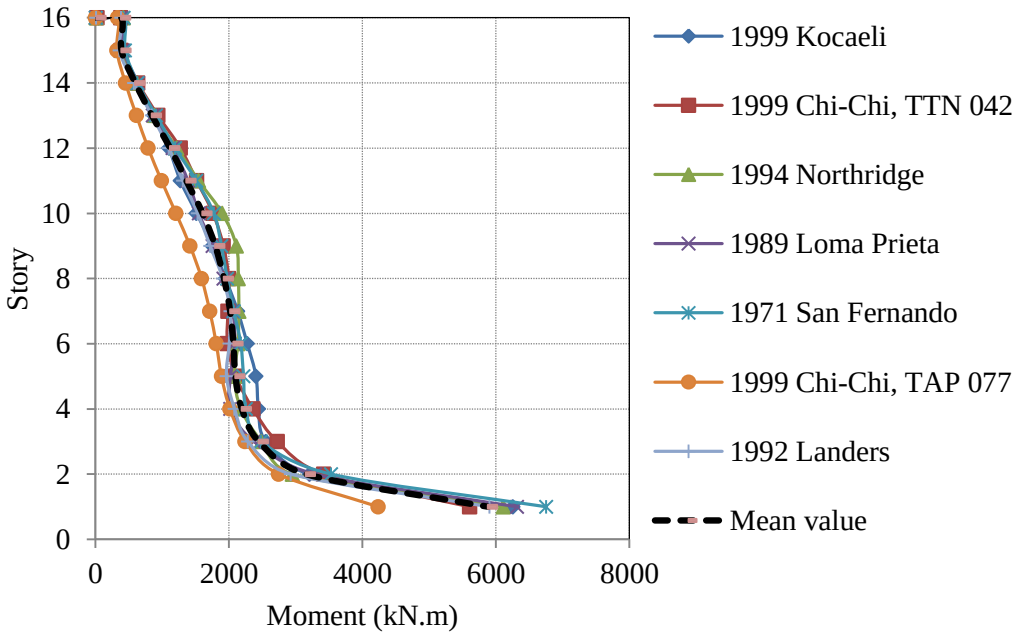

Figure 5.21 Bending moment in wall1 (W1) – NLRHA due to DBE

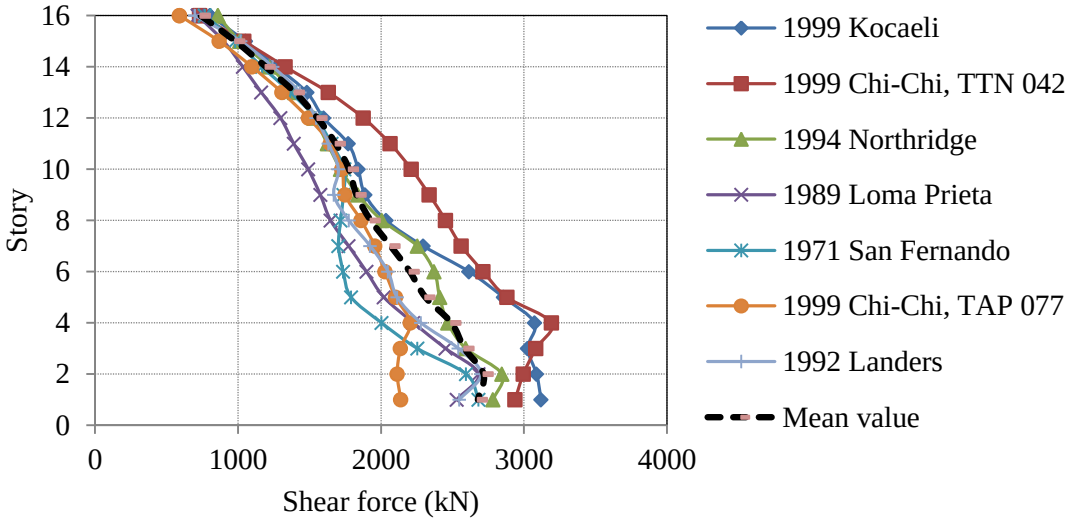

Figure 5.22 Shear force in wall2 (W2) in N-S direction – NLRHA due to DBE

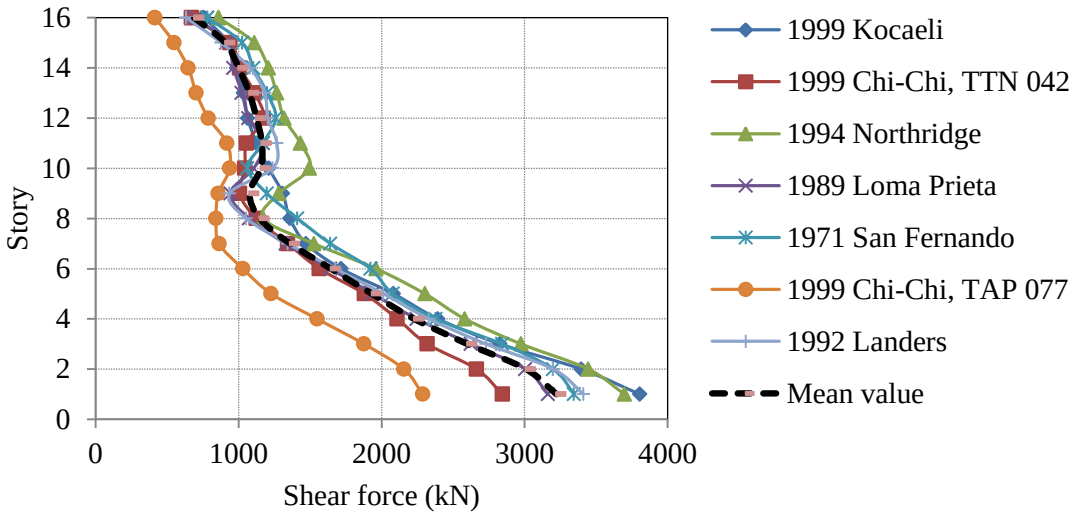

Figure 5.23 Shear force in wall2 (W2) in E-W direction – NLRHA due to DBE

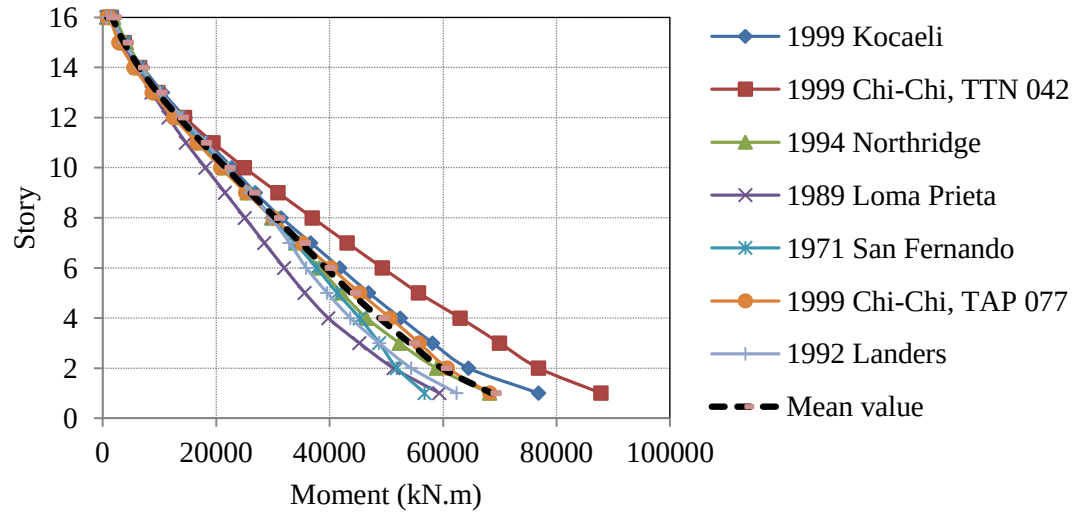

Figure 5.24 Bending moment in wall2 (W2) about E-W direction – NLRHA due to DBE

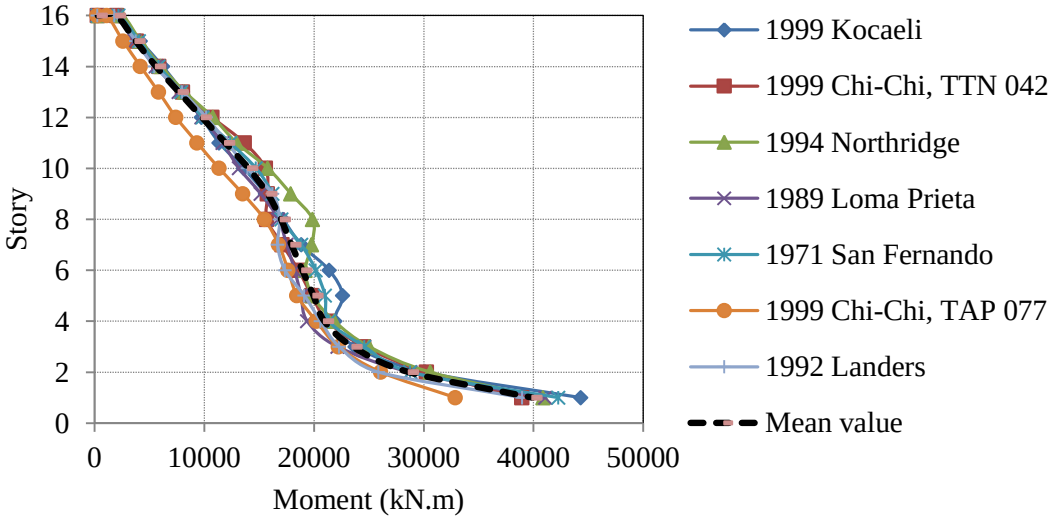

Figure 5.25 Bending moment in wall2 (W2) about N-S direction – NLRHA due to DBE

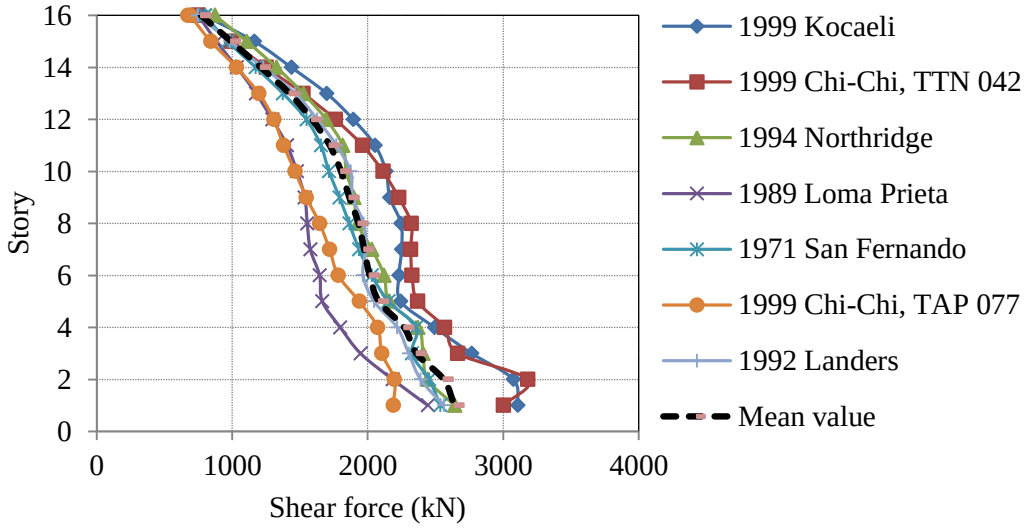

Figure 5.26 Shear force in wall3 (W3) in N-S direction – NLRHA due to DBE

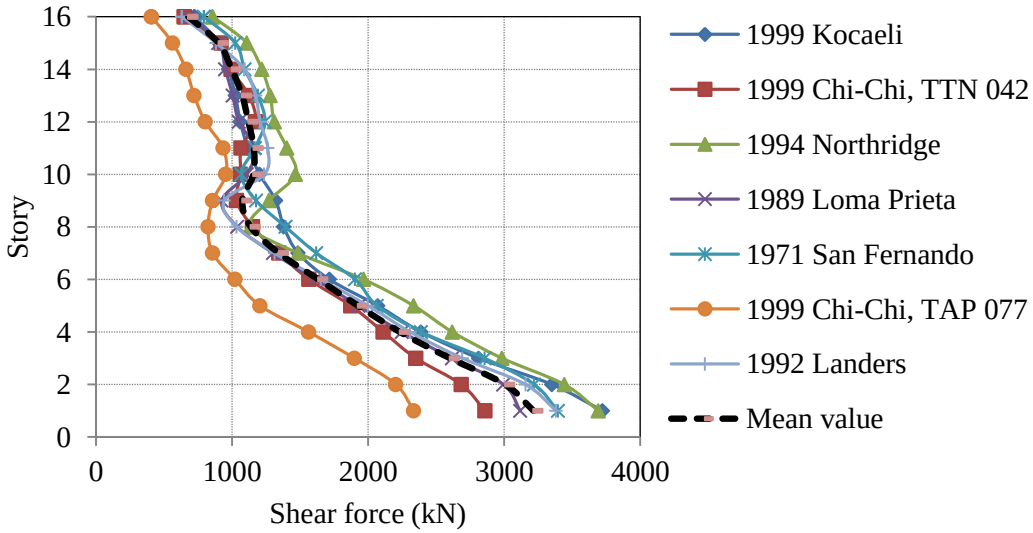

Figure 5.27 Shear force in wall3 (W3) in E-W direction – NLRHA due to DBE

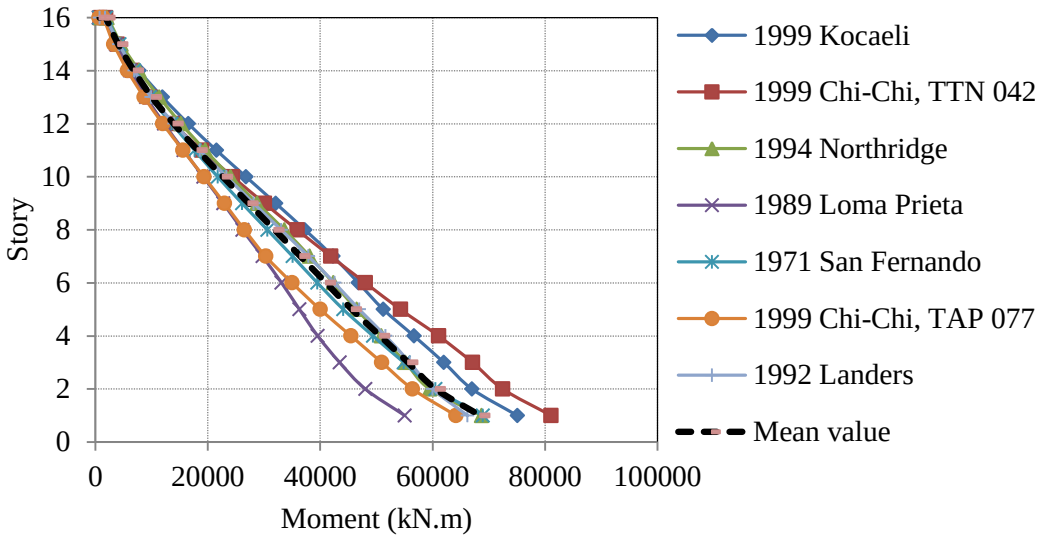

Figure 5.28 Bending moment in wall3 (W3) about E-W direction – NLRHA due to DBE

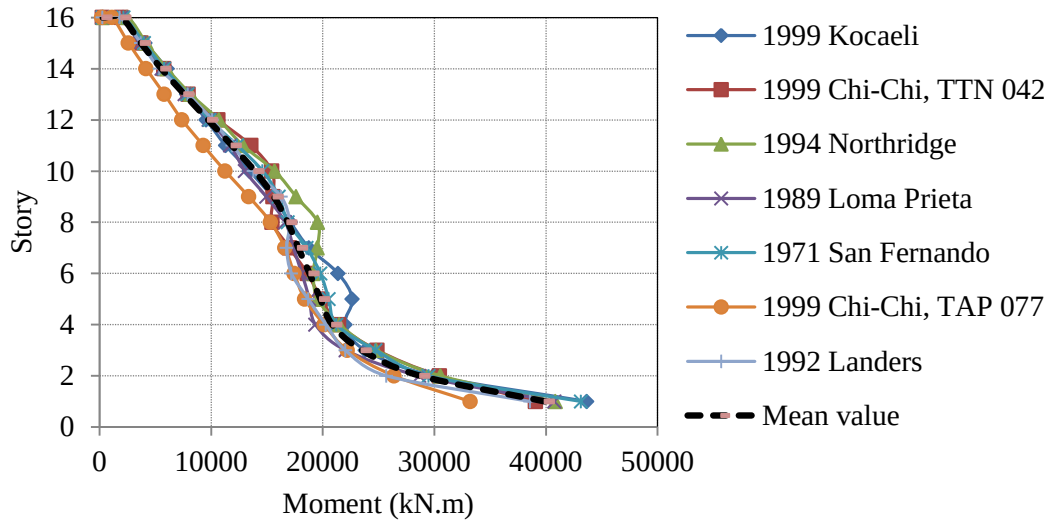

Figure 5.29 Bending moment in wall3 (W3) about N-S direction – NLRHA due to DBE

Like drift ratio, the mean value of demands in NLRHA obtained from averaging out the demands in NLRHA due to the seven DBE ground motions presented earlier from Figure 5.20 through Figure 5.29 are comparing to the demands from RSA procedure for the forces in walls. As shown in Figure 5.30 and Figure 5.31, RSA procedure underestimates the seismic shear demands throughout the entire height of W1 and the moment at middle stories of W1 (from story 4 to story 10). This result agrees quite well with the research by Tuan et al. (2008) in which the seismic shear demand over the entire height of the wall from NLRHA is about 1.25 time the corresponding demand from RSA procedure.

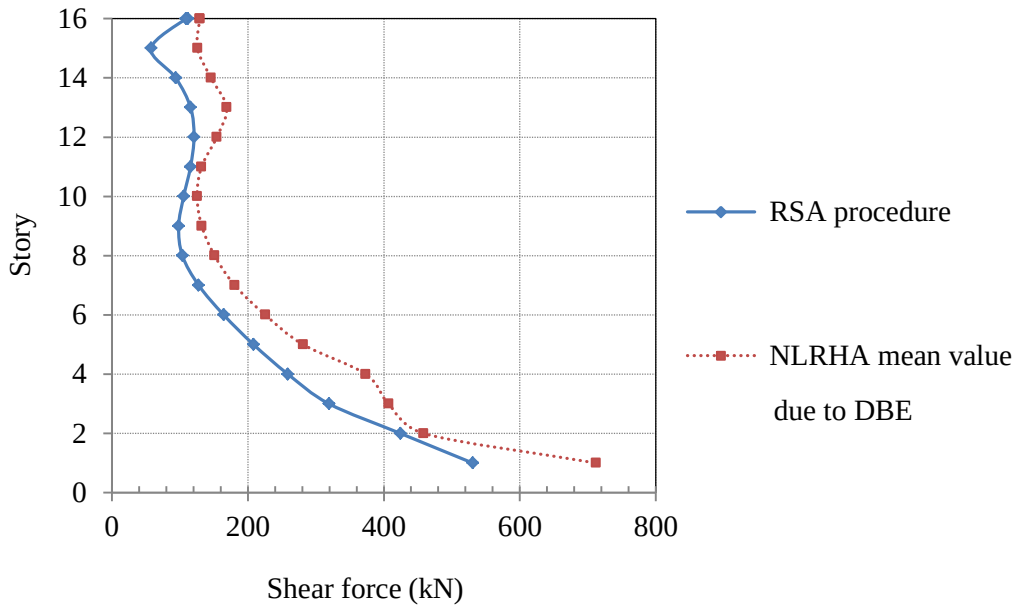

Figure 5.30 Comparison of seismic shear demand in wall1 (W1) – RSA versus NLRHA

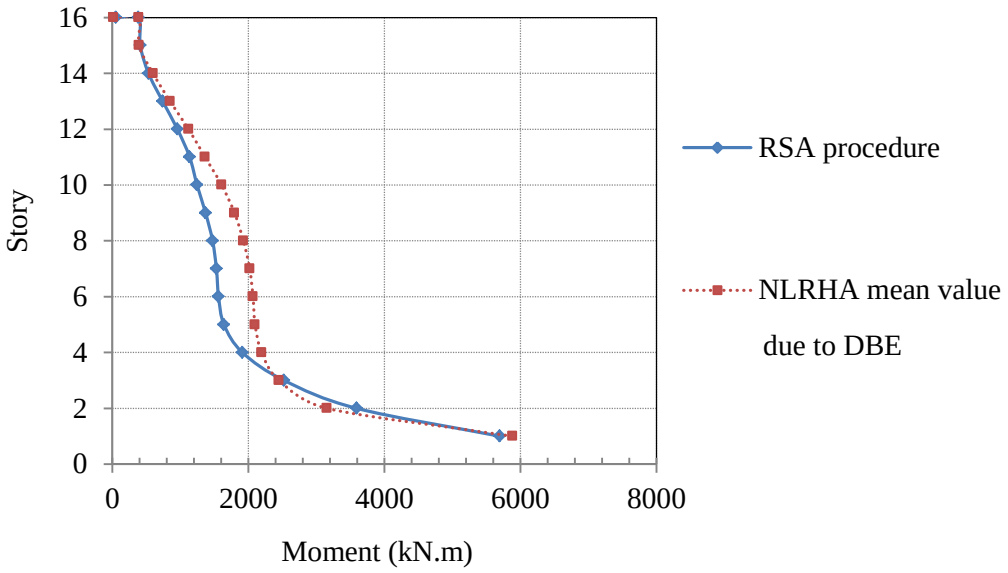

Figure 5.31 Comparison of bending moment in wall1 (W1) – RSA versus NLRHA

It can be seen from Figure 5.32 through Figure 5.35 that the seismic shear demands of W2 and W3 from NLRHA procedure are about 2 times the corresponding shear demands from RSA procedure and that their distribution patterns throughout entire height are almost the same. These results agree quite well with the results of Klemencic et al. (2007), and Munir and Warnitchai (2012). Similarly, the moment

from NLRHA is also about 2 times the corresponding demands from RSA procedure throughout the entire height of the building as depicted in Figure 5.36 through Figure 5.39. This difference for moment may be caused by the fact that flexural strength of W2 and W3 is around 1.5 times the demands from RSA procedure, due to safety factor and P-M_2-M_3 interaction effect (see APPENDIX G), and the material strain hardening used in steel model for NLRHA.

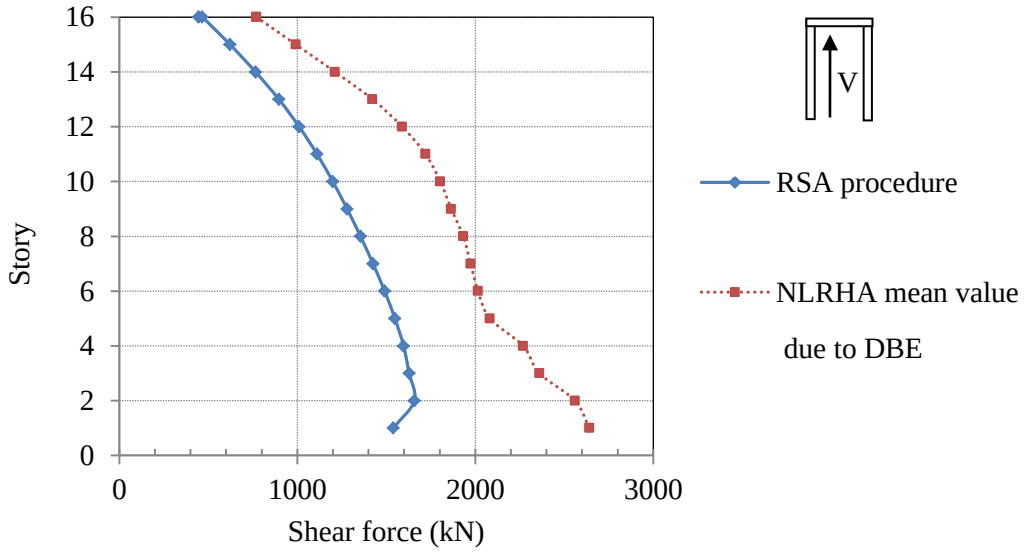

Figure 5.32 Comparison of seismic shear demand in wall2 (W2) in N-S direction – RSA versus NLRHA

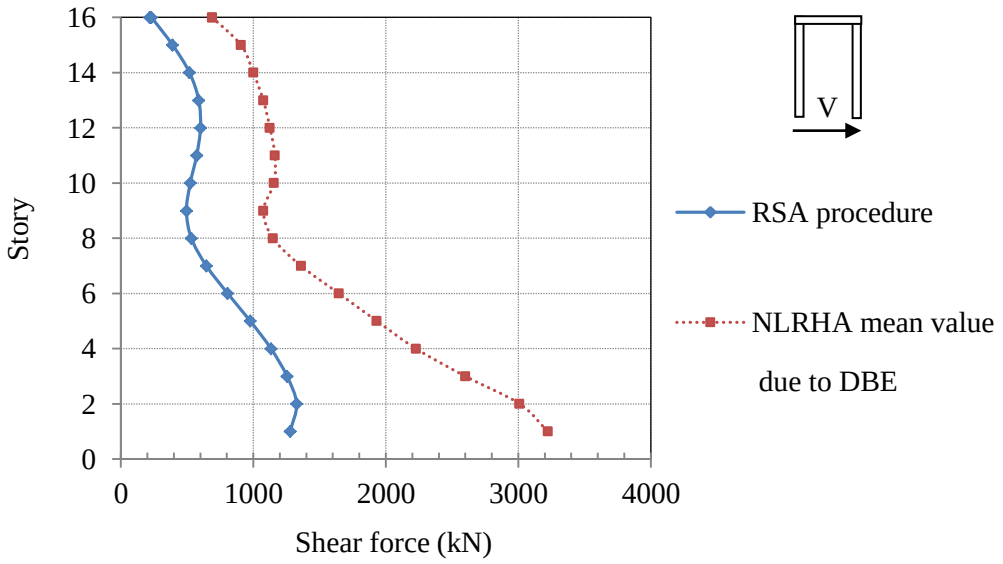

Figure 5.33 Comparison of seismic shear demand in wall2 (W2) in E-W direction – RSA versus NLRHA

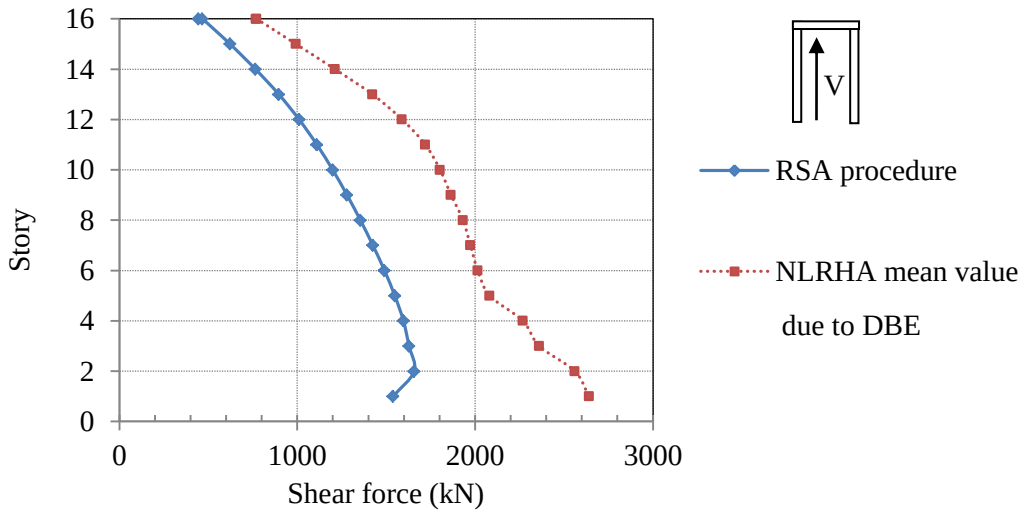

Figure 5.34 Comparison of seismic shear demand in wall3 (W3) in N-S direction – RSA versus NLRHA

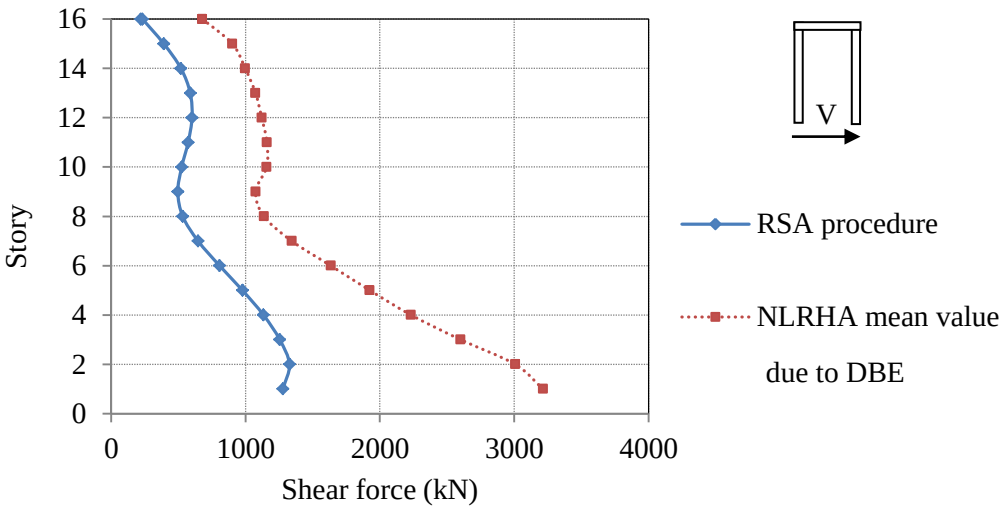

Figure 5.35 Comparison of seismic shear demand in wall3 (W3) in E-W direction – RSA versus NLRHA

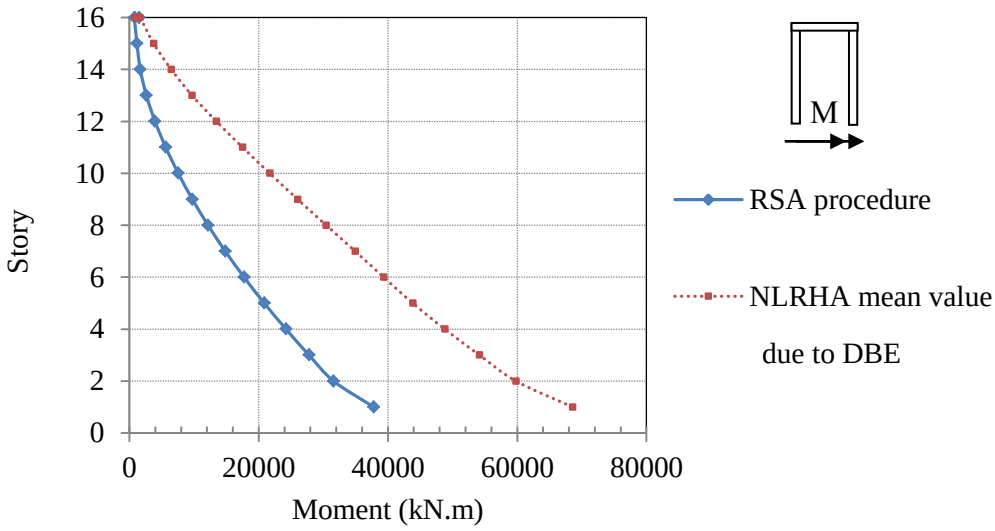

Figure 5.36 Comparison of bending moment in wall2 (W2) about E-W direction – RSA versus NLRHA

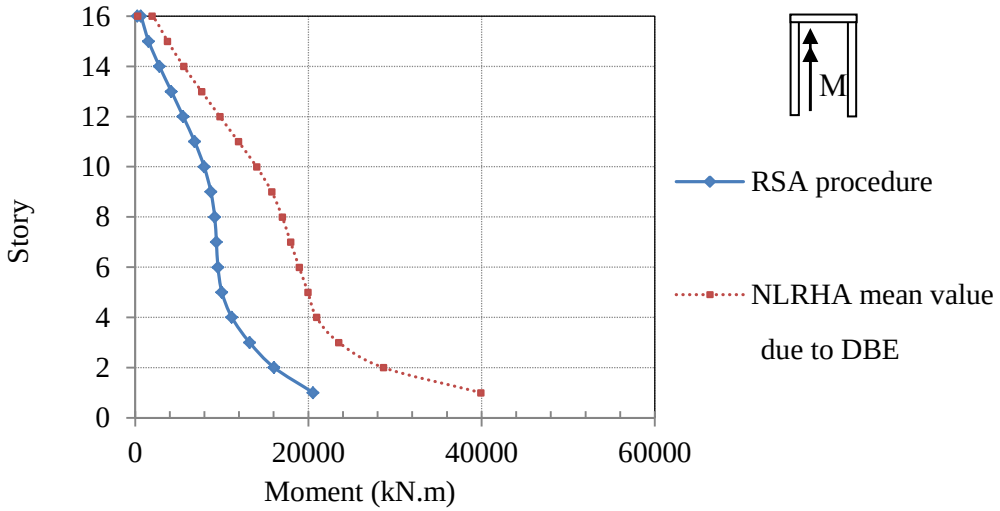

Figure 5.37 Comparison of bending moment in wall2 (W2) about N-S direction – RSA versus NLRHA

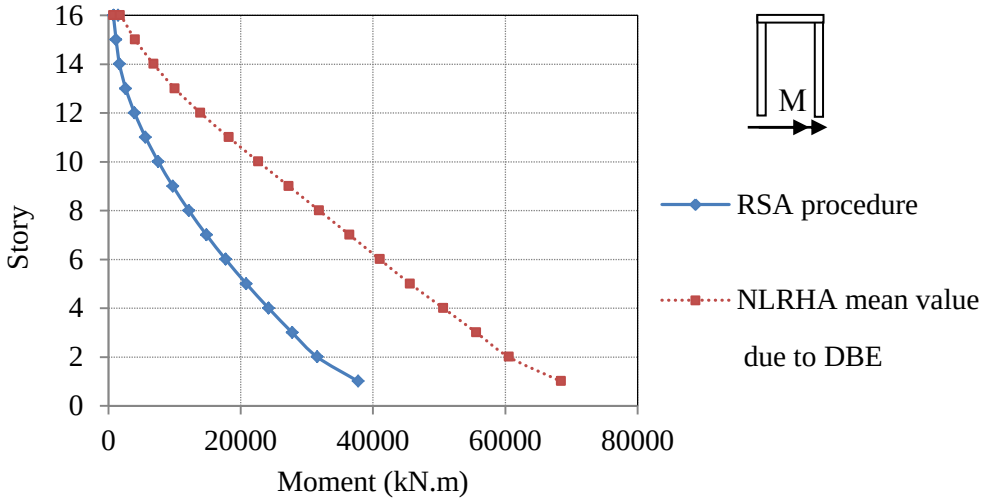

Figure 5.38 Comparison of bending moment in wall3 (W3) about E-W direction – RSA versus NLRHA

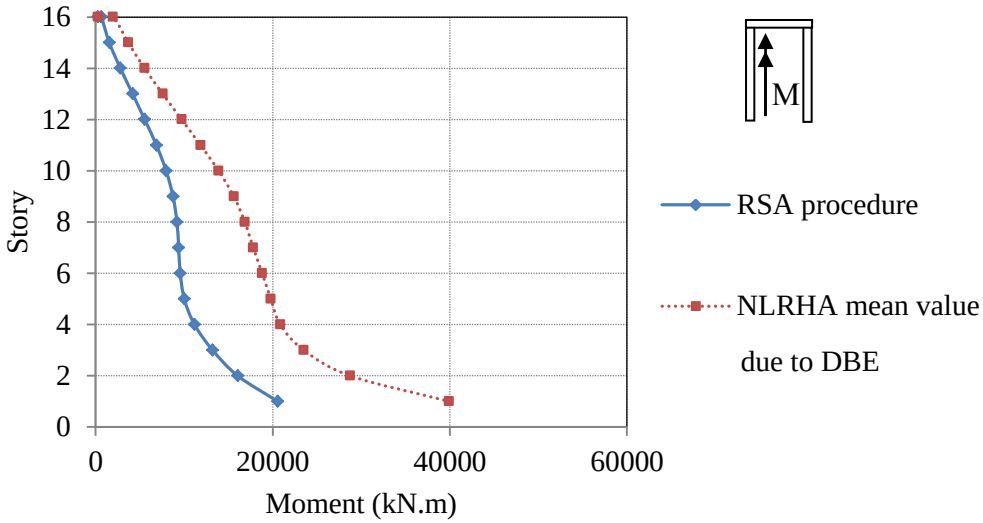

Figure 5.39 Comparison of bending moment in wall3 (W3) about N-S direction – RSA versus NLRHA

5.2.2 Building performance

The building designed by RSA procedure for DBE spectrum is expected to perform well under severe earthquake (MCE level). So MCE ground motions are used in NLRHA to check the performance of the building. The elements to be checked are column hinge rotation, wall shear strength and hinge rotation, and drift ratio against each performance levels proposed in ASCE41-06. The first quantity to be checked is maximum story drift ratio. As shown in Figure 5.40 and Figure 5.41, the story drift ratios in both E-W and N-S directions are much smaller than the allowable limit in the code (about half of the allowable drift ratio).

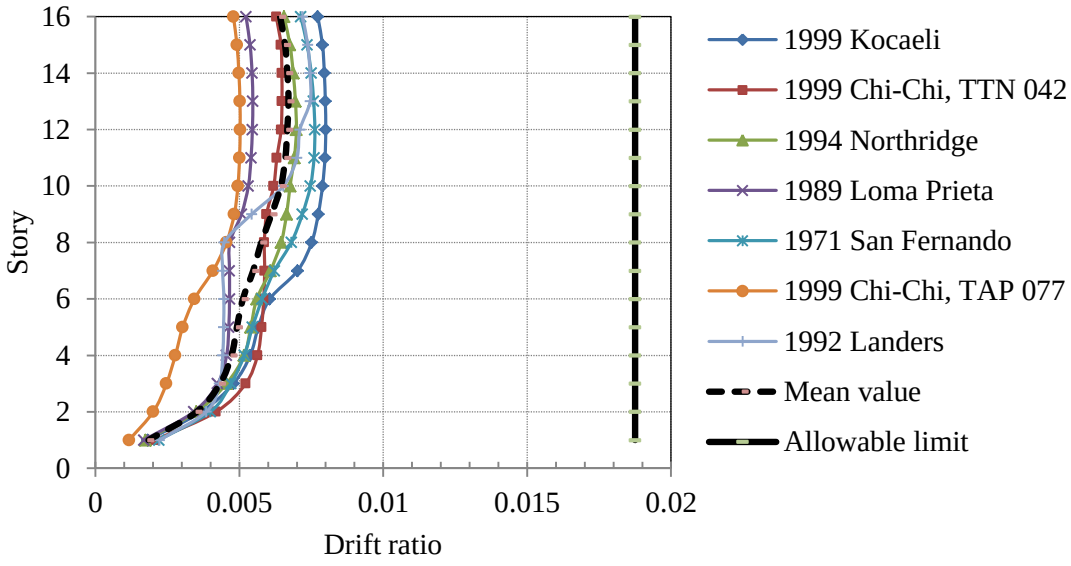

Figure 5.40 Maximum story drift ratios in E-W direction – NLRHA due to MCE

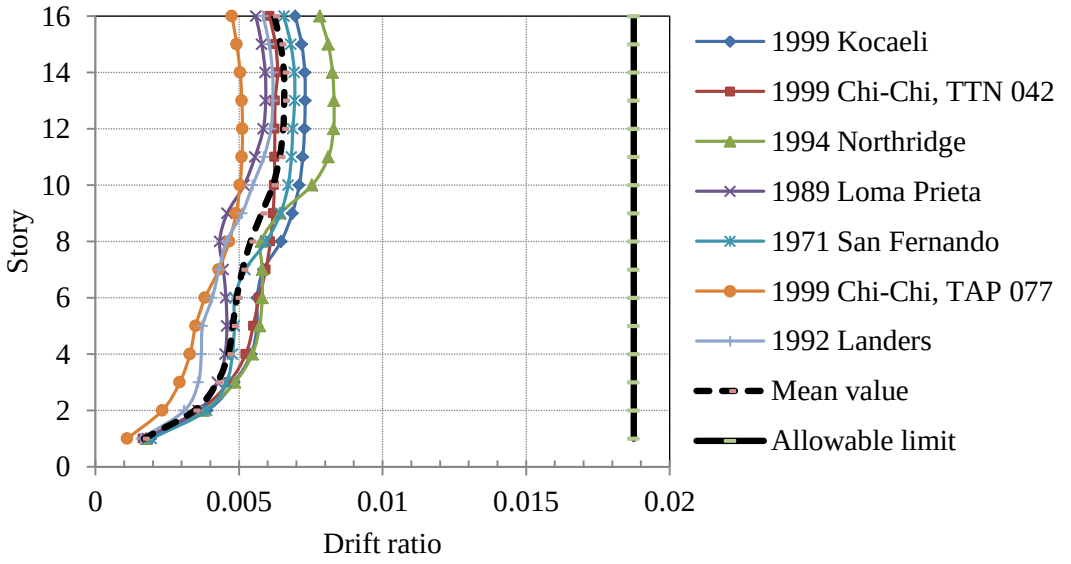

Figure 5.41 Maximum story drift ratios in N-S direction – NLRHA due to MCE

The results are investigated in several aspects. Core wall shear response is particularly critical, as illustrated in Figure 5.42 through Figure 5.46, the shear demands from NLRHA due to MCE ground motions are all exceeding the design capacity, which is equal to the demand divided by a safety factor of 0.75, from RSA procedure of the shear walls. It can be interpreted from the figures that the shear demand of the walls exceeds their capacity designed by RSA procedure, so shear failure could be expected to occur in the wall elements if they were designed to resist the shear demand in RSA procedure. However, in this study, the walls are designed to resist the seismic moment from RSA procedure only, but no shear design is performed. The shear capacity of concrete in wall1 is exceeding the demand in NLRHA except in the first story as shown in Figure 5.42, so using just the minimum shear reinforcement; the wall1 is safe from shear failure. Moreover as illustrated in Figure 5.43 and Figure 5.45, the shear capacity of concrete in wall2 and wall3 in N-S direction is also exceeding the shear demand in NLRHA from the top to the sixth story, nevertheless, the amount of minimum shear reinforcement can help avoid shear failure for the rest of the floor (1^{st} to the 5^{th} story) in these wall elements. Last, as shown in Figure 5.44 and Figure 5.46, the shear failure could be expected to occur in wall2 and wall3 in the E-W direction if the walls are designed based on RSA procedure using minimum shear reinforcement. Whereas the flexural response of the wall elements, evaluated using rotation gage elements included in the model in PERFORM-3D, is within immediate occupancy performance level in ASCE41-06 (Table 5.4). Column hinge rotation is also very critical; the plastic hinge rotations of C8, C9, C16 and C17 at story 16 are all exceeding the rotation limit for collapse prevention level set by ASCE41-06. For column C12 and C13 at story 16, the plastic hinge rotations are satisfied the life safety performance level. And the column hinge rotations in the first story are all within the immediate occupancy performance level. The most critical column hinge rotation is shown in Table 5.5. Figure 5.47 shows the columns failing CP (red color), satisfying LS (light blue color) and IO (green color).

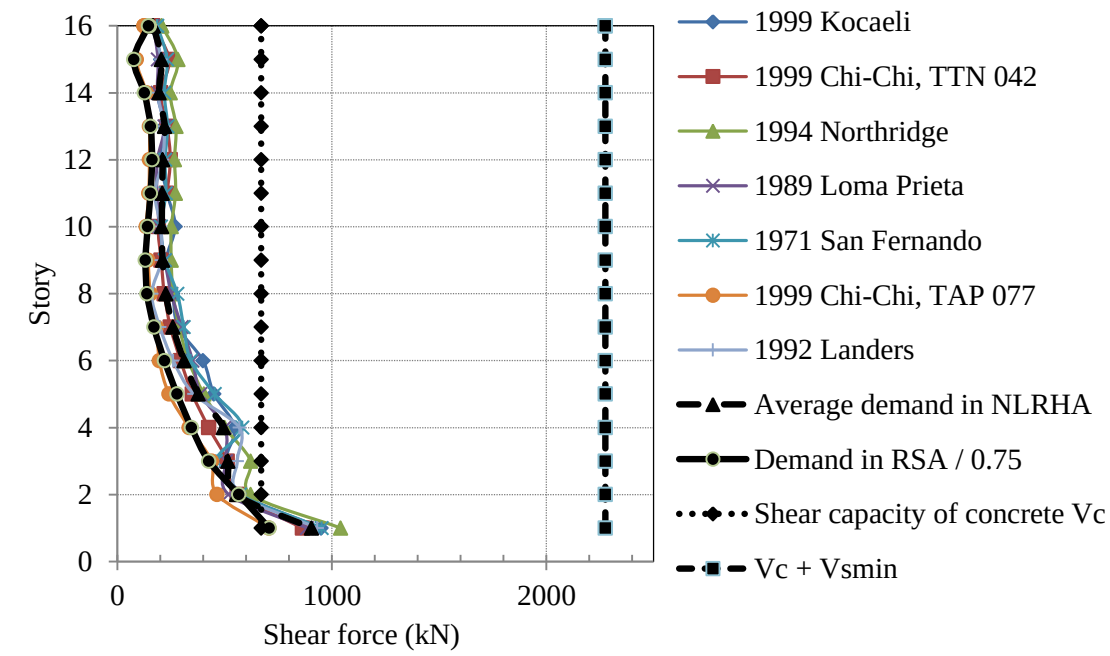

Figure 5.42 Shear force in wall1 (W1) – RSA versus NLRHA due to MCE

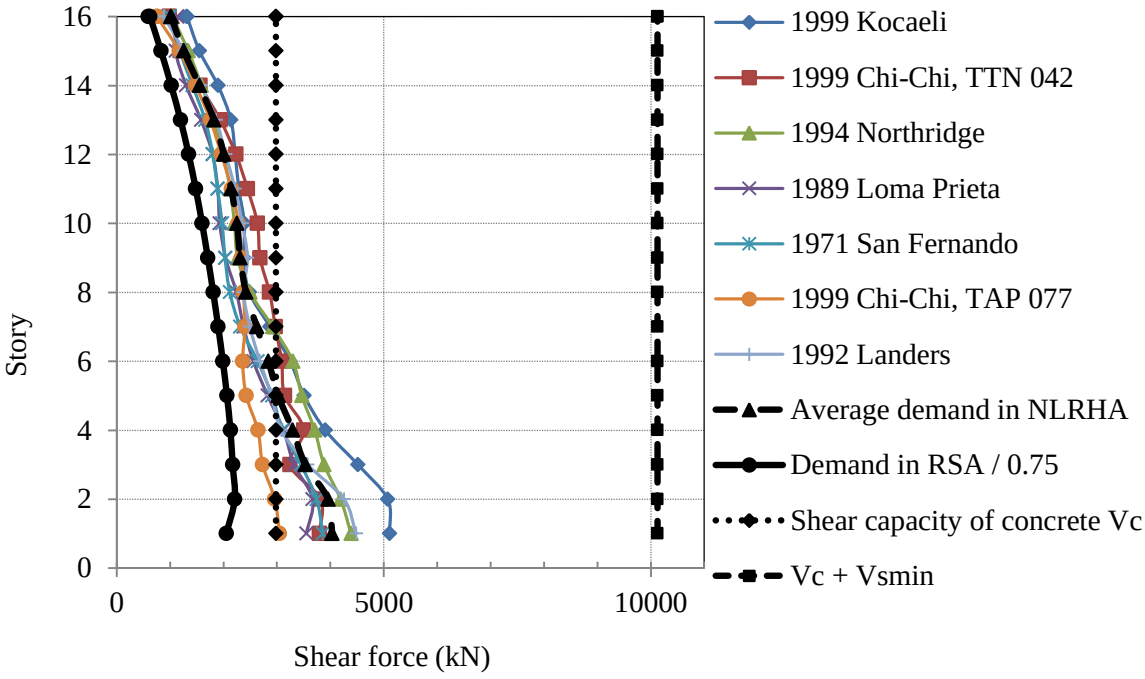

Figure 5.43 Shear force in wall2 (W2) in N-S direction – RSA versus NLRHA due to MCE

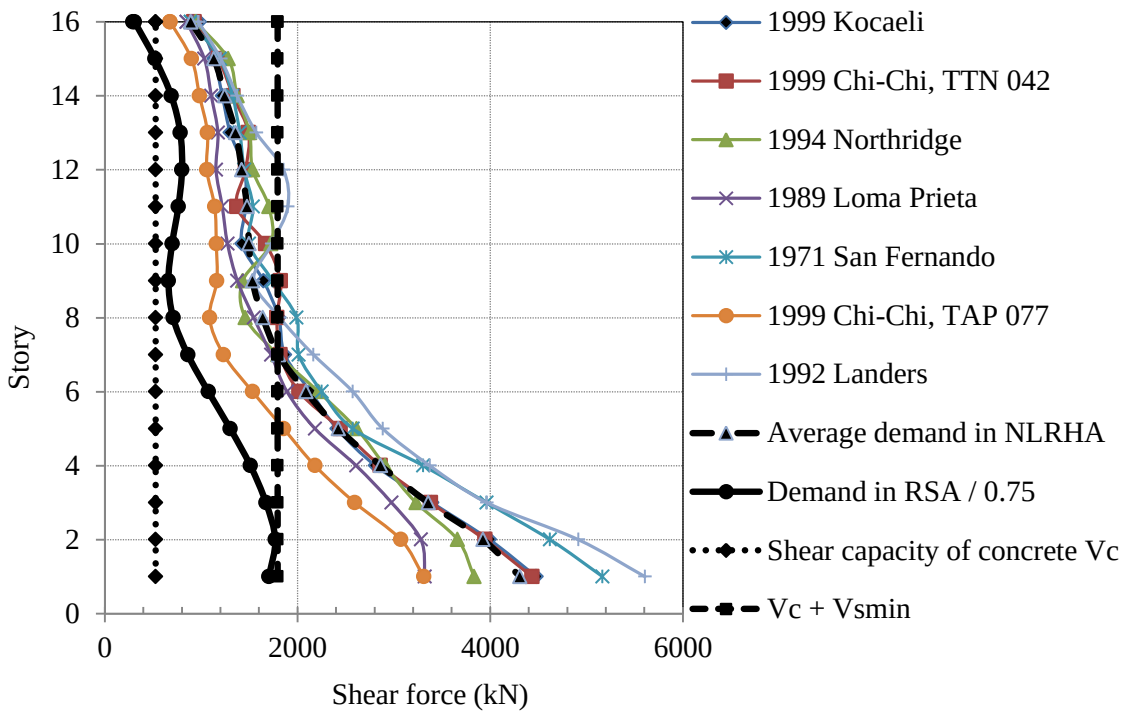

Figure 5.44 Shear force in wall2 (W2) in E-W direction – RSA versus NLRHA due to MCE

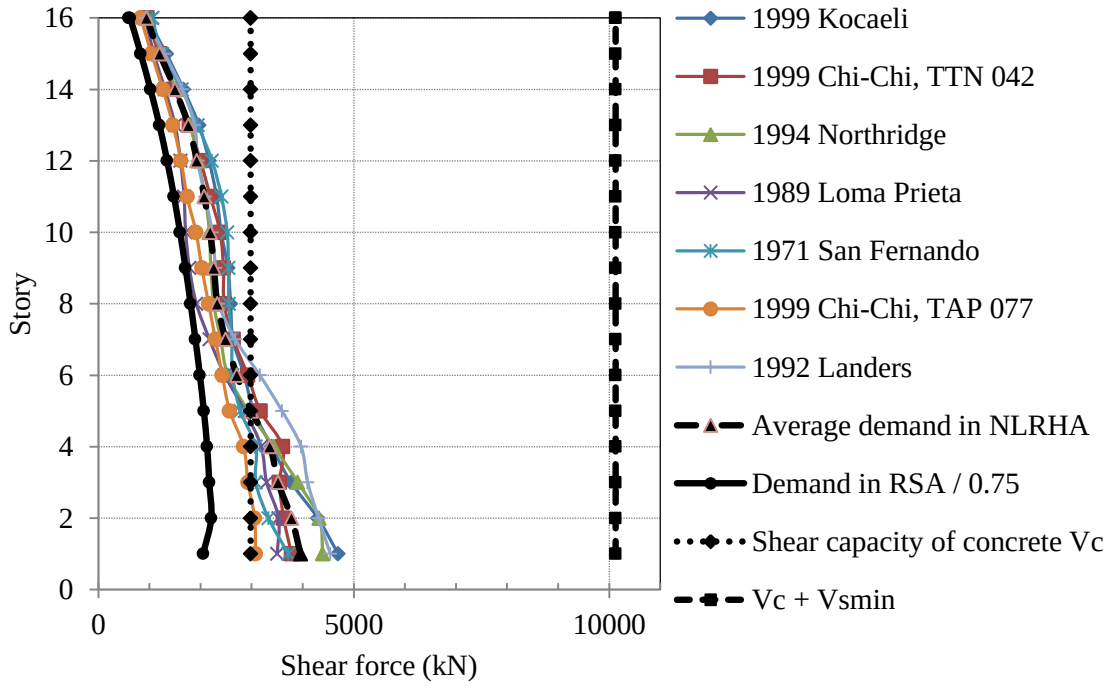

Figure 5.45 Shear force in wall3 (W3) in N-S direction – RSA versus NLRHA due to MCE

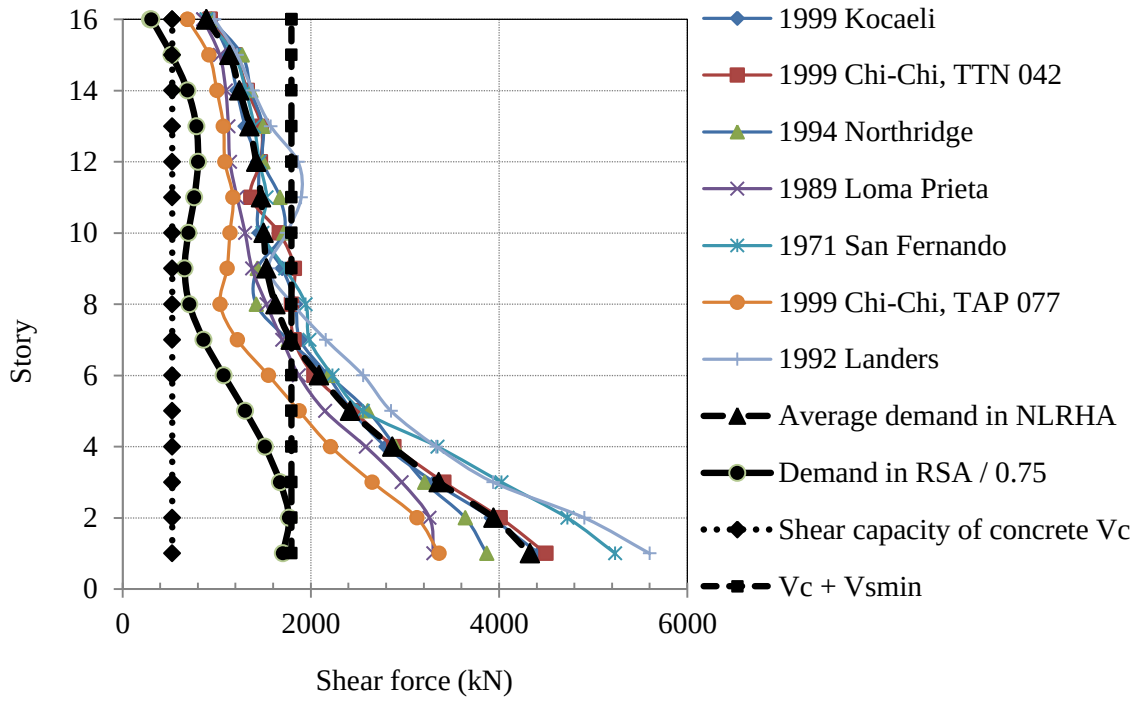

Figure 5.46 Shear force in wall3 (W3) in E-W direction – RSA versus NLRHA due to MCE

Table 5.4 Most critical wall hinge rotation

Earthquake loading	Hinge rotation	ASCE41-06 – Limit		
		IO	LS	CP
Average of 7 ground motions	0.0017	0.002	0.004	0.008
Maximum of 7 ground motions	0.002			

Table 5.5 Most critical column hinge rotation

Earthquake loading	Hinge rotation	ASCE41-06 – Limit		
		IO	LS	CP
Average of 7 ground motions	0.0183	0.004	0.0135	0.0175
Maximum of 7 ground motions	0.0254			

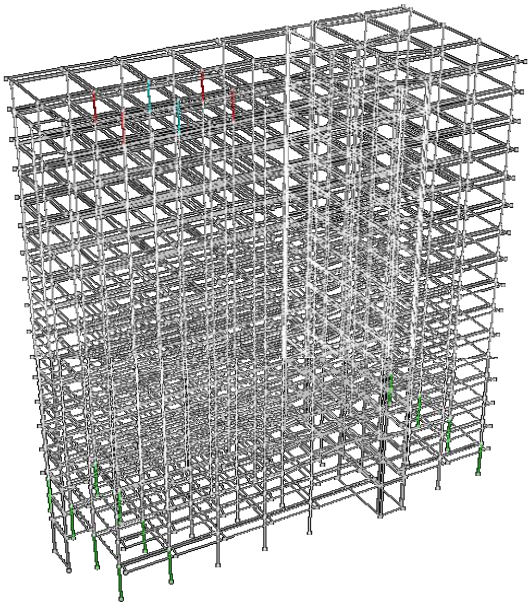

Figure 5.47 Location of columns exceeding CP, satisfying LS and IO performance level due to MCE ground motions

CHAPTER VI
MODIFIED RESPONSE SPECTRUM ANALYSIS PROCEDURE

6.1 Introduction

Priestly and Amaris (2002) attempted to quantify the influence of the higher mode on the response of a wide range of cantilever wall buildings of 2, 4, 8, 12, 16 and 20 stories in multi-mode analysis. They had proposed Modified Modal Superposition (MMS) method to combine the elastic modal shear demand with two main assumptions: (1) ductility limits primarily first mode response, and (2) the inelastic higher modes will not differ significantly from elastic mode, which means it is not appropriate to apply a force reduction factor (R_d) to any mode past the first. In MMS method, the elastic seismic shear demand is reduced by a seismic modification factor only in the first vibration mode and then combined with the elastic shear demand of other higher modes into total response. Priestly and Amaris (2003) compared the results from the MMS method with time history results, at seismic intensities scaled by a factor of 1.0 the results compared well, however at double seismic intensities the MMS method overestimates shears.

Munir and Warnitchai (2012) used a method called uncoupled modal response history analysis (UMRHA) adapted from Chopra and Goel (2002) to decompose the inelastic seismic responses into the contribution of each vibration modes. They applied this method to analyze a 40-story core-wall building designed by response spectrum analysis procedure. Three different types of seismic demands are then compared. The first type of demand is the inelastic demand obtained from UMRHA, the second type is the elastic demand computed from elastic response spectrum at 5% damping ratio, and the third type is the design demand which is set equal to the elastic demand divided by R_{eff}. They found that the demands from UMRHA matched the design demands only in the first mode and reasonably close to elastic demands in second mode.

Hence, it is wise to adapt the modified RSA procedure to MMS method proposed by Priestly and Amaris (2002).

6.2 Modified response spectrum analysis procedure

In this modified RSA procedure, the RSA procedure needs to be conducted first to determine the dynamic seismic base shear and compared with the static base shear from ELF procedure, and then R_{eff} can be calculated using the formula in Table 4.7 of Chapter IV. And then similar to RSA procedure, the elastic responses of all significant vibration modes are determined using the elastic response spectrum in Figure 4.1 of Chapter IV, next only the responses of the first translational mode (E-W direction) and the first torsional mode of the structure are reduced by the effective seismic modification factor "R_{eff}". To do this, we divide the elastic response spectrum mentioned earlier by "R_{eff}" in a range of time starting from 1.5 second to 3 second since only the natural periods of the first translational and torsional modes are within this range and other higher modes are outside this range of time. Finally the responses of all modes being considered are combined into total responses by CQC rule.

It should be noted that this modified RSA procedure is used to improve the seismic shear demand, hence seismic shear strength or shear capacity of the shear walls only, no modification is necessary in computing deformations and seismic moment of the walls. However, the results for the seismic moment of the wall elements using this modified RSA procedure could also be found in the APPENDIX E of this report.

With the same loading and modeling of building in ETABS as presented in Chapter IV, the modified RSA procedure has been performed via ETABS considering both P-delta and accidental torsional effects.

6.2.1 Torsional effect

The same as the RSA procedure, the natural torsional effect needs to be taken into account using the equation (4.1) to calculate the amplification factor. The results are shown in Table 6.1.

Table 6.1 Amplification factors for accidental torsion

Story	Displacement in E-W direction (m)				Displacement in N-S direction (m)				Amplification factor to be used
	max	min	Avg	A_{xx}	max	min	Avg	A_{yy}	A_x
16	0.078	0.055	0.067	0.983	0.157	0.078	0.118	1.112	1.112
15	0.072	0.049	0.060	0.987	0.146	0.073	0.109	1.112	1.112
14	0.065	0.044	0.055	0.991	0.134	0.067	0.100	1.112	1.112
13	0.059	0.040	0.049	0.994	0.122	0.061	0.092	1.111	1.111
12	0.053	0.036	0.045	0.995	0.110	0.055	0.083	1.110	1.110
11	0.049	0.033	0.041	0.993	0.098	0.049	0.074	1.109	1.109
10	0.045	0.031	0.038	0.986	0.086	0.043	0.065	1.110	1.110
9	0.042	0.030	0.036	0.976	0.075	0.037	0.056	1.113	1.113
8	0.039	0.028	0.034	0.965	0.065	0.031	0.048	1.129	1.129
7	0.036	0.027	0.031	0.954	0.057	0.025	0.041	1.154	1.154
6	0.032	0.024	0.028	0.943	0.048	0.020	0.034	1.179	1.179
5	0.027	0.021	0.024	0.934	0.039	0.015	0.027	1.203	1.203
4	0.022	0.017	0.019	0.925	0.030	0.011	0.020	1.226	1.226
3	0.016	0.013	0.014	0.916	0.020	0.007	0.014	1.247	1.247
2	0.010	0.008	0.009	0.907	0.012	0.004	0.008	1.264	1.264
1	0.005	0.004	0.004	0.896	0.005	0.001	0.003	1.272	**1.272**

Note: max = maximum value, min = minimum value, Avg = average value,
A_{xx} = amplification factor in E-W direction, A_{yy} = amplification factor in N-S direction

So we will use A_x =1.272 as amplification factor for diaphragms in all stories and the total eccentricity ratio is $0.05A_x$ = 0.06359

6.2.2 Internal forces

With the new torsional eccentricity of 0.06359, the modified RSA procedure is conducted again via ETABS, the seismic demands of the structural members (columns, shear walls, slab) are then obtained, and the seismic base shear in both E-W and N-S directions are shown in Table 6.2.

Table 6.2 Seismic base shears from modified RSA procedure

Directions	E-W	N-S
Base shear (kN)	5292	6869

6.2.2.1 Seismic shear demand of shear walls

The seismic shear demands of the walls based on three different analyses, RSA procedure, NLRHA and modified RSA procedure, are shown in the Figure 6.1 through Figure 6.5. From these figures, we can observe that the modified RSA procedure overestimates the seismic shear demand in Wall1. For wall2 and wall3, the modified RSA procedure overestimates the seismic shear demand in N-S direction and good agreement between modified RSA and NLRHA can be found in seismic shear demand in E-W direction.

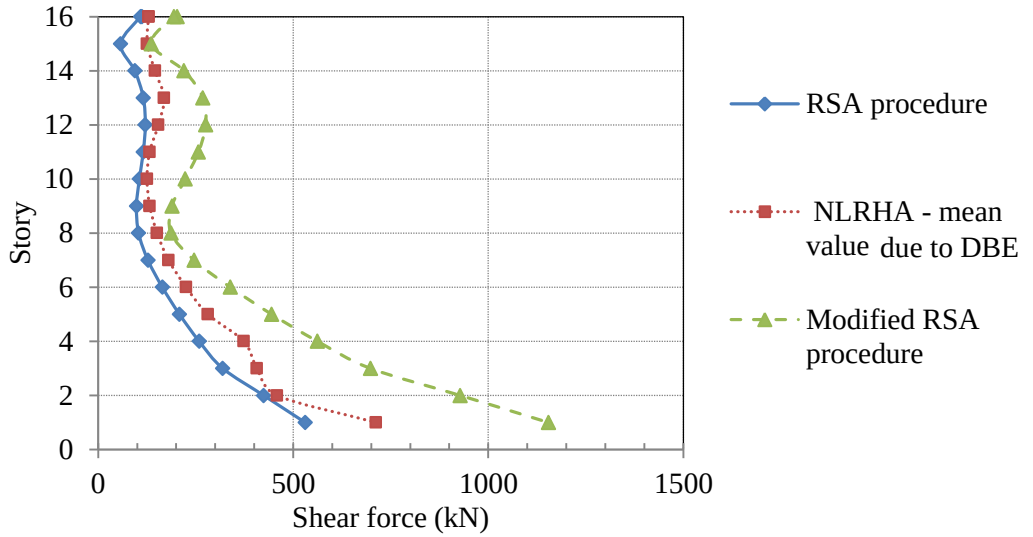

Figure 6.1 Seismic shear demand in Wall1 – RSA vs NLRHA vs modified RSA

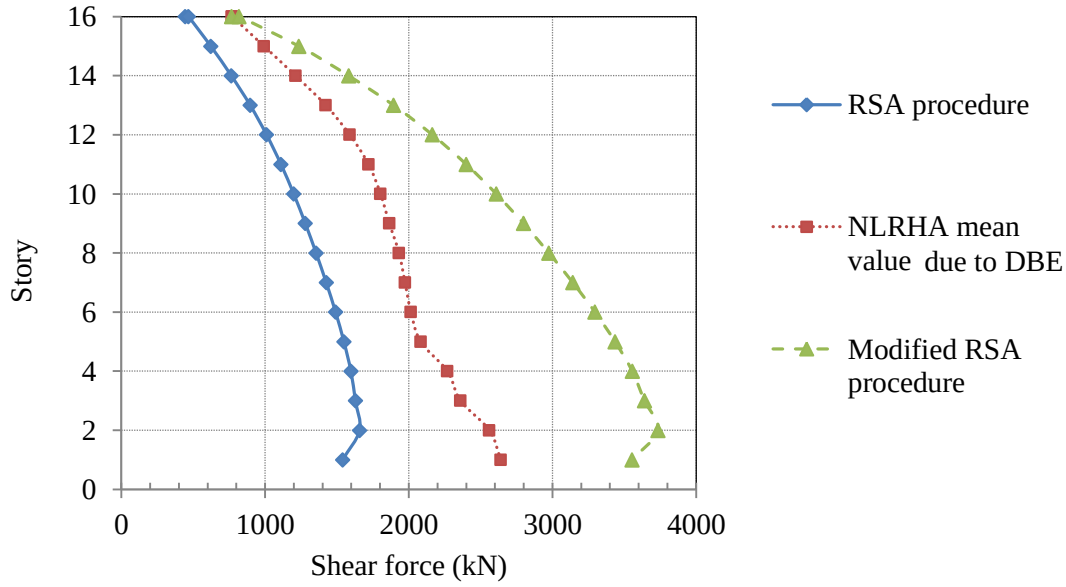

Figure 6.2 Seismic shear demand in Wall2 in N-S direction – RSA vs NLRHA vs modified RSA

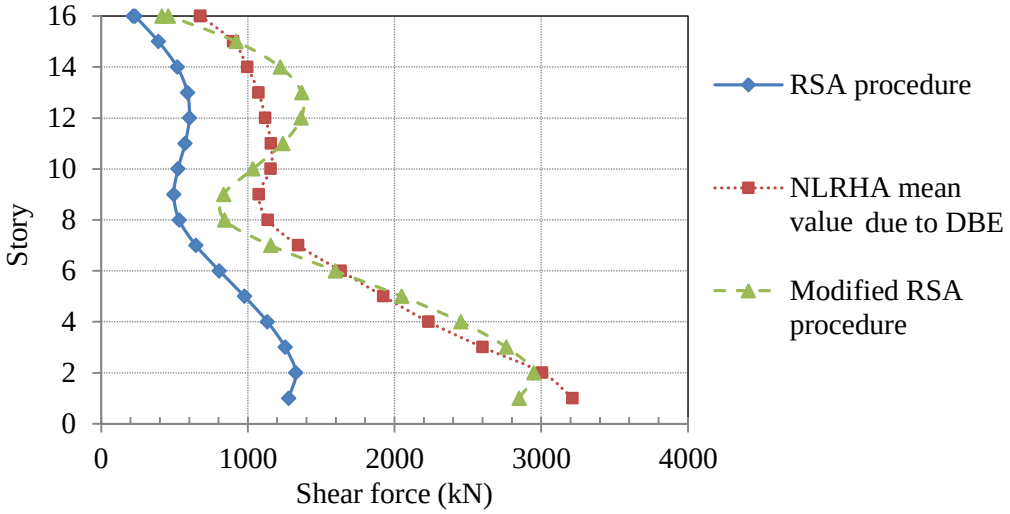

Figure 6.3 Seismic shear demand in Wall2 in E-W direction – RSA vs NLRHA vs modified RSA

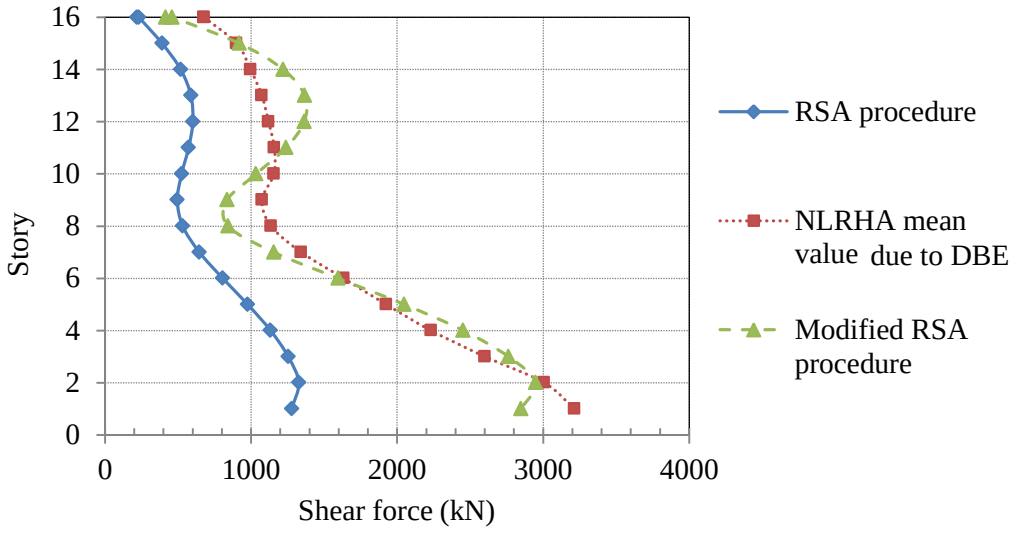

Figure 6.4 Seismic shear demand in Wall3 in N-S direction – RSA vs NLRHA vs modified RSA

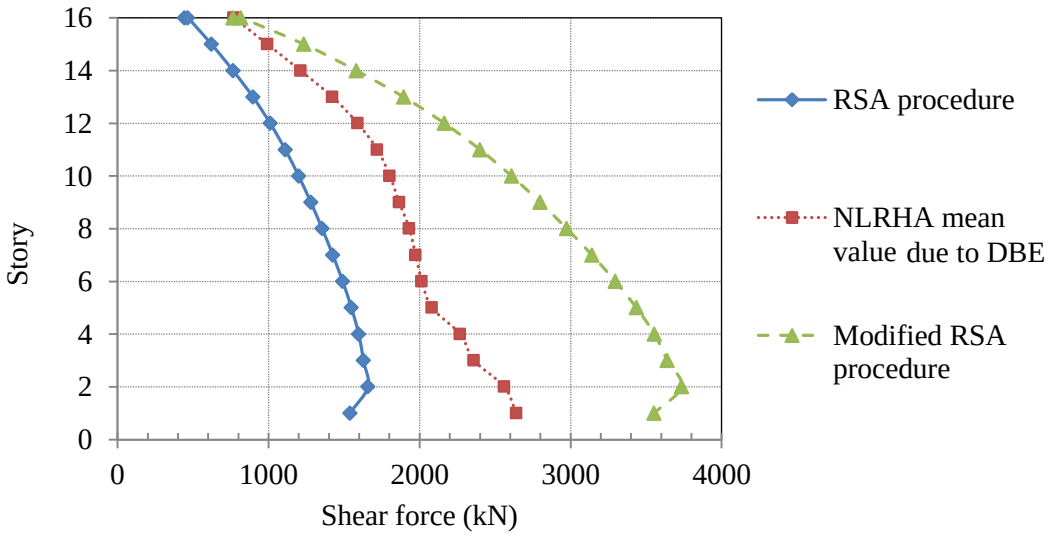

Figure 6.5 Seismic shear demand in Wall3 in E-W direction – RSA vs NLRHA vs modified RSA

Depicted in Figure 6.6 through Figure 6.10 is the shear strength or shear capacity of the walls designed by RSA procedure and modified RSA procedure along with the shear demand in average value obtained from NLRHA using 7 MCE ground motions. Clearly, the shear capacity of the wall designed by modified RSA procedure is greater than the average shear demand obtained from NLRHA, so the shear failure of the wall in RSA procedure could be avoided by this modified RSA procedure. It should be noted that the design RSA and modified RSA in Figure 6.6 through Figure 6.10 are obtained from shear demand in RSA and modified RSA in Figure 6.1 through Figure 6.5 divided by a strength reduction factor or safety factor of 0.75 set by ACI318-08.

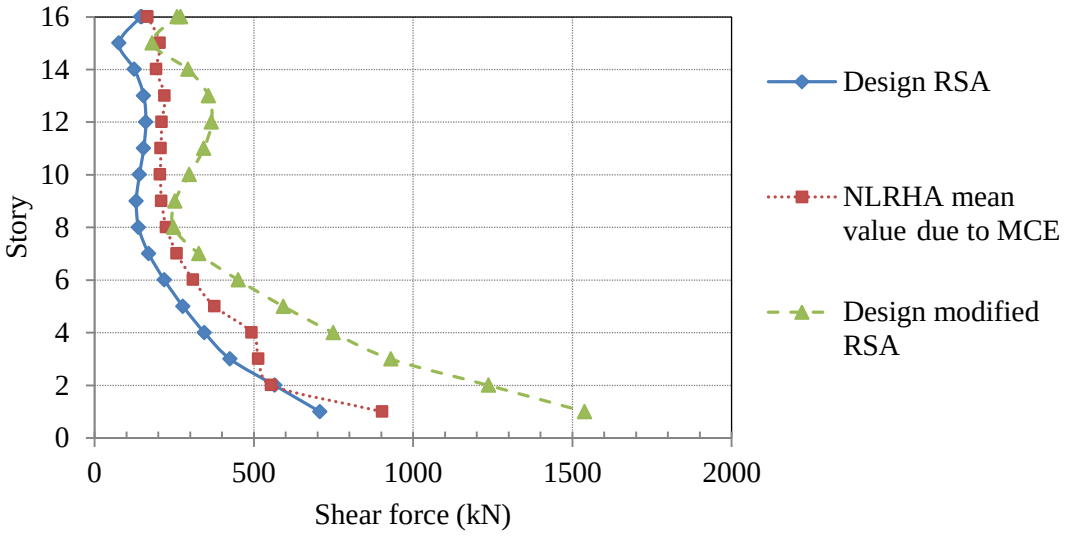

Figure 6.6 Seismic shear capacity and shear demand in Wall1

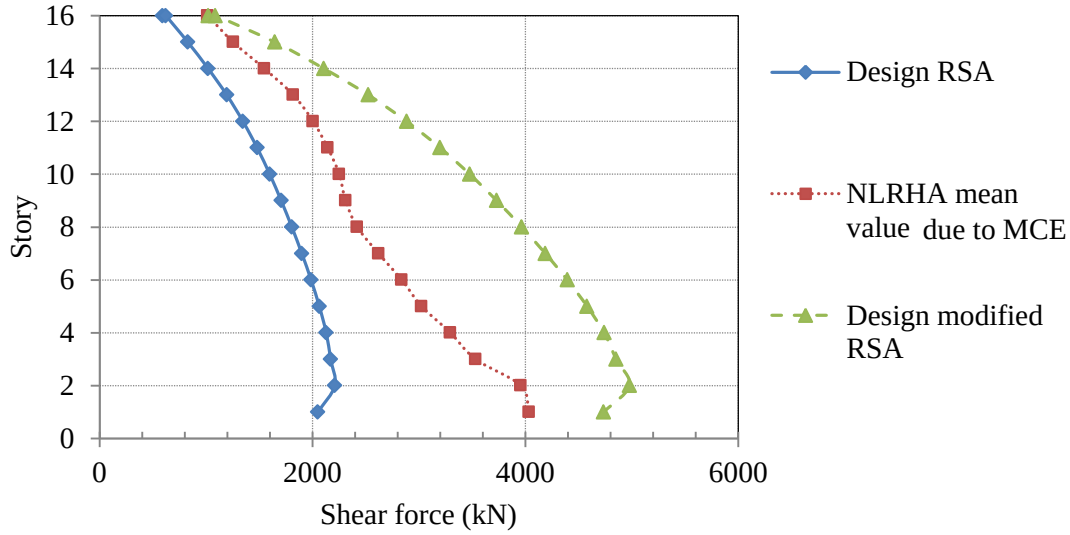

Figure 6.7 Seismic shear capacity and shear demand in Wall2 in N-S direction

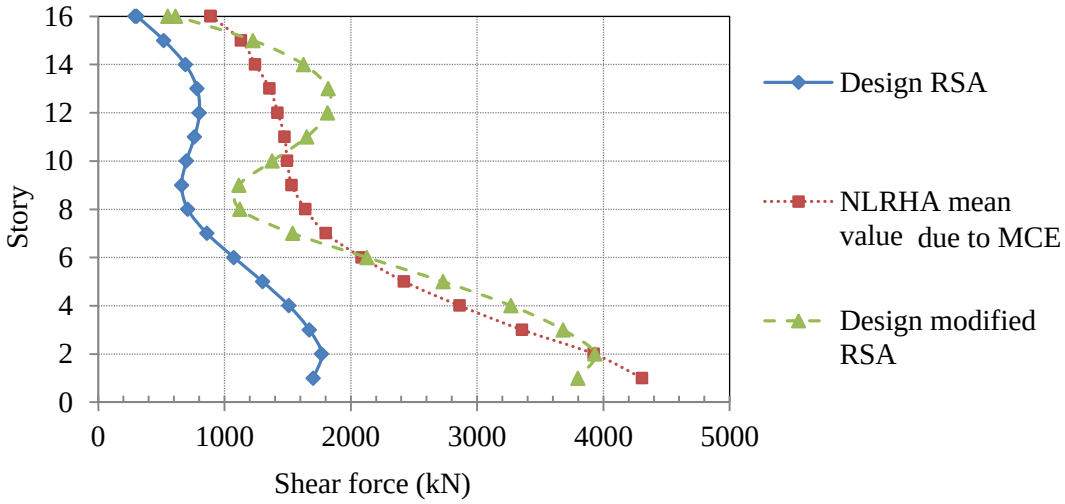

Figure 6.8 Seismic shear capacity and shear demand in Wall2 in E-W direction

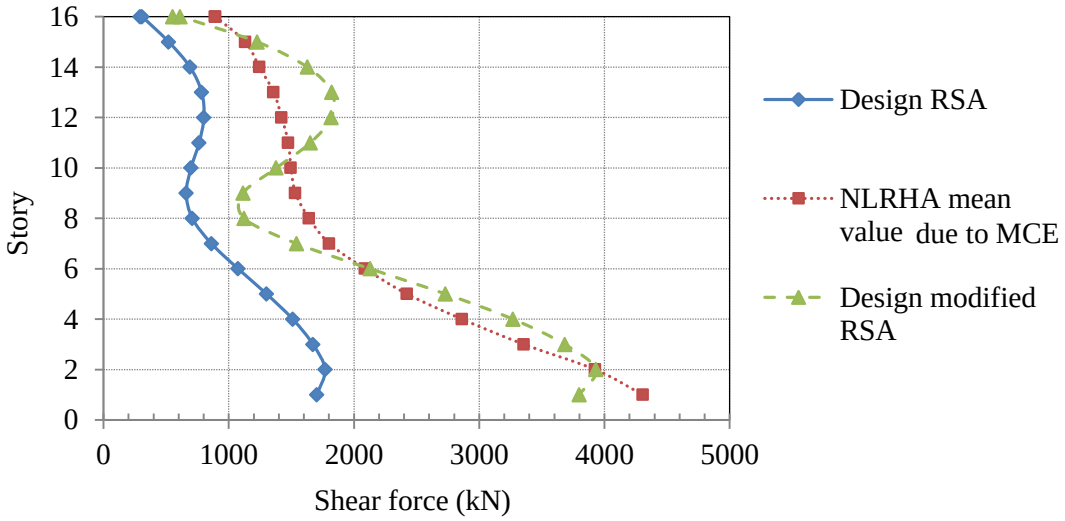

Figure 6.9 Seismic shear capacity and shear demand in Wall3 in N-S direction

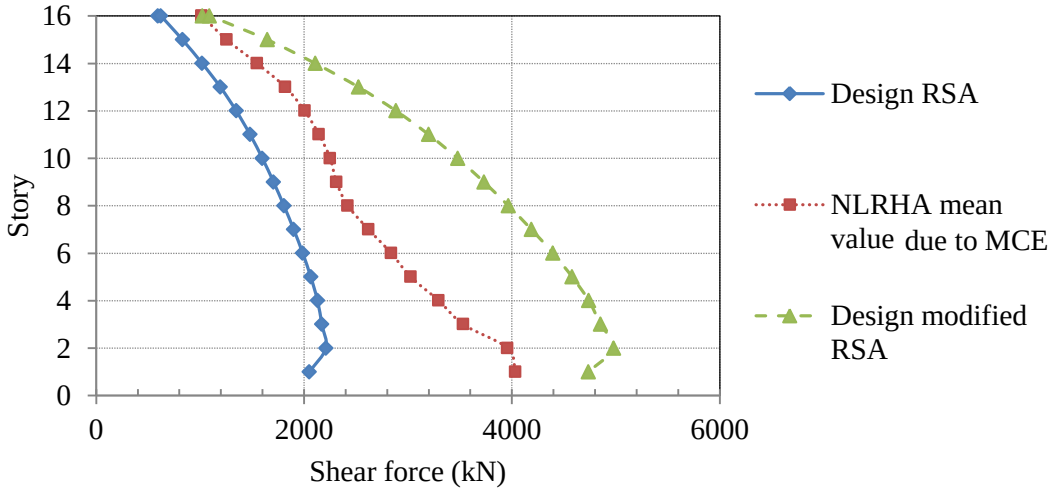

Figure 6.10 Seismic shear capacity and shear demand in Wall3 in E-W direction

CHAPTER VII
CONCLUSIONS AND RECOMMENDATIONS

By using the 16-story case-study building, the following conclusions can be drawn:

1. RSA procedure prescribed in the current Thai seismic design code (based on ASCE7-05), in which the responses of every vibration modes are divided by "R_{eff}" factor, underestimates the demands in shear wall elements. The best estimation of seismic demands obtained from NLRHA could be as high as 2 time the corresponding demands from RSA procedure for wall 2 throughout the entire height of the wall.
2. RSA procedure underestimates the story drift ratios in E-W direction, which is predominated by frame action, and overestimates the story drift ratios in N-S direction, which is predominated by shear wall action. The maximum story drift ratios of the building in both E-W and N-S directions are within the limit set by ASCE07-05.
3. For the performance of the building, inelastic analysis results show that seismic shear failure is expected to occur in the shear wall elements if the walls were designed to resist the seismic shear demand in RSA procedure, whereas the flexural responses of the wall measured in term of wall rotation satisfy all performance levels namely immediate occupancy (IO), life safety (LS) and collapse prevention (CP) performance levels. Four of the plastic hinge rotations of the yielded columns at floor 16 exceed admissible rotation from the ASCE41-06 for the CP performance level among all the yielded columns on floor 16, and the rests satisfy LS performance level, whereas all the yielded columns in the first floor are within IO performance level.
4. To avoid shear failure in the shear wall elements, a modified RSA procedure adapted from Priestly and Amaris (2002) has been implemented. In this new method, only the responses of the first vibration mode of the translational and

torsional mode are divided by "R_{eff}". The results indicate that this new method works quite well in estimating the seismic shear demands in shear walls; the shear capacity of the walls is now exceeding the seismic shear demand from NLRHA if the walls were designed to resist the seismic shear demand in modified RSA procedure, so shear failure is no longer a problem. However, it overestimates the shear forces in wall2 (W2) and wall3 (W3) in N-S direction; the seismic shear demand from this modified RSA procedure is as high as 1.3 times the corresponding demand obtained from NLRHA.

Recommendations for future work:

To confirm the insufficiency of the RSA procedure prescribed in ASCE7-05 and the sufficiency of the modified RSA procedure, more works should be done based on different building configurations; unsymmetrical buildings, buildings with base isolation system. Building height can also be one of parameter to be considered in the next study.

In the modified RSA procedure, slightly change in the procedure such as use the "R_{eff}" in the first translational modes (both E-W and N-S directions) and first torsional mode instead of using the "R_{eff}" in the first translational mode (E-W direction only) and first torsional mode is suggested.

REFERENCES

ACI Committee 318, (2008), Building Code Requirements for Structural Concrete and Commentary, ACI 318-08.

American Society of Civil Engineers, (2005), Minimum Design Loads for Buildings and Other Structures, ASCE7-05.

American Society of Civil Engineers, (2006), Seismic Rehabilitation of the Existing Buildings, ASCE41-06.

Car, A.,J., (2007), Ruaumoko2D, Inelastic Dynamic Analysis, Department of Civil Engineering, University of Canterbury, Christchurch, New Zealand.

CEN (1998) – Eurocode EC8, Design of structures for earthquake resistance – part 1: General rules, seismic actions and rules for buildings, prEN – 1998 -1

Chopra, A. K. (2007). Dynamics of structures: Theory and applications to earthquake engineering. 3rd Edition. Upper Saddle River, NJ : Pearson Prentice Hall.

Chopra, A. K. and Goel, R. K. (2002). A modal pushover analysis procedure for estimating seismic demands for buildings. Earthquake Engineering and Structural Dynamics, 31(3): 561-582. DOI: 10.1002/eqe.144.

Clough, R. W. Benuska, K. L. and Wilson, E. L. (1965). Inelastic earthquake response of tall buildings.

Department of Public Work and Town & Contry Planning. (2009). Thai Seismic Design Code. DPT 1302-52.

EduPro Civil System, Inc. (2004). ProShake Ground Response Analysis Program. Version 1.1. User's Manual, Redmond, Washington.

Eibl, J., and Keintzel, E., (1988). Seismic shear forces in RC cantilever shear walls, Proceedings of ninth world conference on earthquake engineering 6: 2-9. Tokyo-Kyoto, Japan.

EI-Tawil, S., and Deierlein, G., Jin, L., (2001). Nonlinear analysis of mixed steel-concrete frames, Part I and II, Journal of Structural Engineering, June, 126(6).

ETABS, Extended 3D Analysis of Building System Software, Nonlinear Version 9.5.0 Computers and Structures, Inc.: Berkeley CA.

Faculty of Engineering. (2010). Chulalongkorn University, Seismic evaluation of reactor pool no.1 and its housing structure submitted to Thailand Institute of Nuclear Technology (Public organization).

Haselton, C. B., Liel, A. B., Lange, S. T., and Deierlein, G. G., (2007). Beam-column element model calibrated for predicting flexural response leading to global collapse of RC frame buildings, Report 2007/03, Pacific Earthquake Engineering Research Center 3.

International conference of building officials. (1997) Uniform Building Code, 2, Whittier, CA.

Keintzel, E., (1984). Ductility requirements for shear wall structures in seismic areas.

Klemencic, R., (2008). Performance based seismic design-rising, Structure magazine. 10-13.

Klemencic, R., Fry, J. A. and Hooper, J. D. (2006). Performance-based design of tall reinforced concrete ductile core wall systems, The Structural Design of Tall and Special Buildings 15(5): 571-579.

Klemencic, R., Fry, J. A. Hooper, J. D. and Morgen, B. G. (2007). Performance-based design of ductile concrete core wall buildings—issues to consider before detailed analysis, The Structural Design of Tall and Special Buildings 16(5): 599-614.

Los Angeles Tall Building Structural Design Council (2005), An alternative procedure for seismic analysis and design of tall building located in the Los Angeles Region Los Angeles Tall Buildings, Structural design council Los Angeles 27.

Lukkunaprasit, P., Chintanapakdee, C., Ruangrassamee, A., Palasri, C., Chareonyuth, M., and Anantanavanich, T. (2008). Damage to buildings due to earthquakes and considerations for building design in Bangkok, The 13th National Convention on Civil Engineering, STR 313-319.

Maffei, J., and Yuen, N., (2007). Seismic performance and design requirements for high-rise concrete buildings, Structure Magazine, April, 28-32.

Munir, A., and Warnitchai, P., (2012) The cause of unproportionately large higher mode contributions in the inelastic seismic responses of high-rise core-wall buildings Earthquake Engineering and Structural Dynamics, 41(15): 2195-2214, DOI: /10.1002eqe.2182.

Palasri, C., and Ruangrassamee, A., (2010), Probabilistic seismic hazard maps of Thailand, Journal of Earthquake and Tsunami, 4(4): 369-386.

Panagiotakos, T. B., and Fardis, M. N., (2001). Deformations of reinforced concrete members at yielding and ultimate, ACI Structural Journal, 98(2).

Perform-3D, Nonlinear Analysis and Performance Assessment for 3D Structures Software, Version 5.0.0. Computers and Structures, Inc.: Berkeley, CA.

Priestley, M. J. N., and Amaris, A. D., (2002). Dynamic amplification of seismic moments and shear forces in cantilever walls, Master's Thesis, ROSE School.

Reddiar, M.K.M., (2009), Stress-strain model of confined and unconfined concrete and stress-block parameters, Master's Thesis, Texas A&M University.

Sangarayakul, C., and Warnitchai, P., (2004). Approximate modal decomposition of inelastic dynamic responses of wall buildings, Earthquake engineering and structural dynamics, 33(9): 999-1022.

Sezen, H., (2000), Seismic behavior and modeling of reinforced concrete building columns, Doctoral dissertation, UC Berkeley.

Sullivan, T. J. Priestley, M. J. N. and Calvi, G. M. (2008). Estimating the higher- mode response of ductile structures, Journal of Earthquake Engineering 12(3): 456-472.

Tospol Kaewnurachadasorn. (2012). Seismic evaluation and retrofit of a bridge, Master's Thesis, Department of Civil Engineering, Faculty of Engineering, Chulalongkorn University.

Hiep Pham Tuan. (2008) Seismic design considerations for tall buildings. Master's Thesis, ROSE School.

Zekioglu, A., Willford, M., Jin, L., and Melek, M., (2007). Case study using the Los Angeles tall buildings structural design council guidelines: 40-storey concrete core wall building, Structural Design of Tall and Special Buildings, 16: 583-597.

APPENDICES

APPENDIX A

The first 20 mode shapes and periods of the case-study building

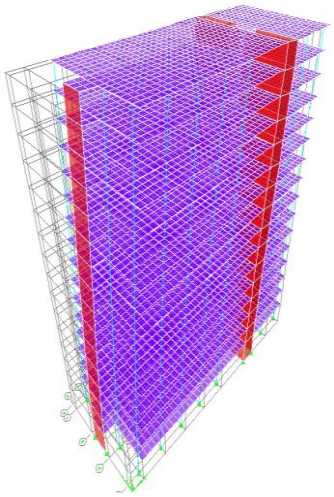

1st mode, T_1 = 2.92s

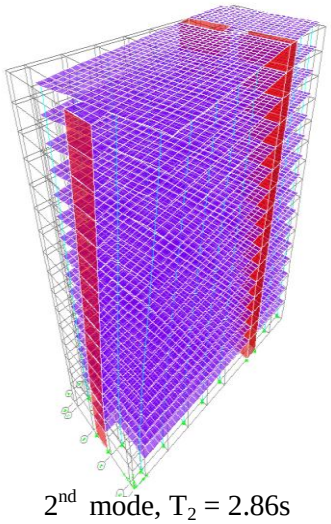

2nd mode, T_2 = 2.86s

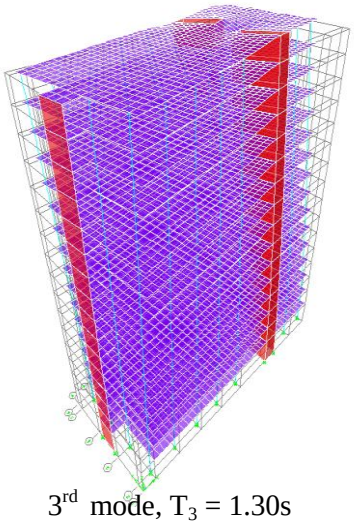

3rd mode, T_3 = 1.30s

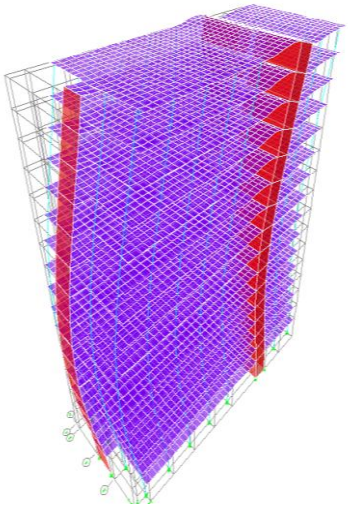

4th mode, T_4 = 0.70s

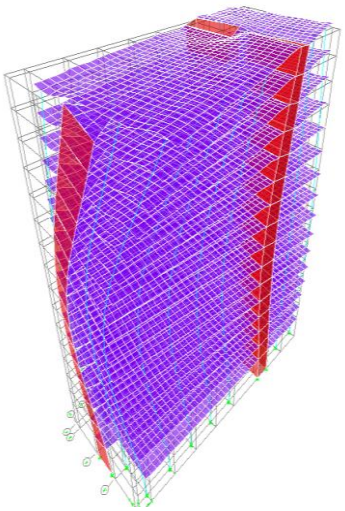

5th mode, T_5 = 0.67s

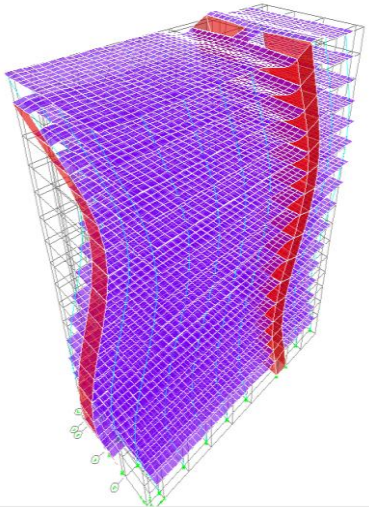

6th mode, T_6 = 0.32s

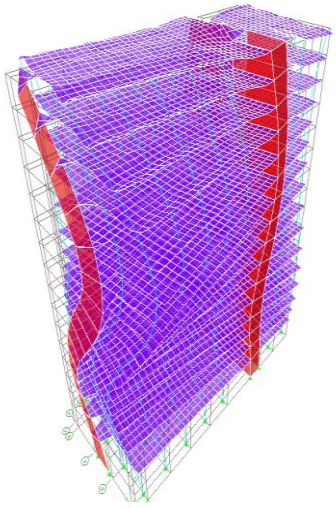

7th mode, T_7 = 0.29s

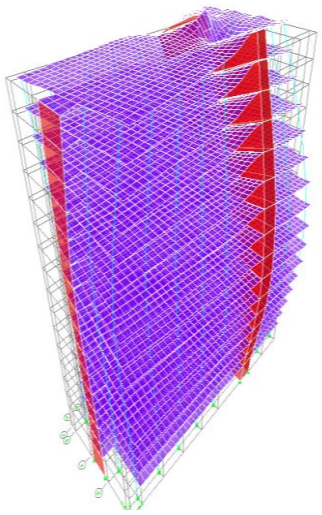

8th mode, T_8 = 0.27s

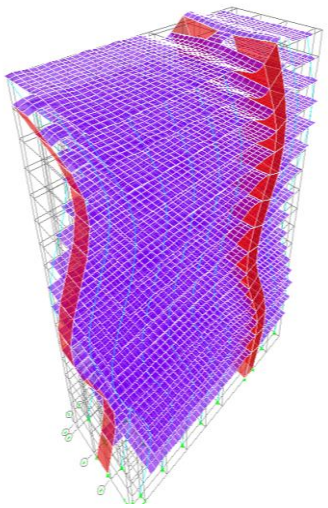

9th mode, T_9 = 0.20s

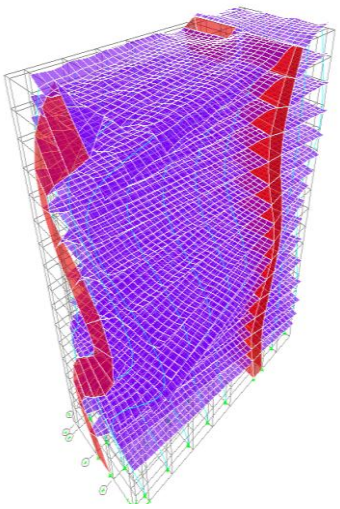

10^{th} mode, T_{10} = 0.17s

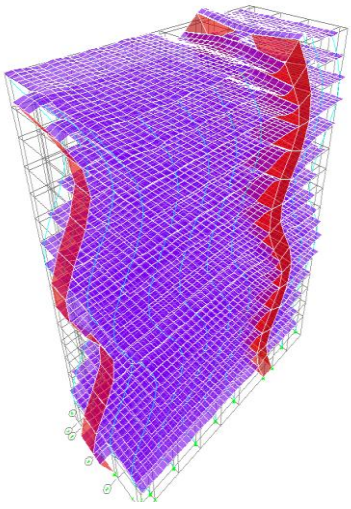

11^{th} mode, T_{11} = 0.15s

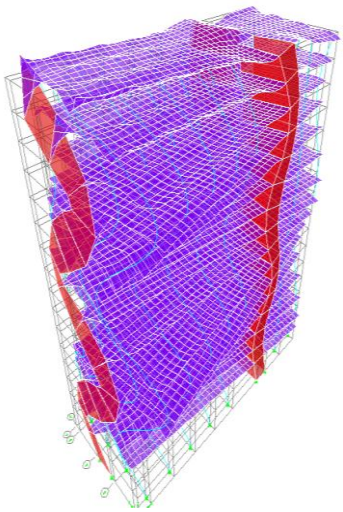

12^{th} mode, T_{12} = 0.113s

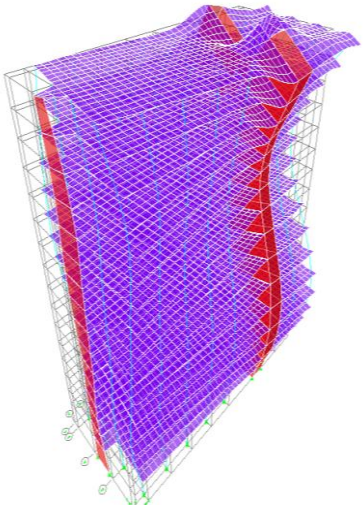

13^{th} mode, T_{14} = 0.112s

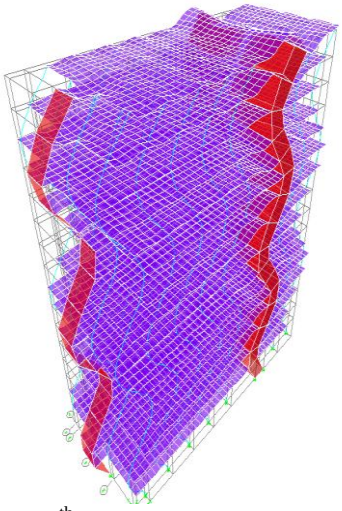

14^{th} mode, T_{14} = 0.111s

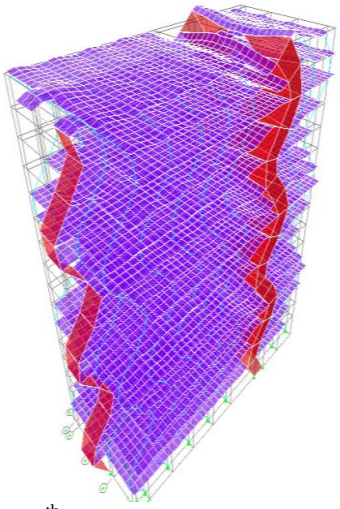

15^{th} mode, T_{15} = 0.092s

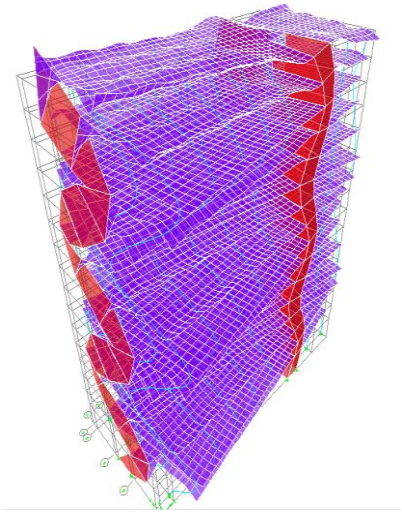

16^{th} mode, T_{16} = 0.082s

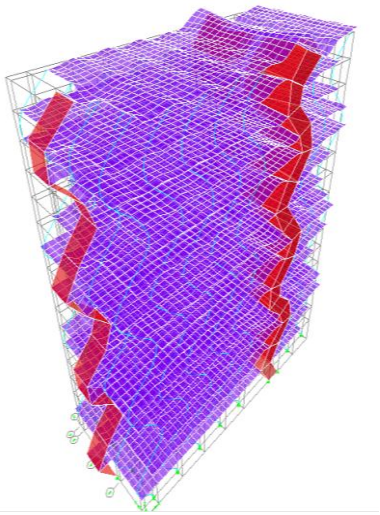

17^{th} mode, T_{17} = 0.078s

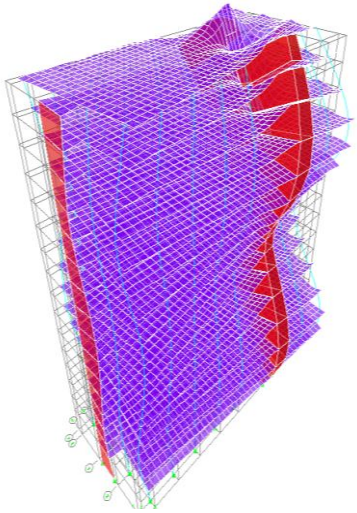

18^{th} mode, T_{18} = 0.069s

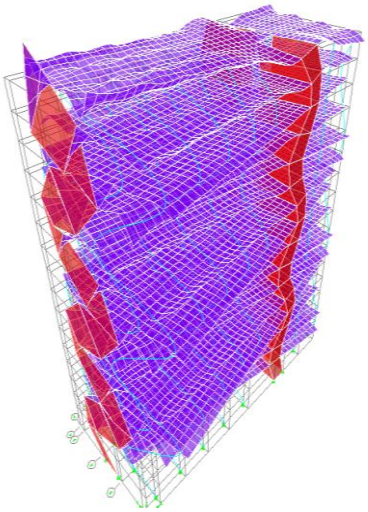

19th mode, T_{19} = 0.066s

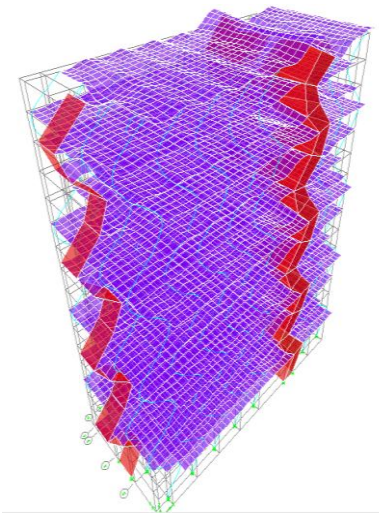

20th mode, T_{20} = 0.063s

APPENDIX B

MatLab codes
(Response spectrum of the 7 ground motions and P-M diagrams of column and wall)

Response spectrum of the 7 ground motions

```
% Response Spectrum using Newmark's Method %
%%%%%%%%%%%%%%%%%%%%%%%%%%%%%%%%%%%%%%%%%%%%%%%%%%%%%%%%%%%%%%%%

clc
clear all

% Average acceleration method
gamma=0.5;
belta=0.25;

zeta=0.05;

% input ground motions
for ground_motion=1:7
    if ground_motion==1
    Ground_motions_1;
      TSPAN=0.005;
    else if ground_motion==2
           Ground_motions_2;
             TSPAN=0.004;
        else if ground_motion==3
                Ground_motions_3;
                  TSPAN=0.01;
            else if ground_motion==4
                    Ground_motions_4;
                      TSPAN=0.005;
                else if ground_motion==5
                        Ground_motions_5;
                          TSPAN=0.01;
                    else if ground_motion==6
                            Ground_motions_6;
                              TSPAN=0.004;
                        else Ground_motions_7;
                              TSPAN=0.02;
                        end
                    end
                end
            end
        end
    end

    Ag=Ag*9.81*1.5;
    Agt=zeros(32768,1);
        for row=1:4096
            Agr=Ag(row,:);
            for column=1:8
             Agt(column+8*(row-1))=Agt(column+8*(row-1))+Agr(column);
            end
        end
    p=-Agt;
    p0=-Agt(1);

    for Tn=0:0.05:3
    l=Tn/0.05+1;
```

```
    l=floor(l);
        if Tn==2.15
        l=l+1;
        end
    m=1;
% independent of m
    wn=2*pi()/Tn;
    c=2*zeta*wn;
    k=wn^2;
    u0=0;
    v0=0;

% Initial calculation

    a0=(p0-c*v0-k*u0)/m;              % Initial relative acceleration
    kbar=k+gamma*c/(belta*TSPAN)+m/(belta*TSPAN^2);
    a_c=m/(belta*TSPAN)+c*gamma/belta;
    b=m/(2*belta)+TSPAN*c*(gamma/(2*belta)-1);

    u=zeros(32768,1);
    v=zeros(32768,1);
    a=zeros(32768,1);
    u(1)=u0;
    v(1)=v0;
    a(1)=a0;

% Calculation for time step i
        for i=2:32768;
            delta_p_bar(i)=p(i)-p(i-1)+a_c*v(i-1)+b*a(i-1);
            delta_u(i)=delta_p_bar(i)/kbar;
            delta_v(i)=delta_u(i)*gamma/(belta*TSPAN)-v(i-
1)*gamma/belta+TSPAN*a(i-1)*(1-gamma/(2*belta));
            delta_a(i)=delta_u(i)/(belta*TSPAN^2)-v(i-
1)/(belta*TSPAN)-a(i-1)/(2*belta);
            u(i)=delta_u(i)+u(i-1);
            v(i)=delta_v(i)+v(i-1);
            a(i)=delta_a(i)+a(i-1);
        end

    U=max(u);
    V_pseudo=wn*U;
    A_pseudo=wn^2*U;

    peak_u(l)=U;
    peak_V_pseudo(l)=V_pseudo;
    peak_A_pseudo(l)=A_pseudo;

    end
    if ground_motion==1
        peak_u_1=peak_u;
        peak_V_pseudo_1=peak_V_pseudo;
        peak_A_pseudo_1= peak_A_pseudo;
    else if ground_motion==2
            peak_u_2=peak_u;
            peak_V_pseudo_2=peak_V_pseudo;
            peak_A_pseudo_2= peak_A_pseudo;
        else if ground_motion==3
```

```
                peak_u_3=peak_u;
                peak_V_pseudo_3=peak_V_pseudo;
                peak_A_pseudo_3= peak_A_pseudo;
            else if ground_motion==4
                    peak_u_4=peak_u;
                    peak_V_pseudo_4=peak_V_pseudo;
                    peak_A_pseudo_4= peak_A_pseudo;
                else if ground_motion==5
                        peak_u_5=peak_u;
                        peak_V_pseudo_5=peak_V_pseudo;
                        peak_A_pseudo_5= peak_A_pseudo;
                    else if ground_motion==6
                            peak_u_6=peak_u;
                            peak_V_pseudo_6=peak_V_pseudo;
                            peak_A_pseudo_6= peak_A_pseudo;
                        else    peak_u_7=peak_u;
                                peak_V_pseudo_7=peak_V_pseudo;
                                peak_A_pseudo_7= peak_A_pseudo;
                        end
                    end
                end
            end
        end
    end
end

%plot graphic

Tn=0:0.05:3;
Tn=transpose(Tn);

plot(Tn,peak_u_1,Tn,peak_u_2,Tn,peak_u_3,Tn,peak_u_4,Tn,peak_u_5,Tn,p
eak_u_6,Tn,peak_u_7)
xlabel('Natural Period (sec)');
ylabel('Peak deformation (m)');
legend('1999 Kocaeli, Maslak','1999 Chi-Chi, TTN 042','1994
Northridge, Wrightwood','1989 Loma Prieta, Piedmont','1971 San
Fernando, Cedar Springs','1999 Chi-Chi, TAP 077','1992 Landers, San
Gabriel');
grid on

figure;
plot(Tn,peak_V_pseudo_1,Tn,peak_V_pseudo_2,Tn,peak_V_pseudo_3,Tn,peak
_V_pseudo_4,Tn,peak_V_pseudo_5,Tn,peak_V_pseudo_6,Tn,peak_V_pseudo_7)
xlabel('Natural Period (sec)');
ylabel('Pseudo-velocity (m/s)');
legend('1999 Kocaeli, Maslak','1999 Chi-Chi, TTN 042','1994
Northridge, Wrightwood','1989 Loma Prieta, Piedmont','1971 San
Fernando, Cedar Springs','1999 Chi-Chi, TAP 077','1992 Landers, San
Gabriel');
grid on

figure;
plot(Tn,peak_A_pseudo_1/9.81,Tn,peak_A_pseudo_2/9.81,Tn,peak_A_pseudo
_3/9.81,Tn,peak_A_pseudo_4/9.81,Tn,peak_A_pseudo_5/9.81,Tn,peak_A_pse
udo_6/9.81,Tn,peak_A_pseudo_7/9.81)
xlabel('Natural Period (sec)');
```

```
ylabel('Pseudo-acceleration (g)');
legend('1999 Kocaeli, Maslak','1999 Chi-Chi, TTN 042','1994
Northridge, Wrightwood','1989 Loma Prieta, Piedmont','1971 San
Fernando, Cedar Springs','1999 Chi-Chi, TAP 077','1992 Landers, San
Gabriel');
grid on
```

P-M diagrams for a rectangular cross section of column and wall

```
%%% In put %%%%%
%%%%%%%%%%%%%%%

clc;
clear all;

fc = 32 ;                %Concrete compressive strength in MPa
fy = 400;                %Reinforcement strength in MPa
Es = 200000;             %Young modulus of rebar(reinforcement) in MPa
b = 30;                  %Width of the cross section in cm
h = 90;                  %Height of the cross section in cm
Ag = b*h;                %Cross sectional area in cm2
n = 6;                   %number of layers of reinforcement
d = [82.5 67.5 52.5 37.5 22.5 7.5];  %Distance of extreme-compression
fiber to the centroid of the rebar in cm

%Assume that the centroid of the gross section located at the mid
height of the cross section h/2

%%% Main program %%%%%
%%%%%%%%%%%%%%%%%%%%%

for ro = 0.01:0.005:0.08;        %Total reinforcement ratio
    Ast = ro*Ag;                 %Total area of reinforcements in cm2
    As =Ast/n; %Assume reinforcement area equal in each layers in cm2

    P0=(0.85*fc*(Ag-Ast)+fy*Ast)/100;         %Concentric compressive
axial-load capacity
    Pnt=-fy*Ast/100;                          %Axial tension capacity
    clear phiPn phiMn ro_t ro_c;

    for Z=-100:0.25:1;             %Iteration process
        t=4*(Z+101)-3;
        As_t=0;                    %Reinforcement area in Tension
        As_c=0;                    %Reinforcement area in Compression

        apsilon_y=fy/Es;
        c=0.003*d(1)/(0.003-Z*apsilon_y);
        for i=1:n
            apsilon_s(i)=(c-d(i))*0.003/c;
            if apsilon_s(i)<0
                As_t=As_t+As;
            else As_c=As_c+As;
            end
            fs(i)=apsilon_s(i)*Es;
            if fs(i)>fy
                fs(i)=fy;
            else if fs(i)<-fy
                    fs(i)=-fy;
                end
            end
            if fc<28;
                belta = 0.85;
```

```
            else belta=max(0.65,0.85-0.05*(fc-28)/7);
            end
            a=min(h,belta*c);
            Cc=0.85*fc*a*b/100;
            if a<d(i)
                Fs(i)=fs(i)*As/100;
            else Fs(i)=(fs(i)-0.85*fc)*As/100;
            end
        end
        ro_t(t)=As_t/Ag;              %Tension reinforcement ratio
        ro_c(t)=As_c/Ag;              %Compression reinforcement ratio
        Pn(t)=Cc+sum(Fs);             %Axial force P
        Mn(t)=(Cc*(h/2-a/2)+sum(Fs.*(h/2-d)))/100; %Bending moments M
       if Pn(t)>0.8*P0
           Pn(t)=0.8*P0;
       end

       %Determine capacity reduction factor phi
        if Z>=-1
            phi(t)=0.65;
        else if Z<=-2.5
                phi(t)=0.9;
            else phi(t)=0.65+0.25*(1/(c/d(1))-5/3);
            end
        end

    end
    phiPn=phi.*Pn;
    phiMn=phi.*Mn;
    ro_t=[ro ro_t 0];
    ro_c=[0 ro_c ro];
    phiPn=[0.9*Pnt,phiPn,0.65*0.8*P0];
    phiMn=[0,phiMn,0];

%Determine P-M diagram in each case of ro = 1%(min) 1.5% .....8%(max)
 if ro==0.01
        phiPn1=phiPn;
        phiMn1=phiMn;
        ro_t1=ro_t;
        ro_c1=ro_c;
    else if ro==0.015
        phiPn2=phiPn;
        phiMn2=phiMn;
        ro_t2=ro_t;
        ro_c2=ro_c;
        else if ro==0.02
            phiPn3=phiPn;
            phiMn3=phiMn;
            ro_t3=ro_t;
            ro_c3=ro_c;
            else if ro==0.025
                phiPn4=phiPn;
                phiMn4=phiMn;
                ro_t4=ro_t;
                ro_c4=ro_c;
                else if ro==0.03
                    phiPn5=phiPn;
```

```
phiMn5=phiMn;
ro_t5=ro_t;
ro_c5=ro_c;
else if ro==0.035
    phiPn6=phiPn;
    phiMn6=phiMn;
    ro_t6=ro_t;
    ro_c6=ro_c;
    else if ro==0.04
        phiPn7=phiPn;
        phiMn7=phiMn;
        ro_t7=ro_t;
        ro_c7=ro_c;
        else if ro<0.05 && ro>0.04
            phiPn8=phiPn;
            phiMn8=phiMn;
            ro_t8=ro_t;
            ro_c8=ro_c;
            else if ro==0.05
                phiPn9=phiPn;
                phiMn9=phiMn;
                ro_t9=ro_t;
                ro_c9=ro_c;
                else if ro==0.055
                    phiPn10=phiPn;
                    phiMn10=phiMn;
                    ro_t10=ro_t;
                    ro_c10=ro_c;
                    else if ro<0.065 && ro>0.055
                        phiPn11=phiPn;
                        phiMn11=phiMn;
                        ro_t11=ro_t;
                        ro_c11=ro_c;
                        else if ro==0.065
                            phiPn12=phiPn;
                            phiMn12=phiMn;
                            ro_t12=ro_t;
                            ro_c12=ro_c;
                         else if ro<0.075 && ro>0.065
                                    phiPn13=phiPn;
                                    phiMn13=phiMn;
                                    ro_t13=ro_t;
                                    ro_c13=ro_c;
                                 else if ro==0.075
                                     phiPn14=phiPn;
                                     phiMn14=phiMn;
                                       ro_t14=ro_t;
                                       ro_c14=ro_c;
                                     else if ro==0.08
                                       phiPn15=phiPn;
                                       phiMn15=phiMn;
                                         ro_t15=ro_t;
                                         ro_c15=ro_c;
                                            end
                                      end
                                 end
                            end
                        end
```

```
                                        end
                                    end
                                end
                            end
                        end
                    end
                end
            end
        end
    end
end

% Extract P-M for P>0 to create M-M diagram.............

i1=0;
i2=0;
i3=0;
i4=0;
i5=0;
i6=0;
i7=0;
i8=0;
i9=0;
i10=0;
i11=0;
i12=0;
i13=0;
i14=0;
i15=0;
for k=1:407

    if phiPn1(k)>0
        i1=i1+1;
        A1(i1)=phiPn1(k);
        B1(i1)=phiMn1(k);
    end

    if phiPn2(k)>0
        i2=i2+1;
        A2(i2)=phiPn2(k);
        B2(i2)=phiMn2(k);
    end

    if phiPn3(k)>0
        i3=i3+1;
        A3(i3)=phiPn3(k);
        B3(i3)=phiMn3(k);
    end

    if phiPn4(k)>0
        i4=i4+1;
        A4(i4)=phiPn4(k);
        B4(i4)=phiMn4(k);
    end

    if phiPn5(k)>0
        i5=i5+1;
```

```
    A5(i5)=phiPn5(k);
    B5(i5)=phiMn5(k);
end

if phiPn6(k)>0
    i6=i6+1;
    A6(i6)=phiPn6(k);
    B6(i6)=phiMn6(k);
end

if phiPn7(k)>0
    i7=i7+1;
    A7(i7)=phiPn7(k);
    B7(i7)=phiMn7(k);
end

if phiPn8(k)>0
    i8=i8+1;
    A8(i8)=phiPn8(k);
    B8(i8)=phiMn8(k);
end

if phiPn9(k)>0
    i9=i9+1;
    A9(i9)=phiPn9(k);
    B9(i9)=phiMn9(k);
end

if phiPn10(k)>0
    i10=i10+1;
    A10(i10)=phiPn10(k);
    B10(i10)=phiMn10(k);
end

if phiPn11(k)>0
    i11=i11+1;
    A11(i11)=phiPn11(k);
    B11(i11)=phiMn11(k);
end

if phiPn12(k)>0
    i12=i12+1;
    A12(i12)=phiPn12(k);
    B12(i12)=phiMn12(k);
end

if phiPn13(k)>0
    i13=i13+1;
    A13(i13)=phiPn13(k);
    B13(i13)=phiMn13(k);
end

if phiPn14(k)>0
    i14=i14+1;
    A14(i14)=phiPn14(k);
    B14(i14)=phiMn14(k);
```

```
    end

    if phiPn15(k)>0
        i15=i15+1;
        A15(i15)=phiPn15(k);
        B15(i15)=phiMn15(k);
    end
end

%Plot figures

plot
(phiMn1,phiPn1,phiMn2,phiPn2,phiMn3,phiPn3,phiMn4,phiPn4,phiMn5,phiPn
5,phiMn6,phiPn6,phiMn7,phiPn7,phiMn8,phiPn8,phiMn9,phiPn9,phiMn10,phi
Pn10,phiMn11,phiPn11,phiMn12,phiPn12,phiMn13,phiPn13,phiMn14,phiPn14,
phiMn15,phiPn15);
legend('\rho=0.010','\rho=0.015','\rho=0.020','\rho=0.025','\rho=0.03
0','\rho=0.035','\rho=0.040','\rho=0.045','\rho=0.050','\rho=0.055','
\rho=0.060','\rho=0.065','\rho=0.070','\rho=0.075','\rho=0.080')
xlabel('\phiMn (Ton-m)')
ylabel('\phiPn (Ton)')
title('P-M diagram in strong axis')
grid minor
```

APPENDIX C

Time history results of simple models (2-story and 16-story walls) in PERFORM-3D

2-story shear wall model –
Period: T_{LRHA} = 0.8499s, T_{NLRHA1} = 0.8124s, T_{NLRHA2} = 0.858s, T_{NLRHA3} = 0.8124s

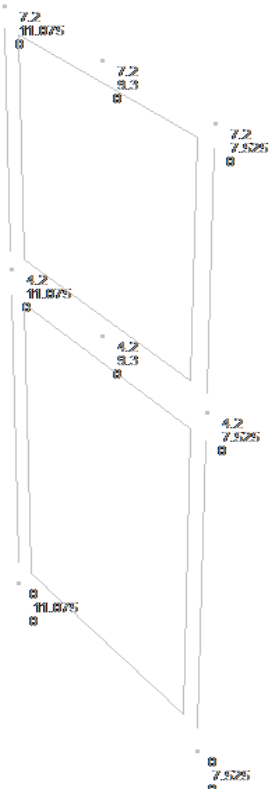

Figure C.1 2-story shear wall model in PERFORM-3D

This simple model is used to perform 4 different analyses, one of which is linear response history analysis and three of the rest are nonlinear response history analyses with different nonlinear material models. The first nonlinear model is the model in which the steel rebar is included and tension in concrete model is neglected, whereas the second model is the model in which the steel rebar is excluded and tension in concrete model is included and equal to the compressive strength of the concrete, and the third model is the model in which both the steel rebar and tension equalling to the compressive strength of the concrete in concrete model are included. As shown in Figure C2 and Figure C3, the linear model and the second nonlinear model coincide before yielding occur, while the third nonlinear model is slightly different caused by the effect of the steel rebar. The first nonlinear model has longer period since the stiffness reduces in hysteretic loop caused by the opening and closing of concrete in cyclic behavior.

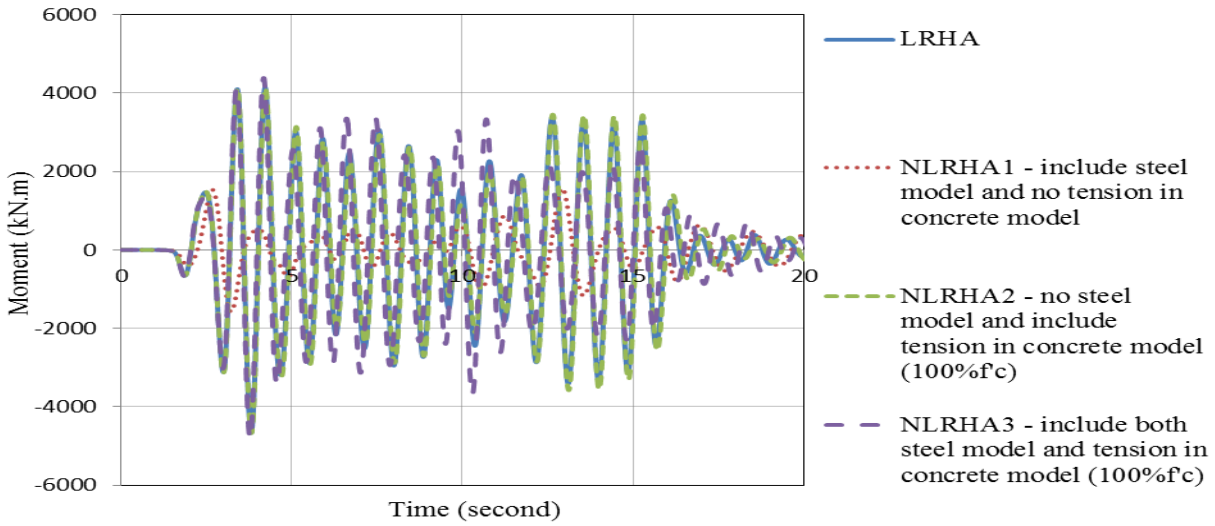

Figure C.2 Time history response of the 2-story shear wall model due to MCE5 scaled by 0.05 – story 1

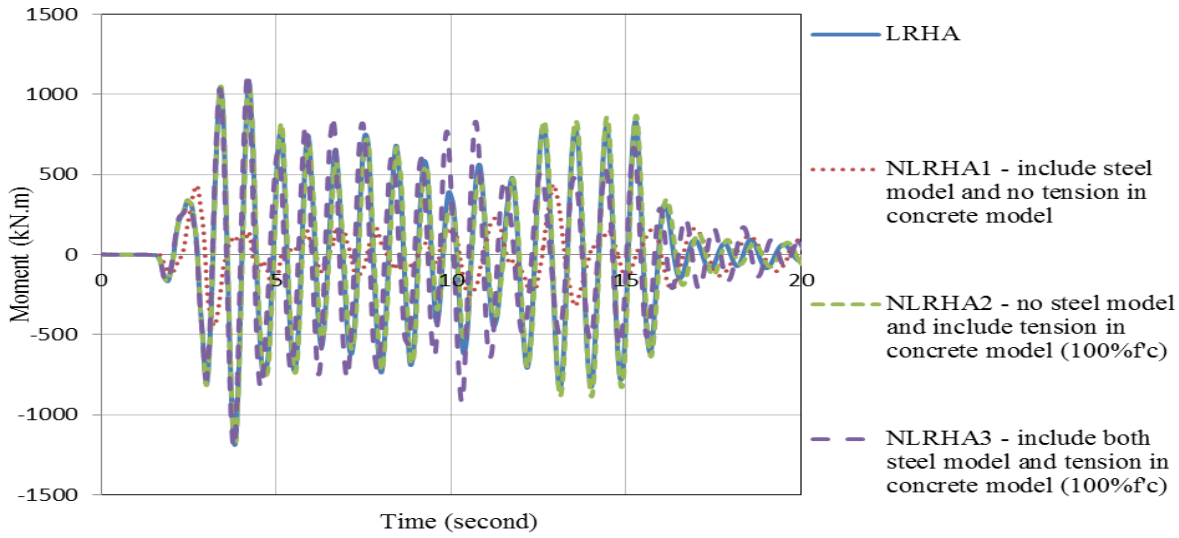

Figure C.3 Time history response of the 2-story shear wall model due to MCE5 scaled by 0.05 – story 2

To study the behaviour of this simple model after yielding, the magnitude of ground motions are increase by 9 times. The results indicate that after yielding, nonlinear models (the second and the third model) start to separate from the linear model and limited to the yielding moment as illustrated in Figure C4 and C5. The first nonlinear model is also limited to its yielding moment.

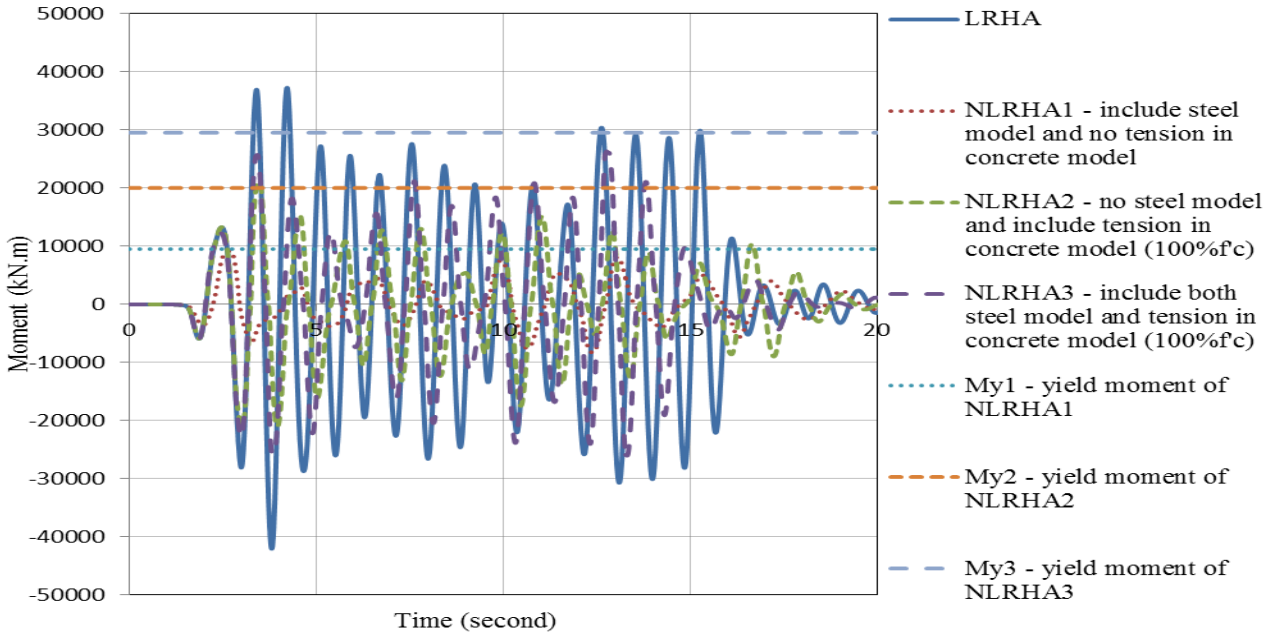

Figure C.4 Time history response of the 2-story shear wall model due to MCE5 scaled by 0.45 – story 1

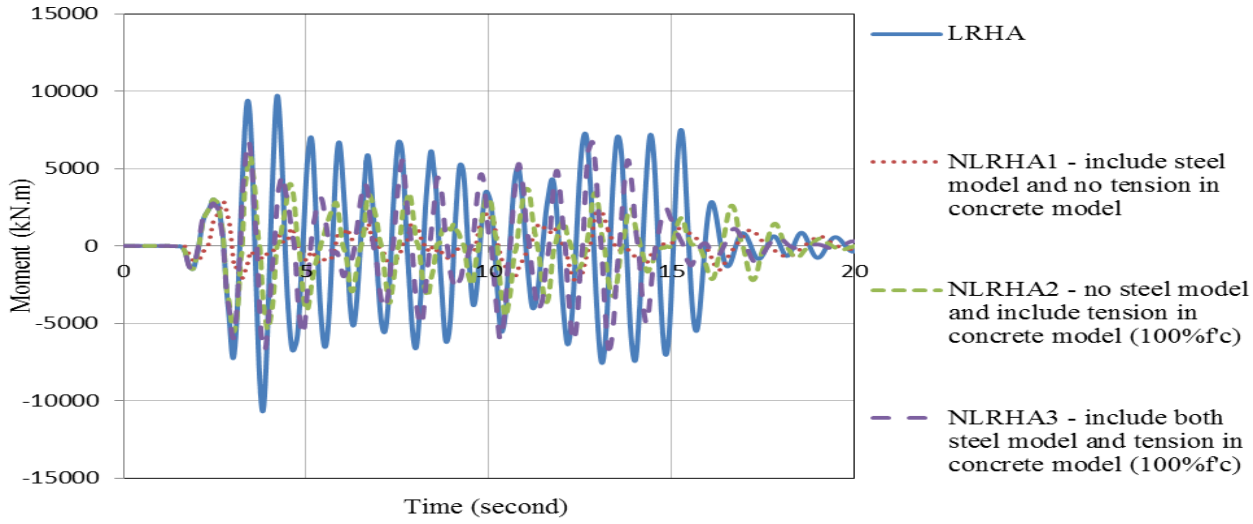

Figure C.5 Time history response of the 2-story shear wall model due to MCE5 scaled by 0.45 – story 2

Figure C6 and Figure C7 show the seismic moment of the simple model due to different magnitudes of ground motions before and after yielding in the first and second story. The results show that before yielding, scaling the ground motion up by a factor of 3 will also increase the seismic demand of the wall in the first and second story by 3 times, on the other hand, after yielding, scaling the ground motion up by a factor of 3 will no longer increase the seismic demand of the wall by 3 times anymore

since the demand of the wall is limited to the yielding moment in the first story, moreover, in the second story, even the wall does not yield yet, but the demand does not increase by 3 times; this is due to the effect of yielding in the first story which limit the demand in the second story.

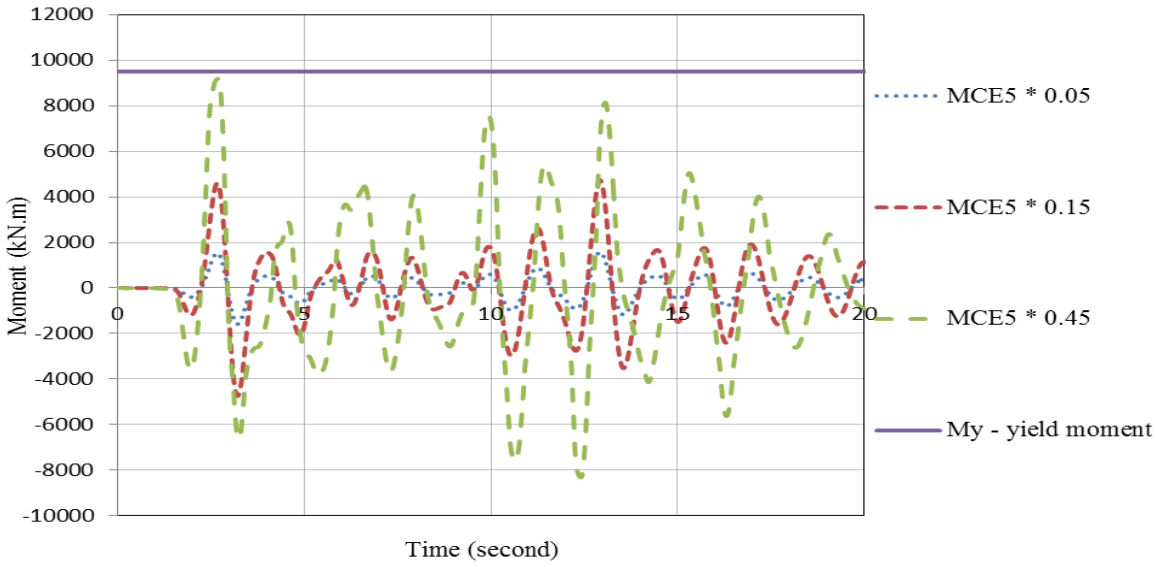

Figure C.6 Time history response of the 2-story shear wall – NLRHA1 model due to MCE5 – story 1

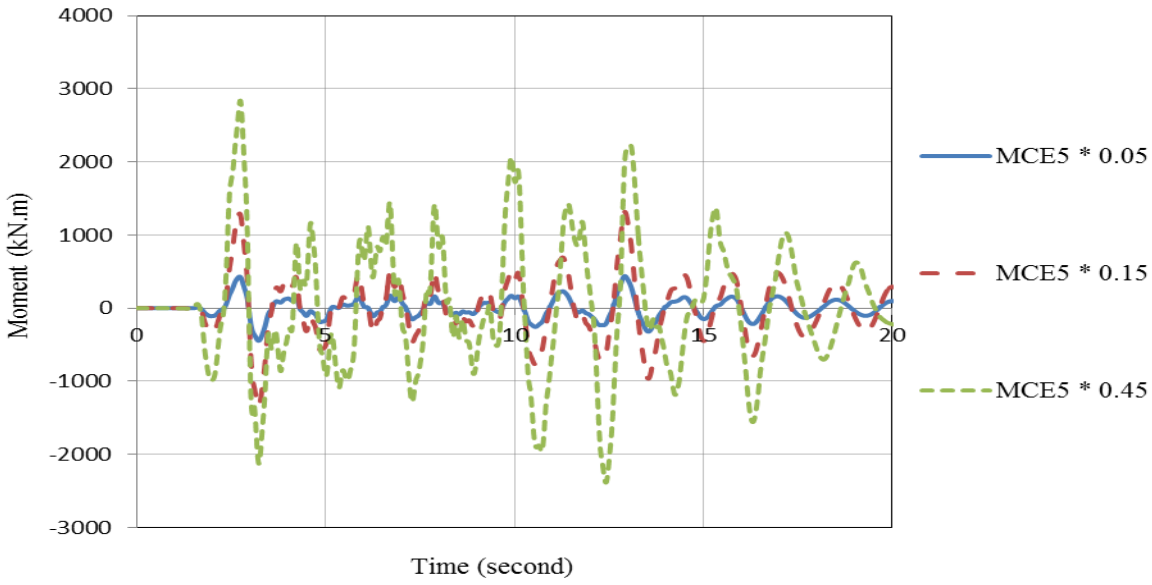

Figure C.7 Time history response of the 2-story shear wall – NLRHA1 model due to MCE5 – story 2

16-story shear wall model –
Period: T_{LRHA} = 0.8251s, T_{NLRHA1} = 0.782s, T_{NLRHA2} = 0.8342s, T_{NLRHA3} = 0.782s

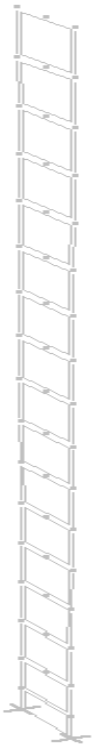

Figure C.8 16-story shear wall model in PERFORM-3D

The same observation as the 2-story model can be found for this 16-story model. Before yielding occurs, the linear and nonlinear models (NLRHA2) coincide, the NLRHA 3 which includes steel model is a little bit stiffer and so experiences higher demand, while the NLRHA 1 has longer period hence lower demand. After yielding, the nonlinear model started to separate from the linear model and the demand is limited to the yielding moment. Finally, the yielding in the first story limits or decreases the demand in other higher stories even though there is no yielding in those stories.

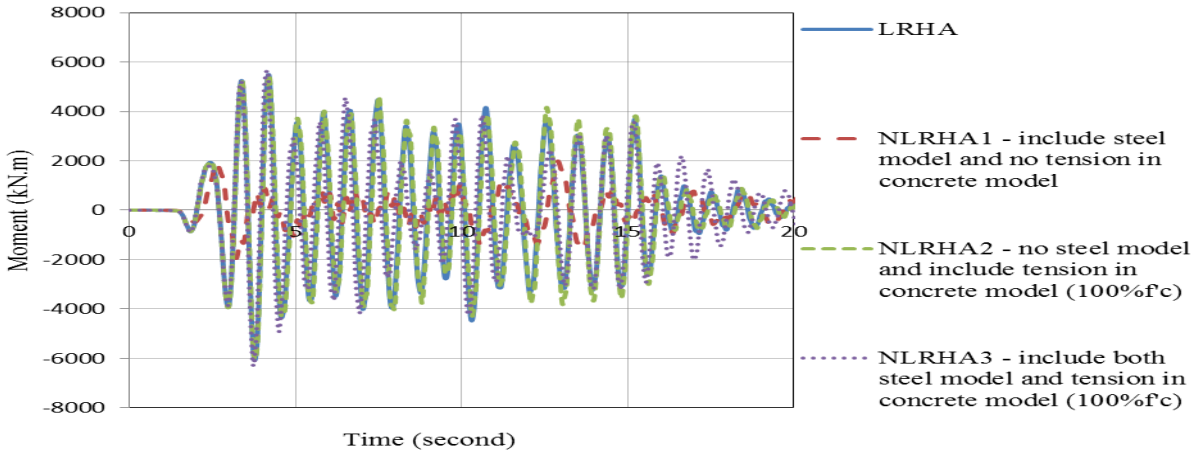

Figure C.9 Time history response of the 16-story shear wall model due to MCE5 scaled by 1.5 – story 1

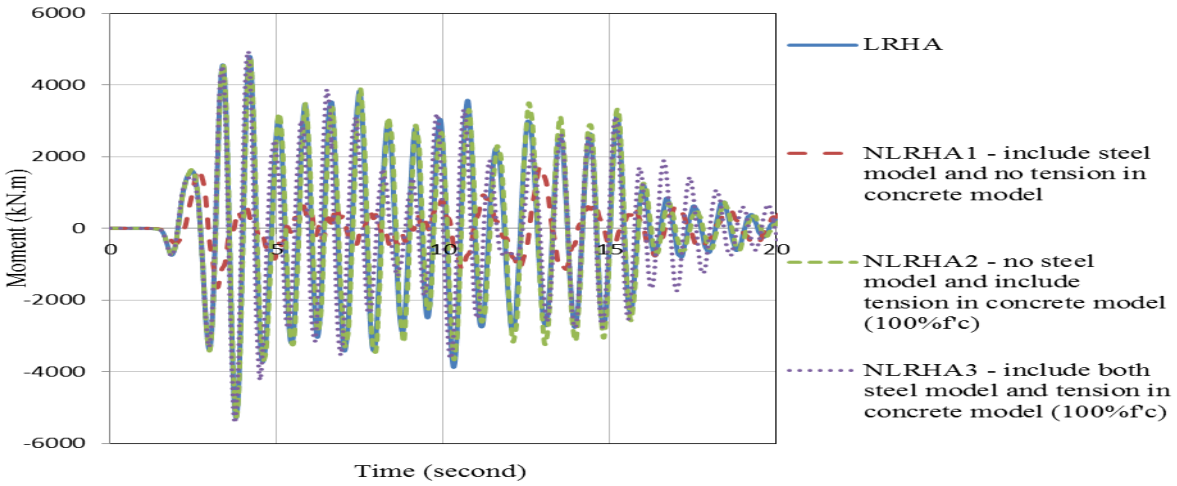

Figure C.10 Time history response of the 16-story shear wall model due to MCE5 scaled by 1.5 – story 2

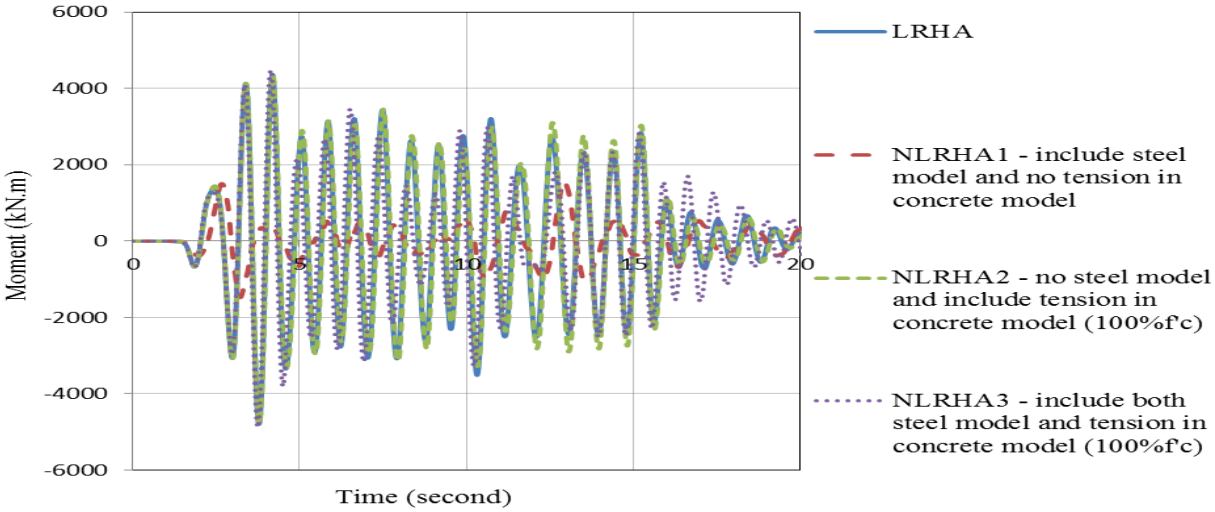

Figure C.11 Time history response of the 16-story shear wall model due to MCE5 scaled by 1.5 – story 3

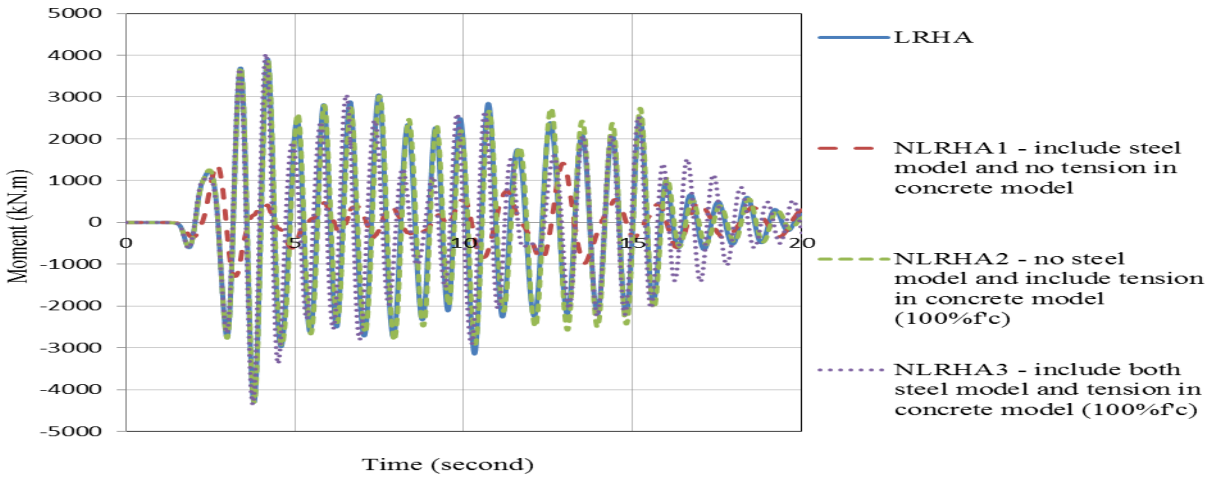

Figure C.12 Time history response of the 16-story shear wall model due to MCE5 scaled by 1.5 – story 4

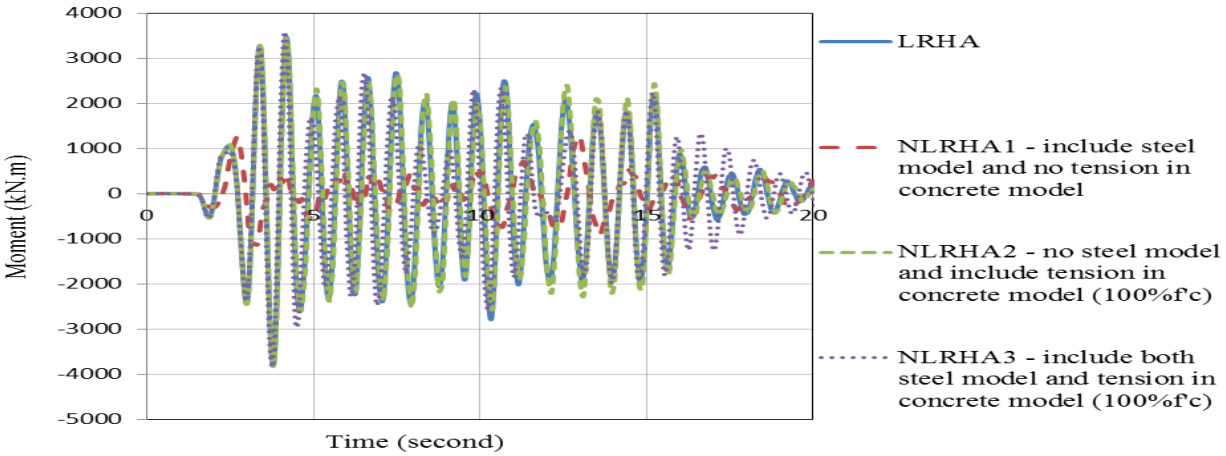

Figure C.13 Time history response of the 16-story shear wall model due to MCE5 scaled by 1.5 – story 5

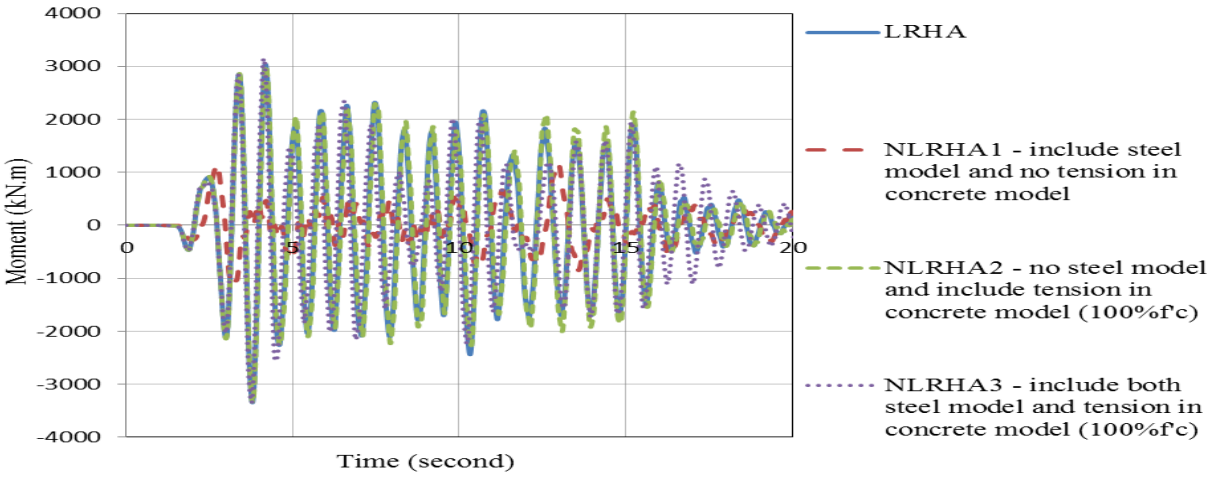

Figure C.14 Time history response of the 16-story shear wall model due to MCE5 scaled by 1.5 – story 6

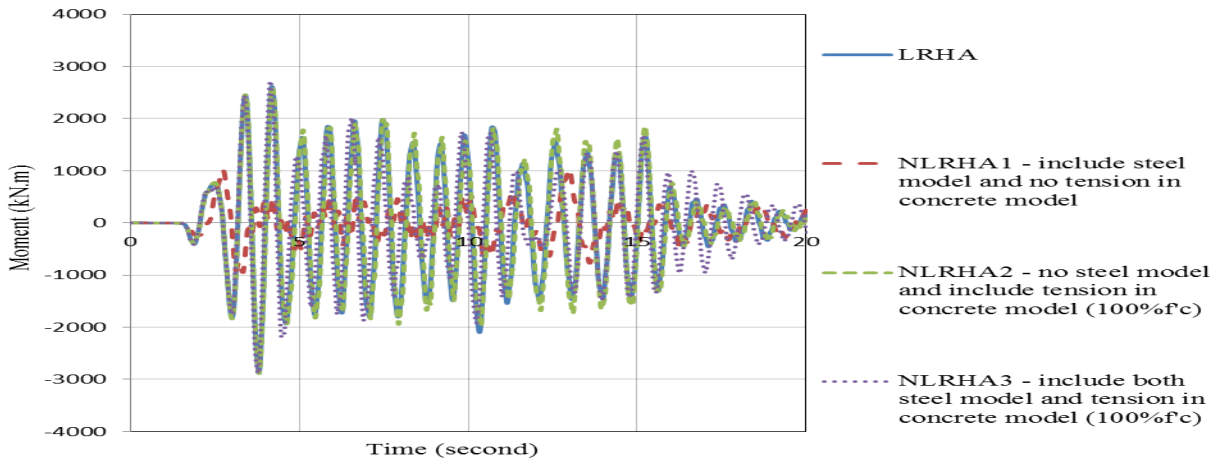

Figure C.15 Time history response of the 16-story shear wall model due to MCE5 scaled by 1.5 – story 7

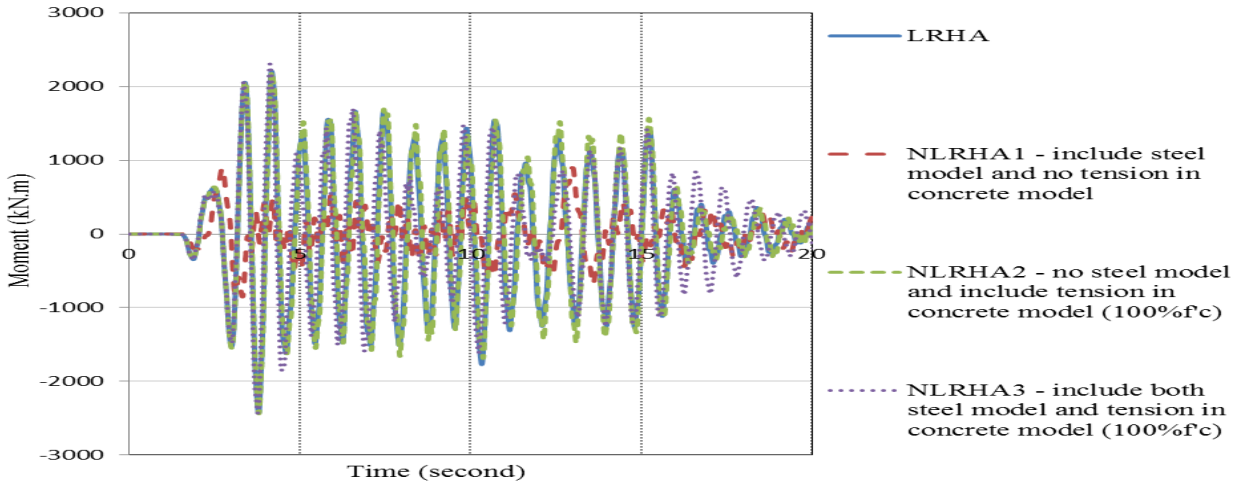

Figure C.16 Time history response of the 16-story shear wall model due to MCE5 scaled by 1.5 – story 8

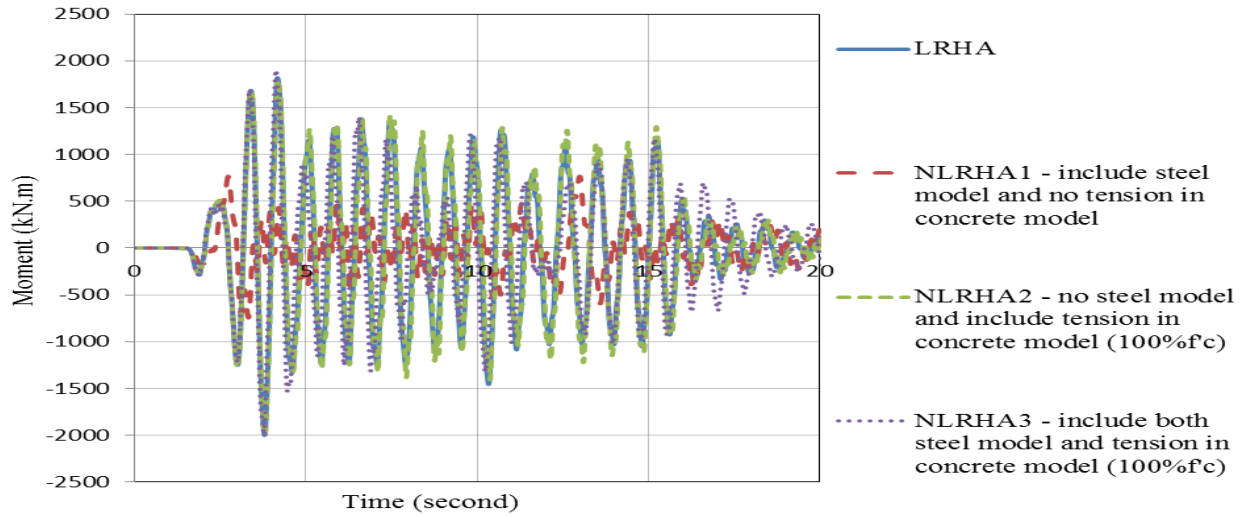

Figure C.17 Time history response of the 16-story shear wall model due to MCE5 scaled by 1.5 – story 9

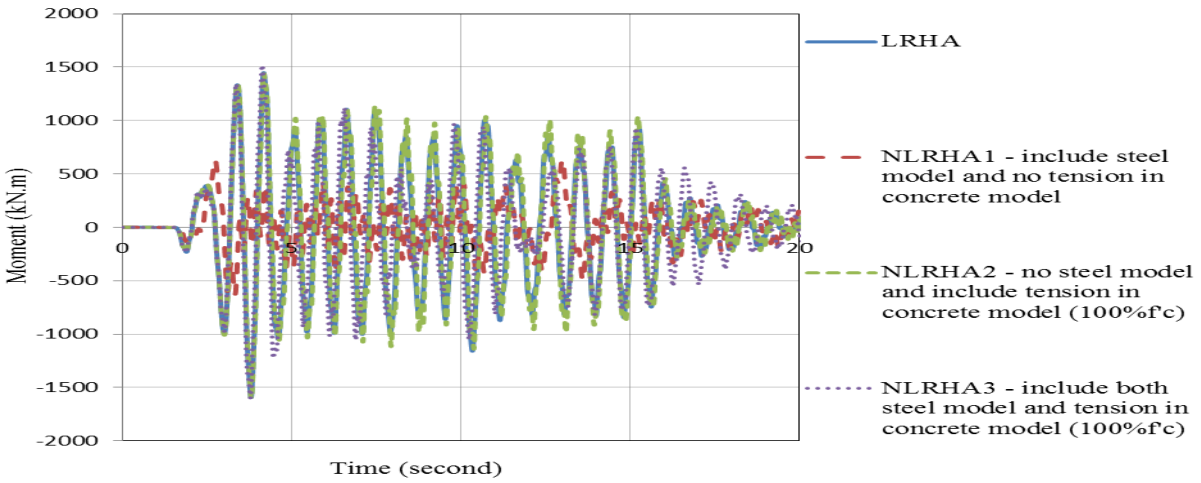

Figure C.18 Time history response of the 16-story shear wall model due to MCE5 scaled by 1.5 – story 10

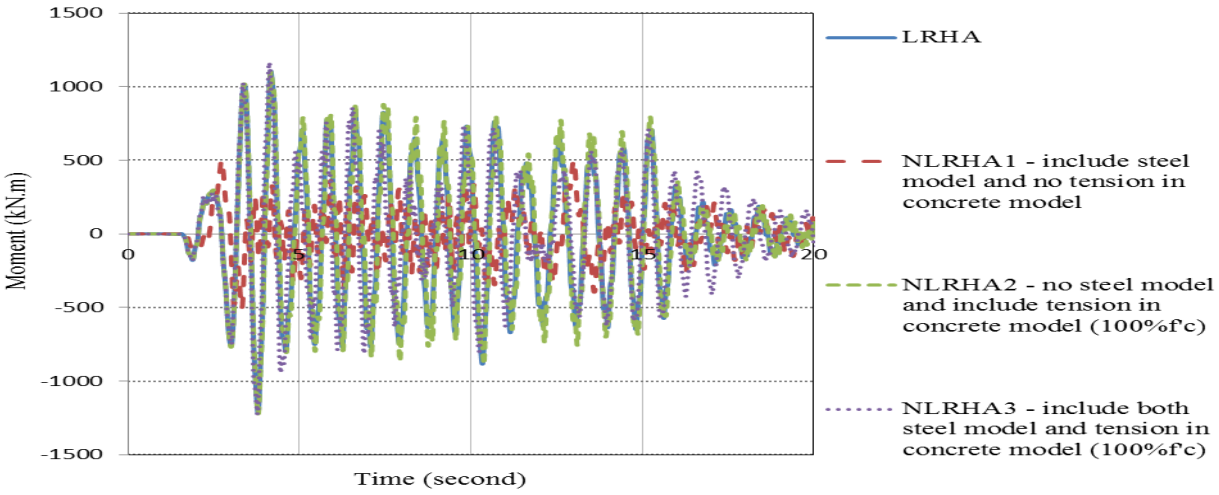

Figure C.19 Time history response of the 16-story shear wall model due to MCE5 scaled by 1.5 – story 11

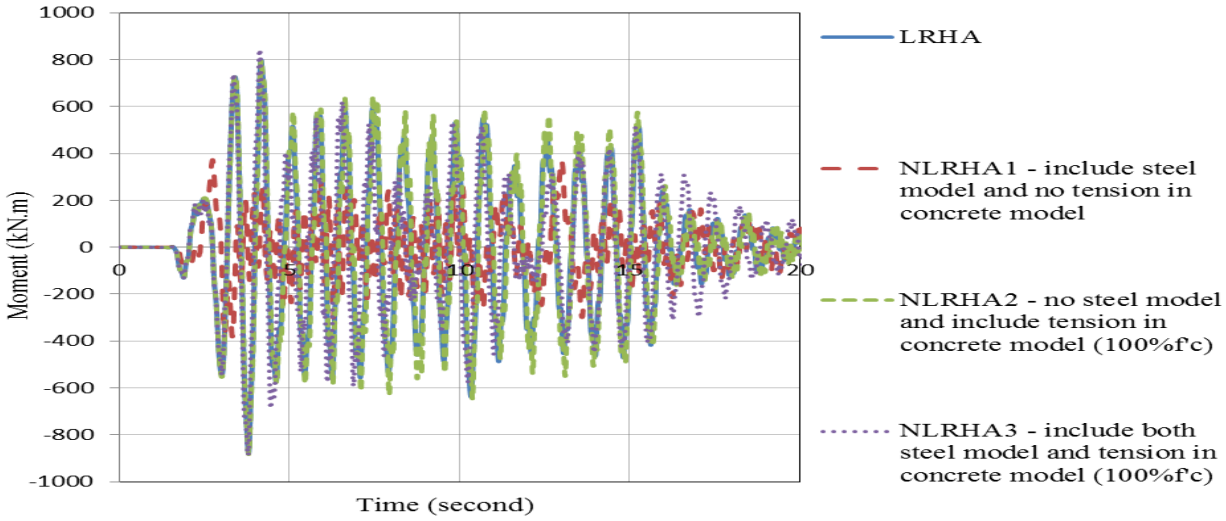

Figure C.20 Time history response of the 16-story shear wall model due to MCE5 scaled by 1.5 – story 12

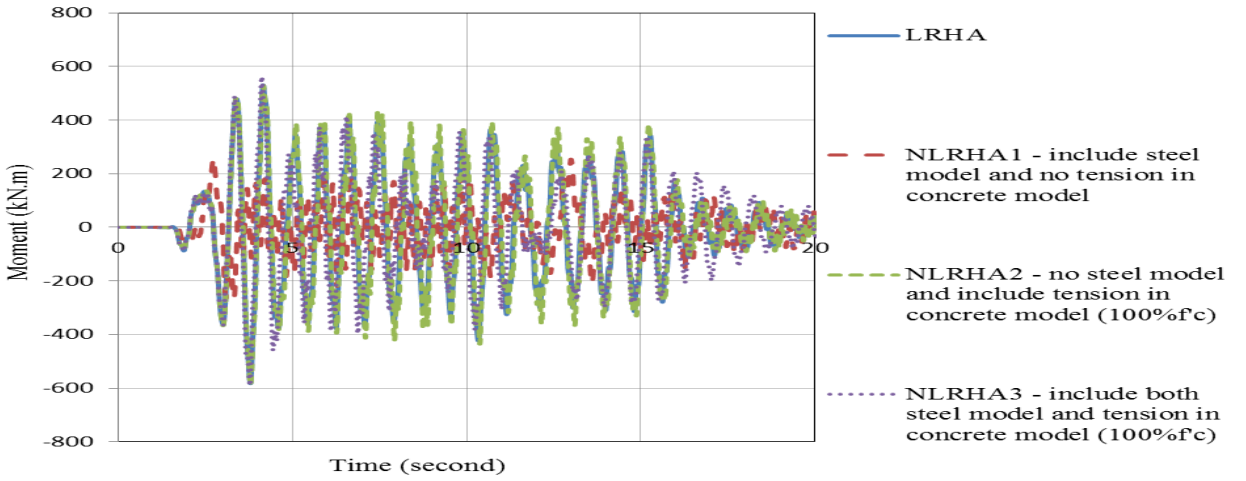

Figure C.21 Time history response of the 16-story shear wall model due to MCE5 scaled by 1.5 – story 13

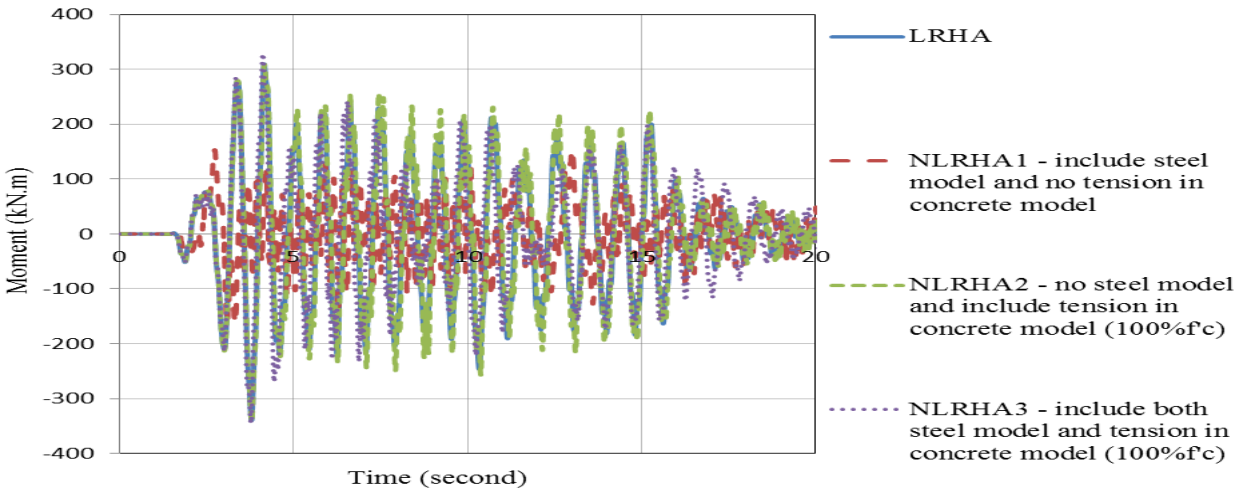

Figure C.22 Time history response of the 16-story shear wall model due to MCE5 scaled by 1.5 – story 14

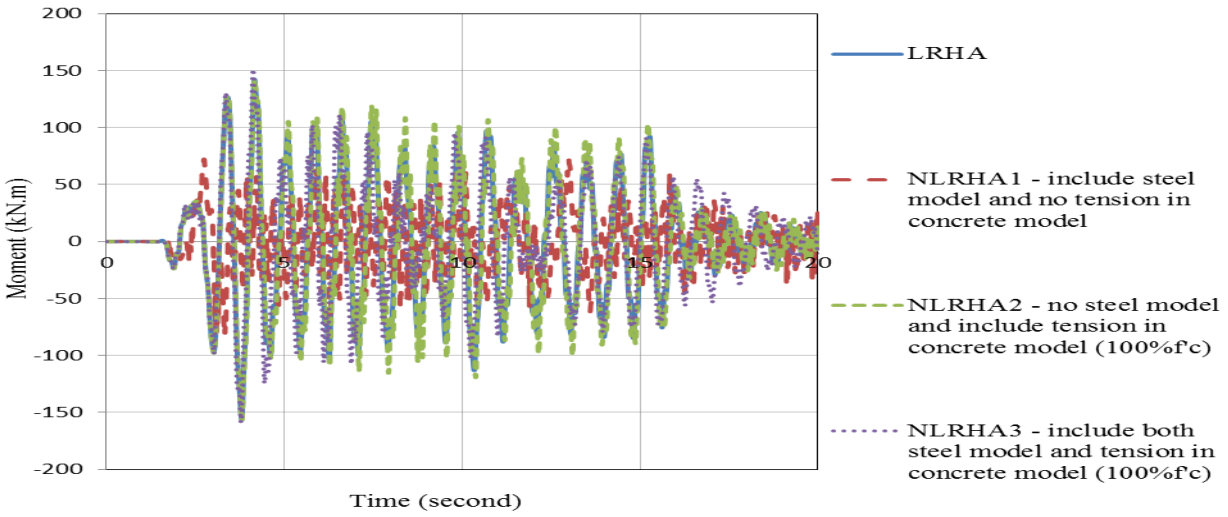

Figure C.23 Time history response of the 16-story shear wall model due to MCE5 scaled by 1.5 – story 15

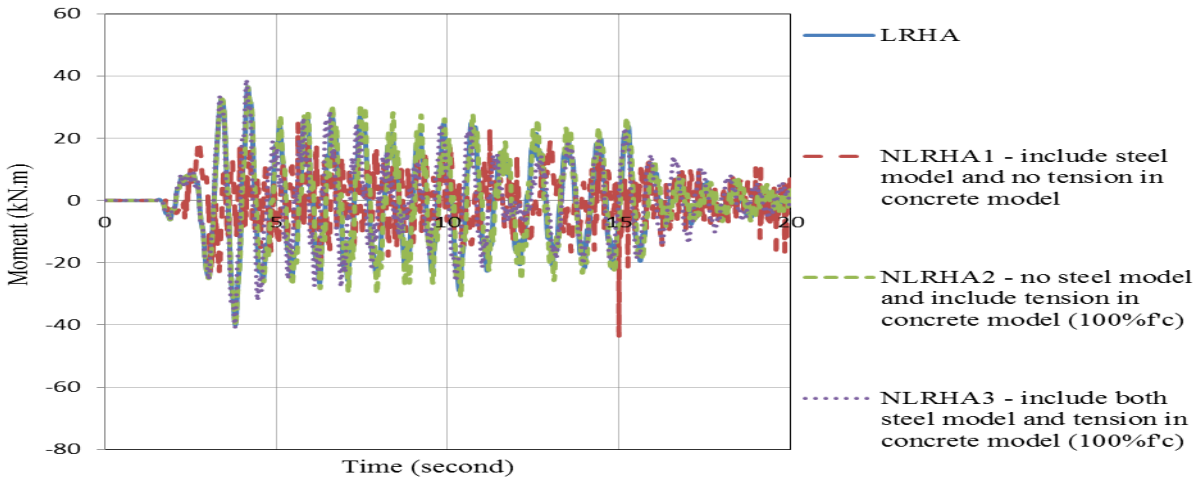

Figure C.24 Time history response of the 16-story shear wall model due to MCE5 scaled by 1.5 – story 16

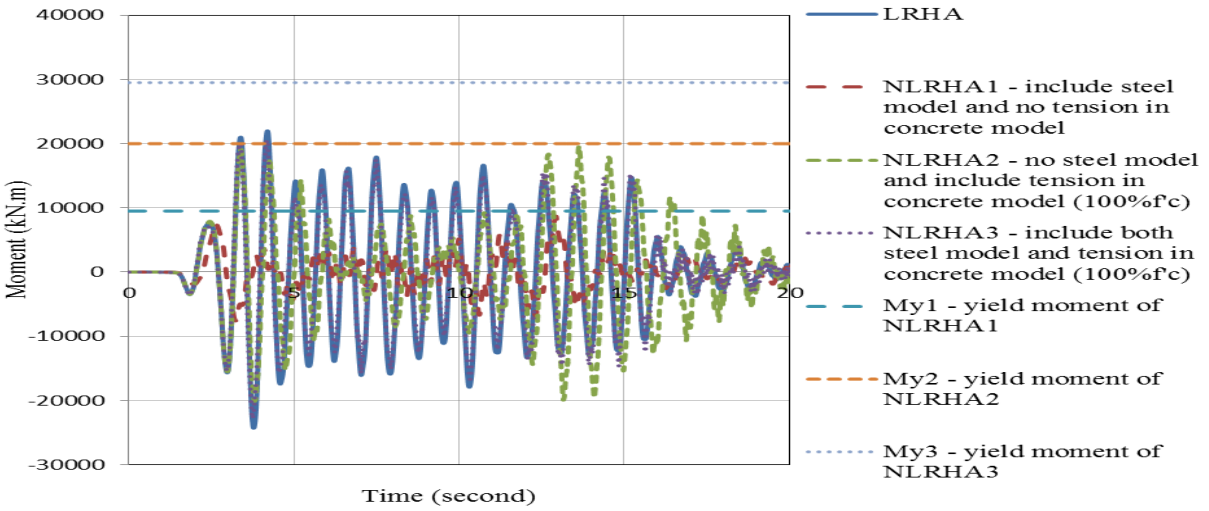

Figure C.25 Time history response of the 16-story shear wall model due to MCE5 scaled by 6 – story 1

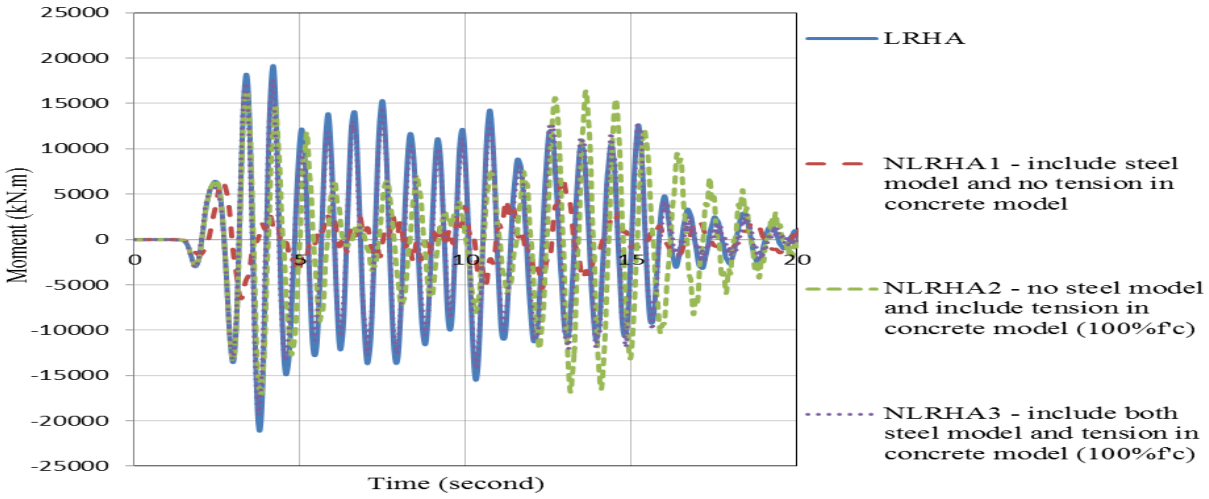

Figure C.26 Time history response of the 16-story shear wall model due to MCE5 scaled by 6 – story 2

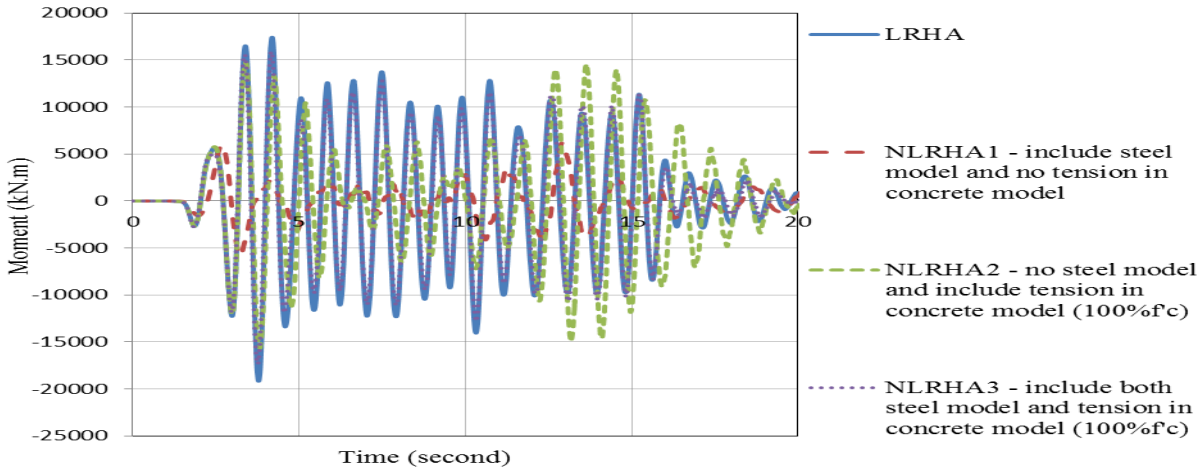

Figure C.27 Time history response of the 16-story shear wall model due to MCE5 scaled by 6 – story 3

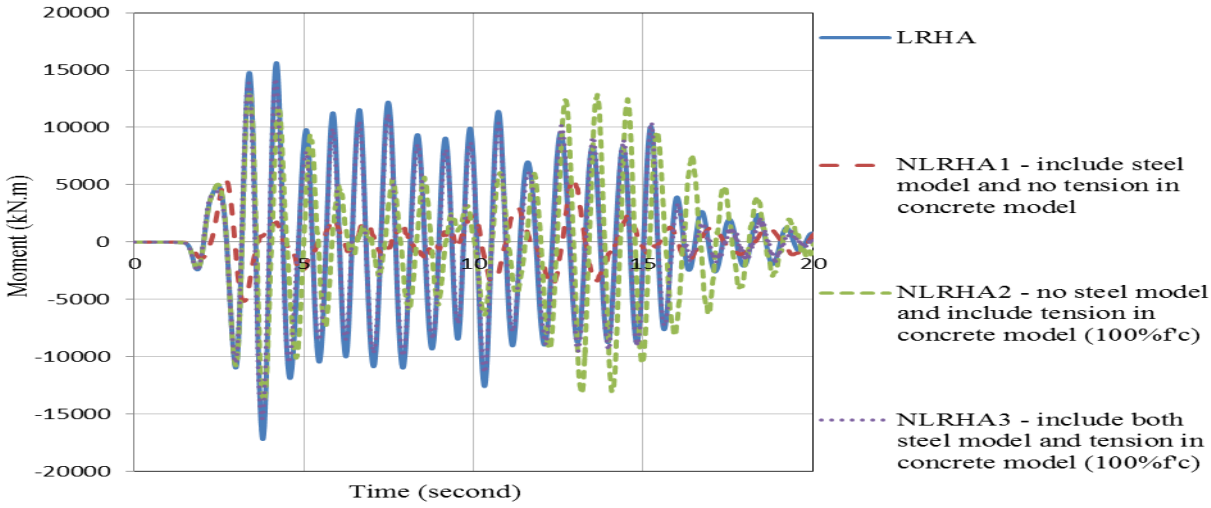

Figure C.28 Time history response of the 16-story shear wall model due to MCE5 scaled by 6 – story 4

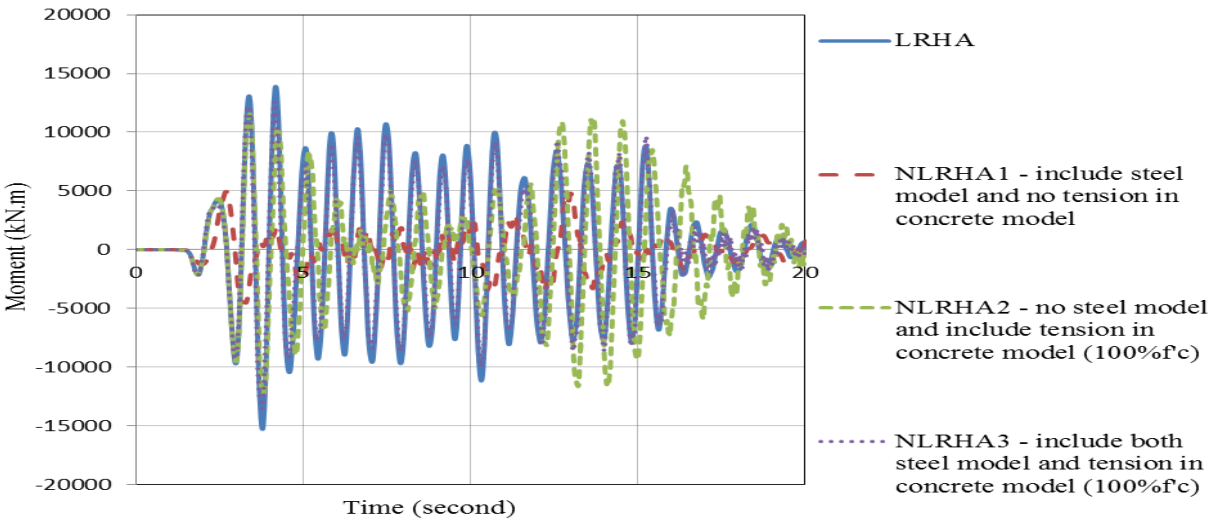

Figure C.29 Time history response of the 16-story shear wall model due to MCE5 scaled by 6 – story 5

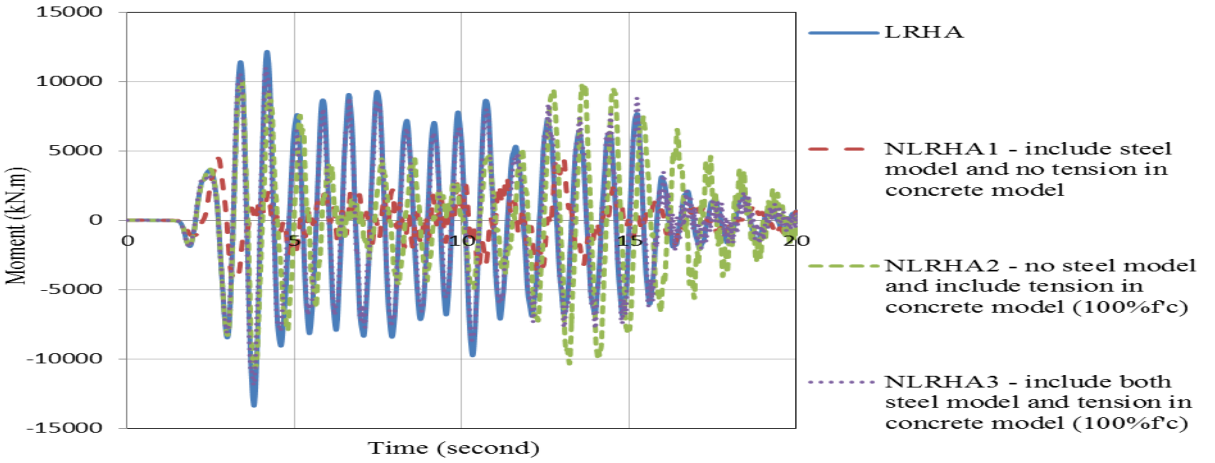

Figure C.30 Time history response of the 16-story shear wall model due to MCE5 scaled by 6 – story 6

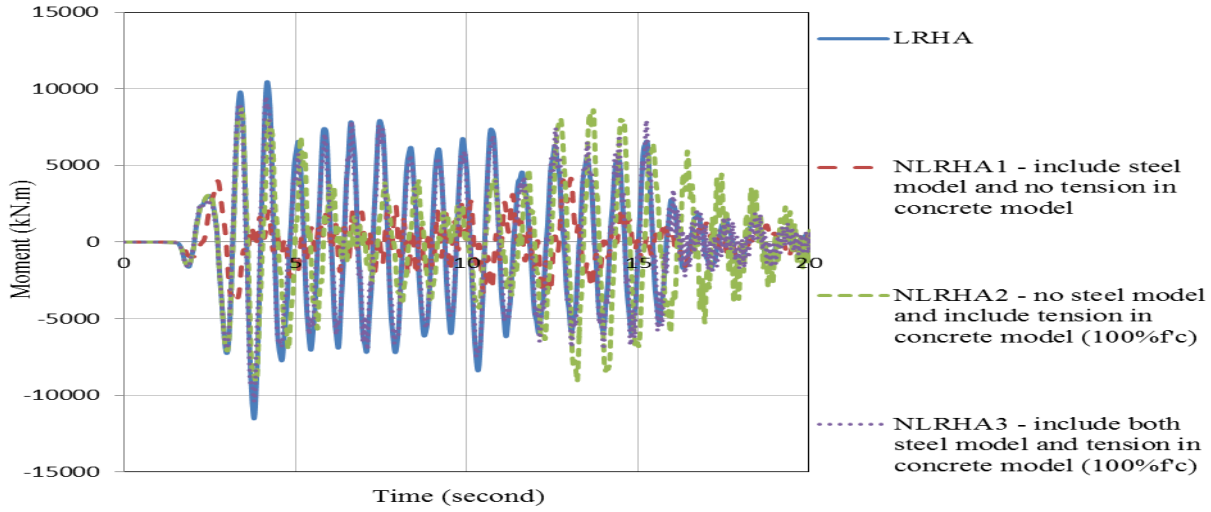

Figure C.31 Time history response of the 16-story shear wall model due to MCE5 scaled by 6 – story 7

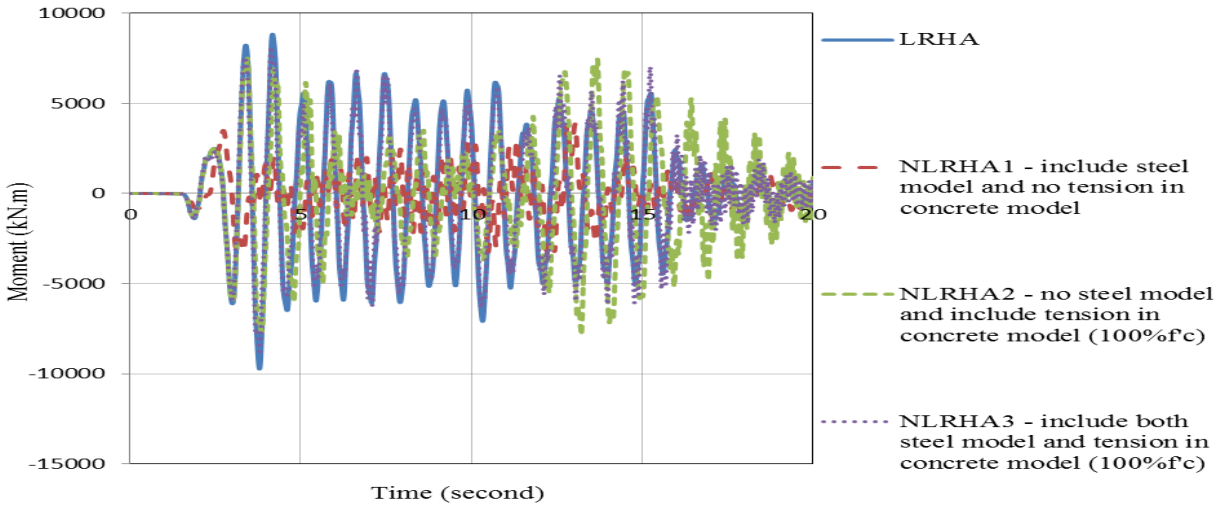

Figure C.32 Time history response of the 16-story shear wall model due to MCE5 scaled by 6 – story 8

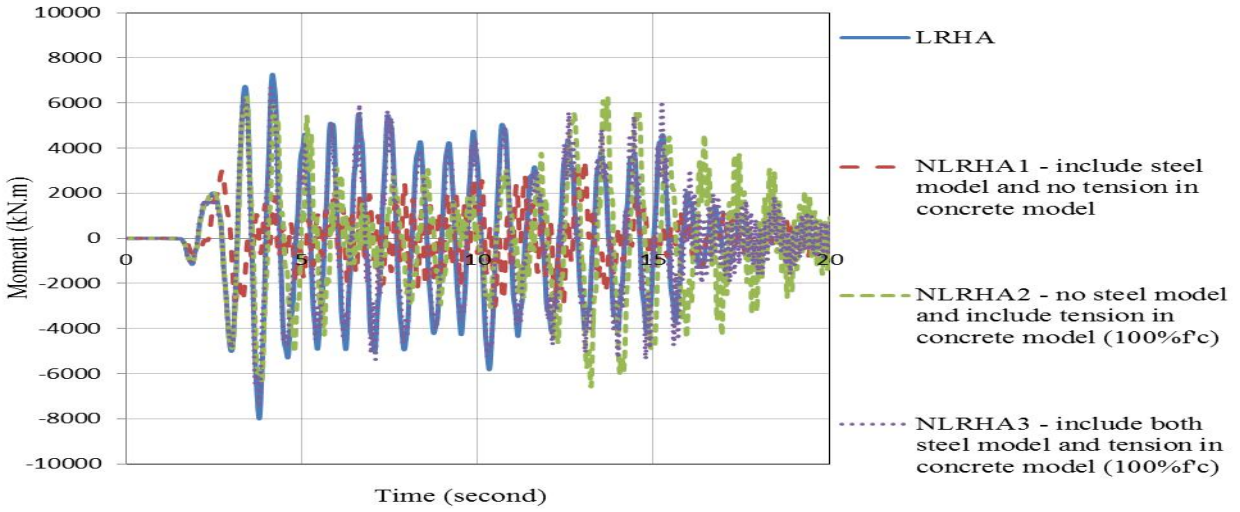

Figure C.33 Time history response of the 16-story shear wall model due to MCE5 scaled by 6 – story 9

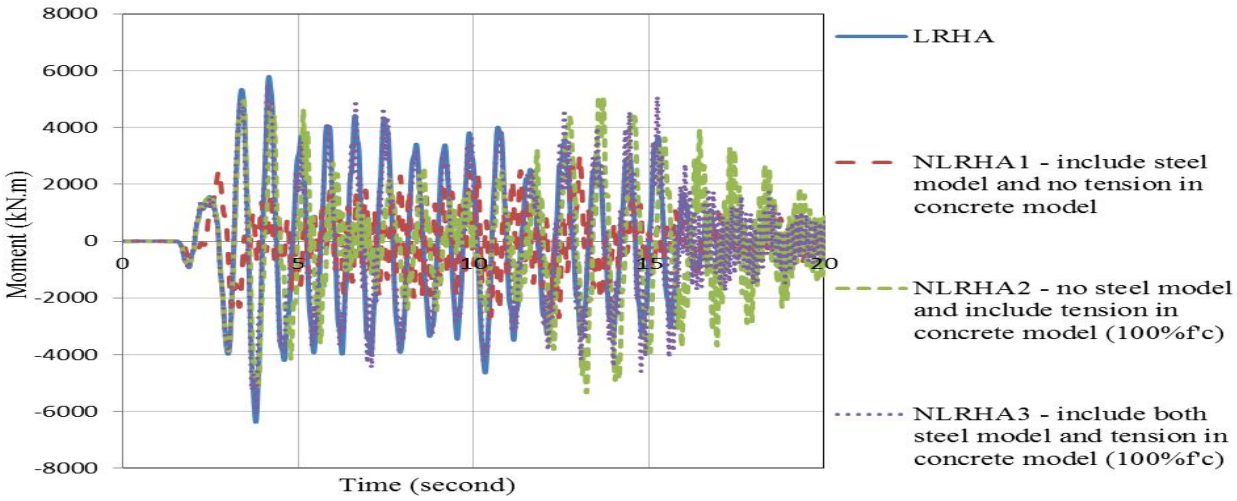

Figure C.34 Time history response of the 16-story shear wall model due to MCE5 scaled by 6 – story 10

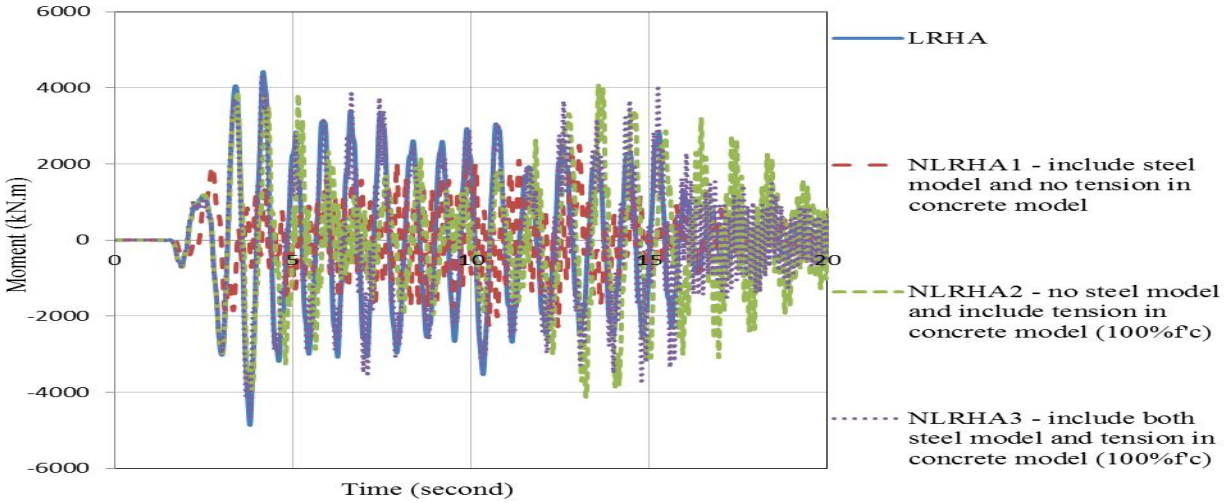

Figure C.35 Time history response of the 16-story shear wall model due to MCE5 scaled by 6 – story 11

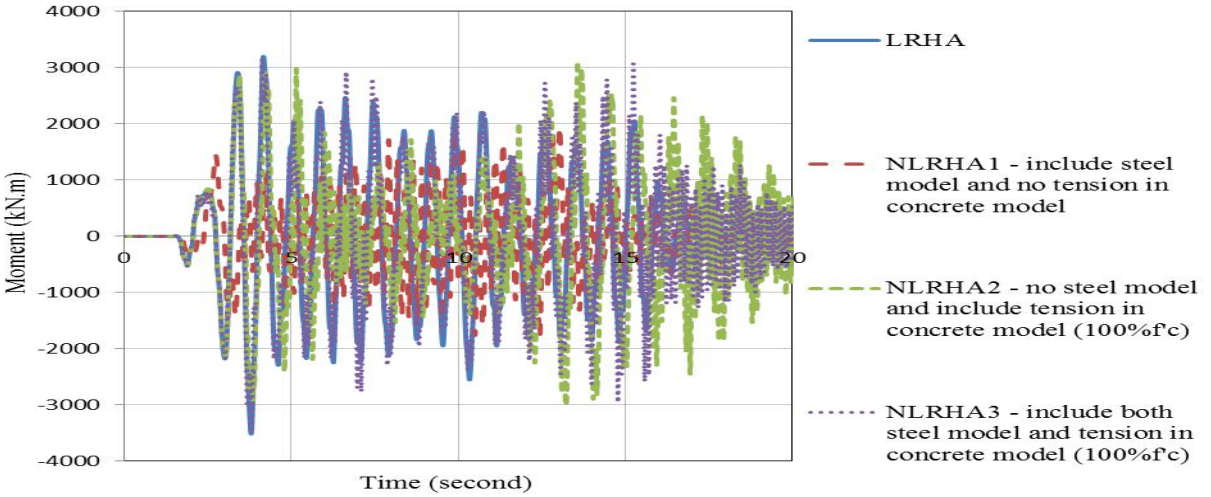

Figure C.36 Time history response of the 16-story shear wall model due to MCE5 scaled by 6 – story 12

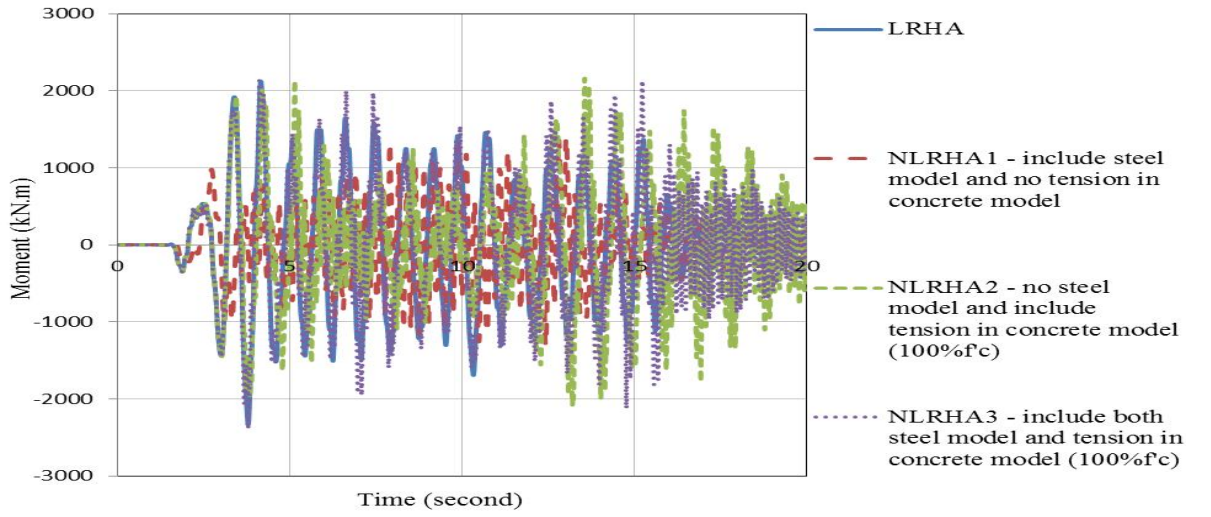

Figure C.37 Time history response of the 16-story shear wall model due to MCE5 scaled by 6 – story 13

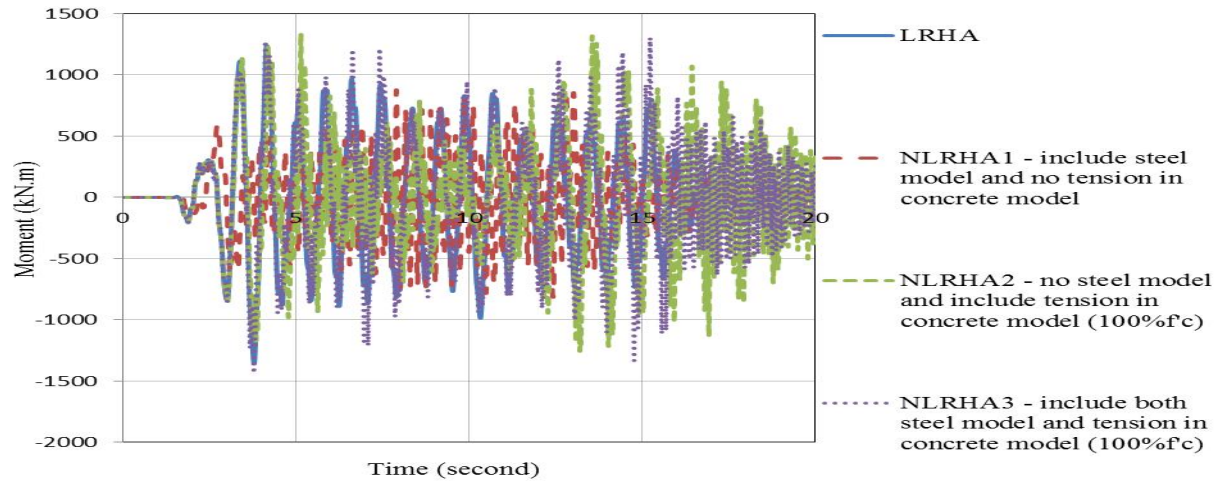

Figure C.38 Time history response of the 16-story shear wall model due to MCE5 scaled by 6 – story 14

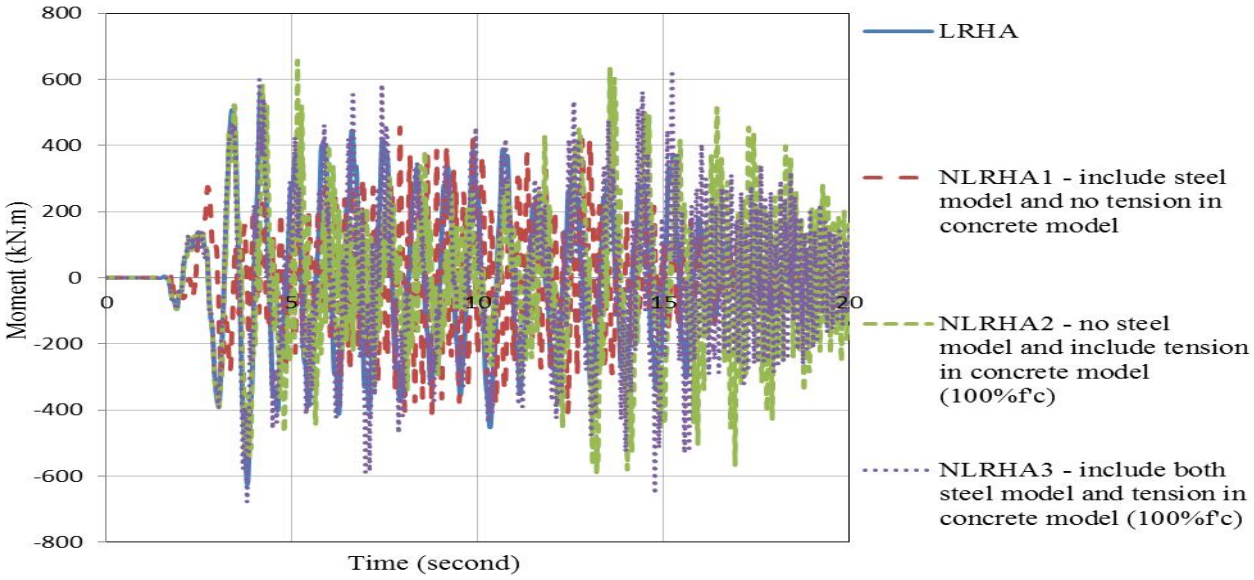

Figure C.39 Time history response of the 16-story shear wall model due to MCE5 scaled by 6 – story 15

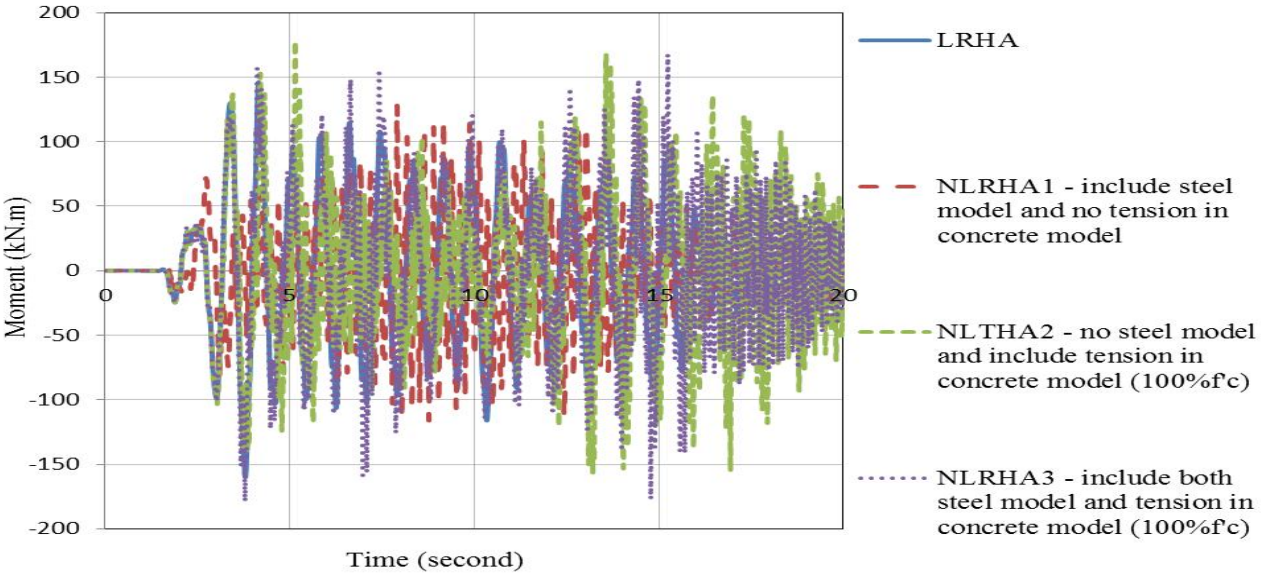

Figure C.40 Time history response of the 16-story shear wall model due to MCE5 scaled by 6 – story 16

APPENDIX D

Seismic demands of shear wall (W1 and W2) with varying nonlinear model in the wall elements of the whole structure modeled in PERFORM-3D

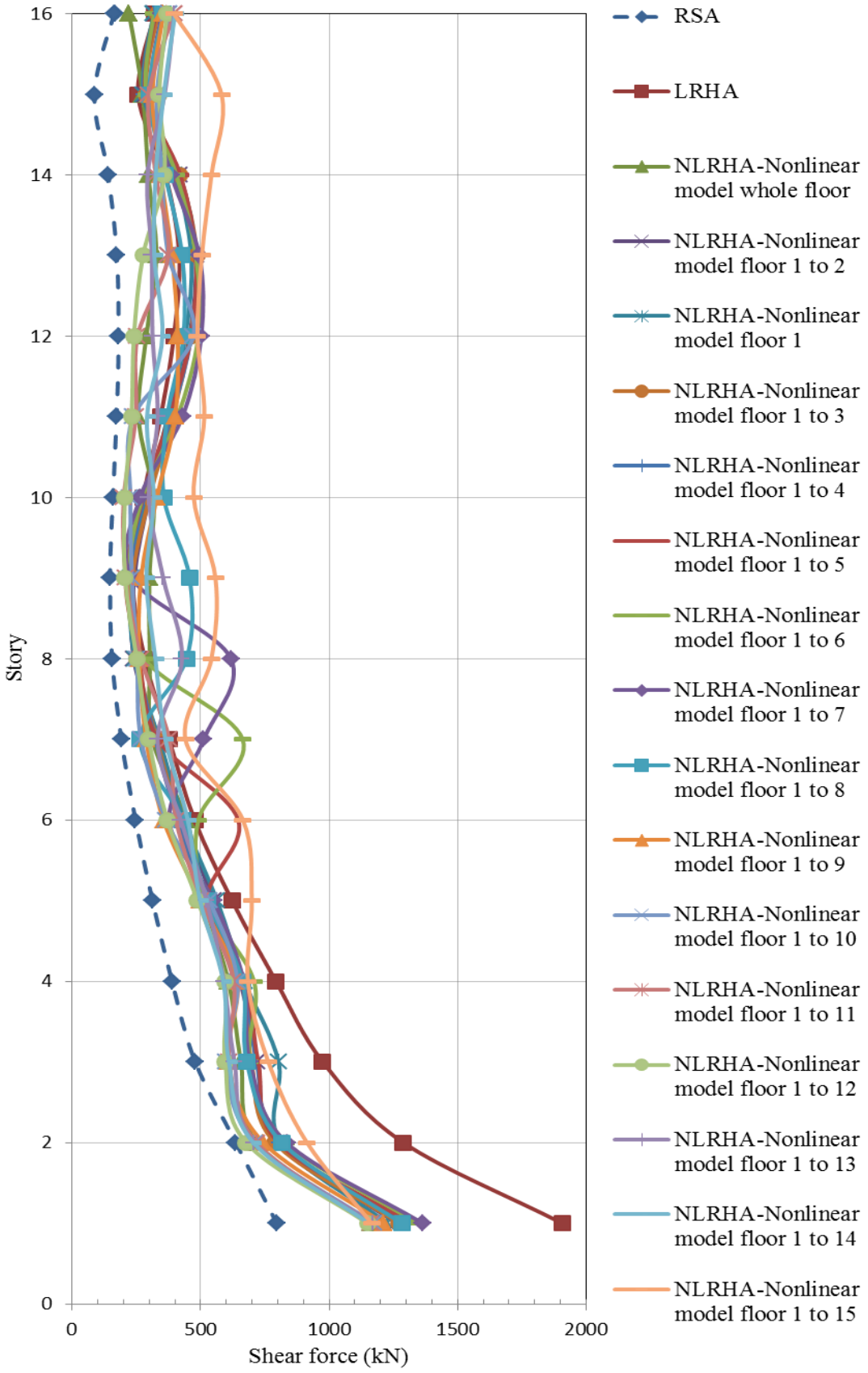

Figure D.1 Seismic shear demand of W1 due to MCE5

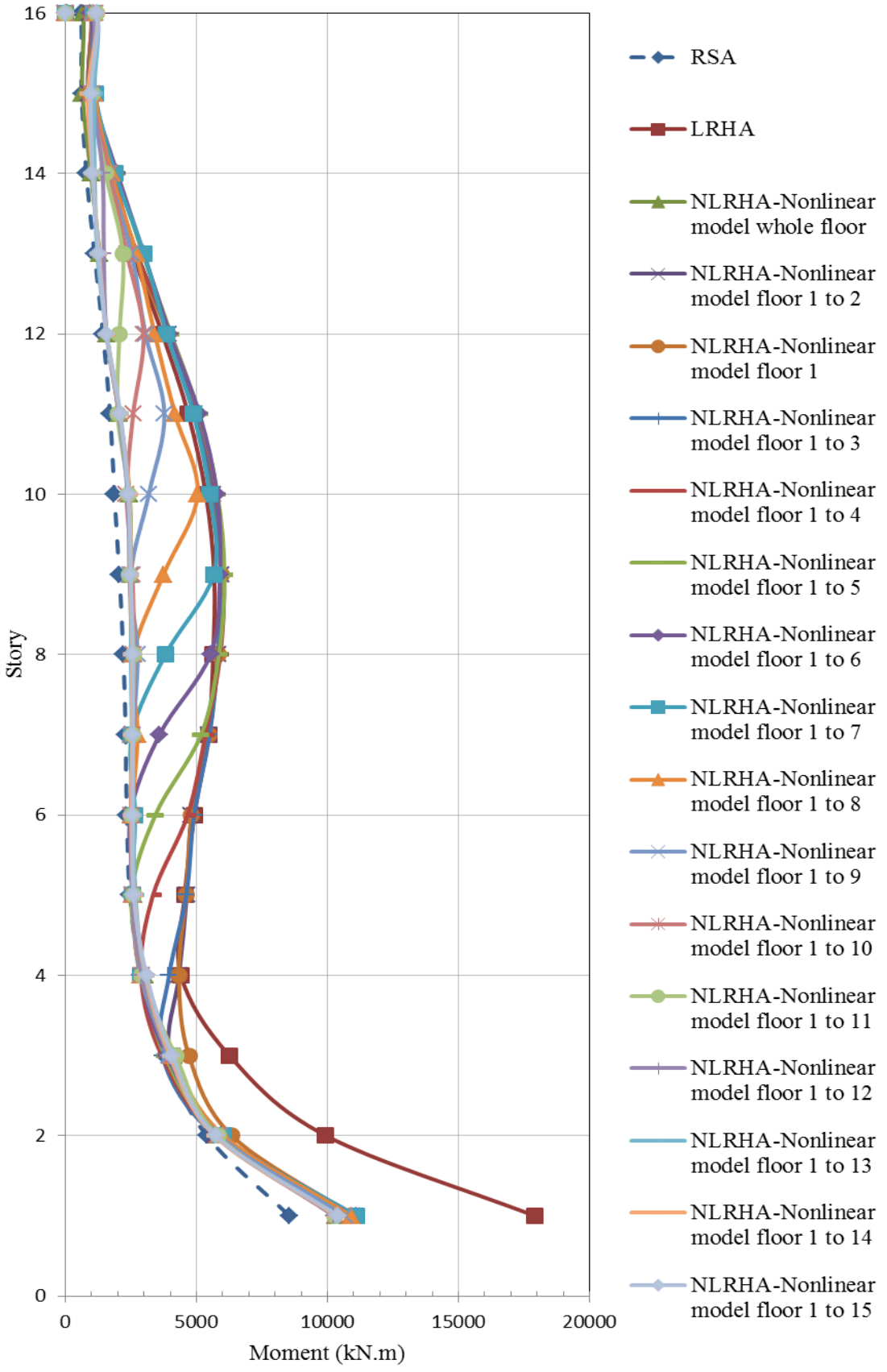

Figure D.2 Bending moment of W1 due to MCE5

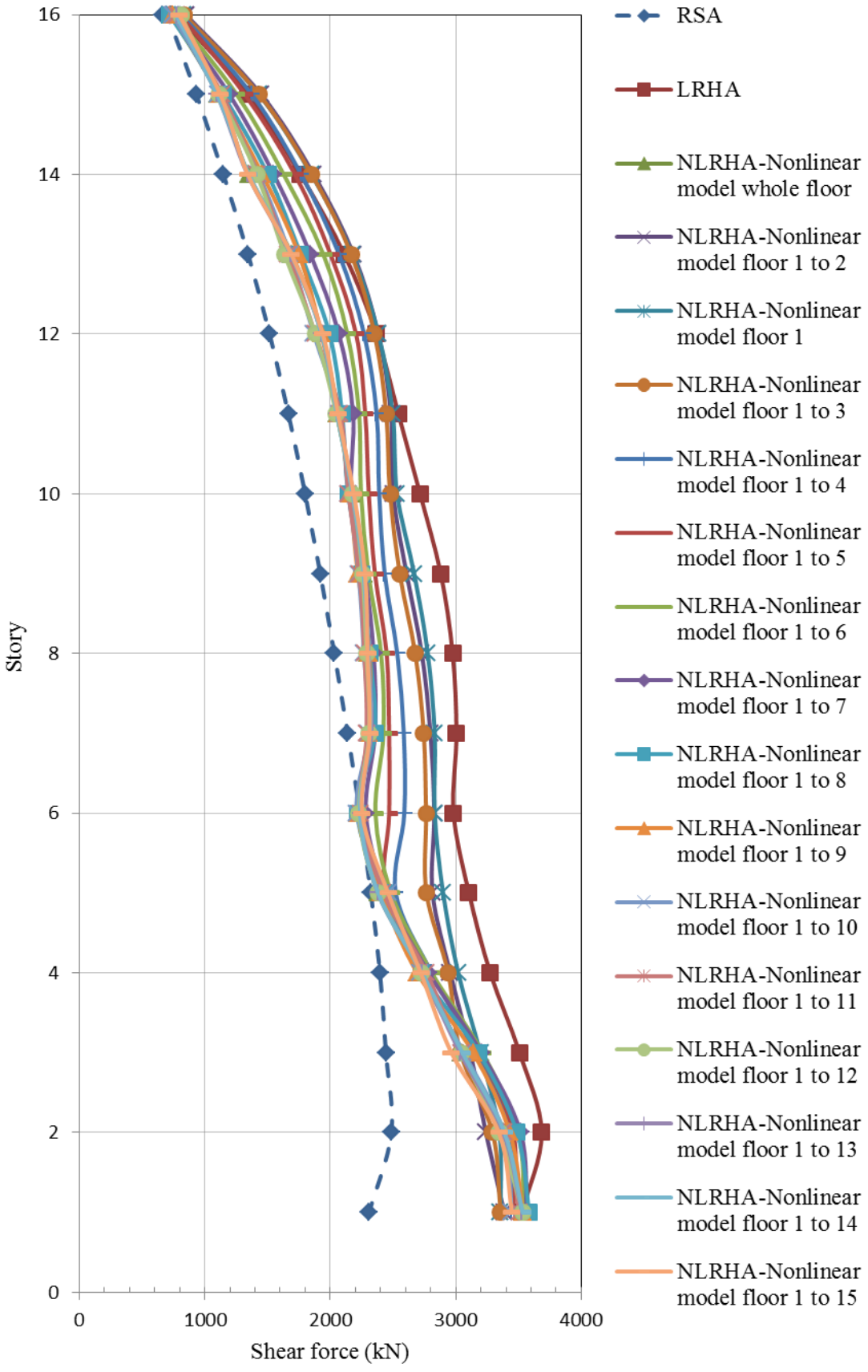

Figure D.3 Seismic shear demand of W2 due to MCE5 – N-S direction

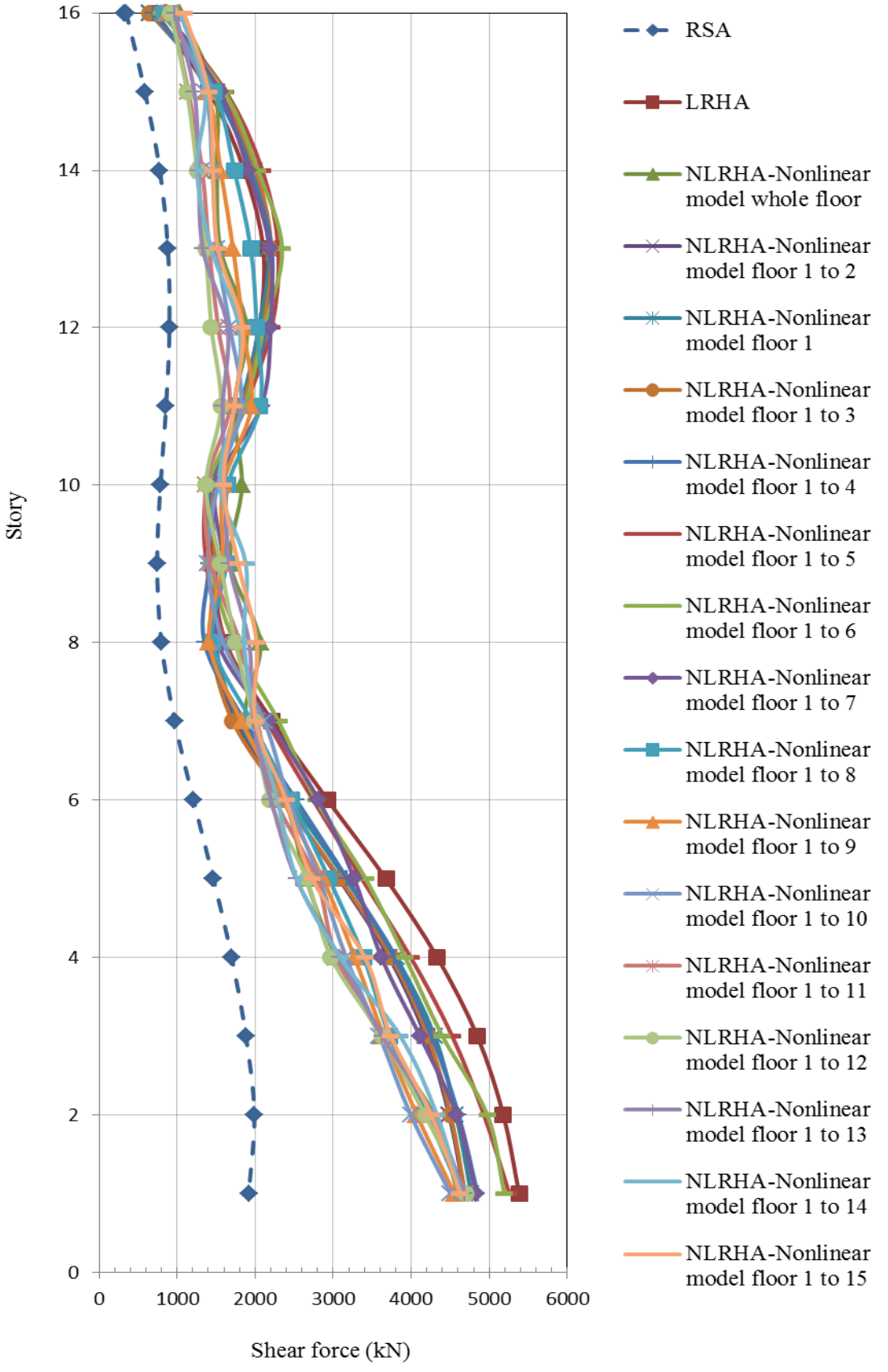

Figure D.4 Seismic shear demand of W2 due to MCE5 – E-W direction

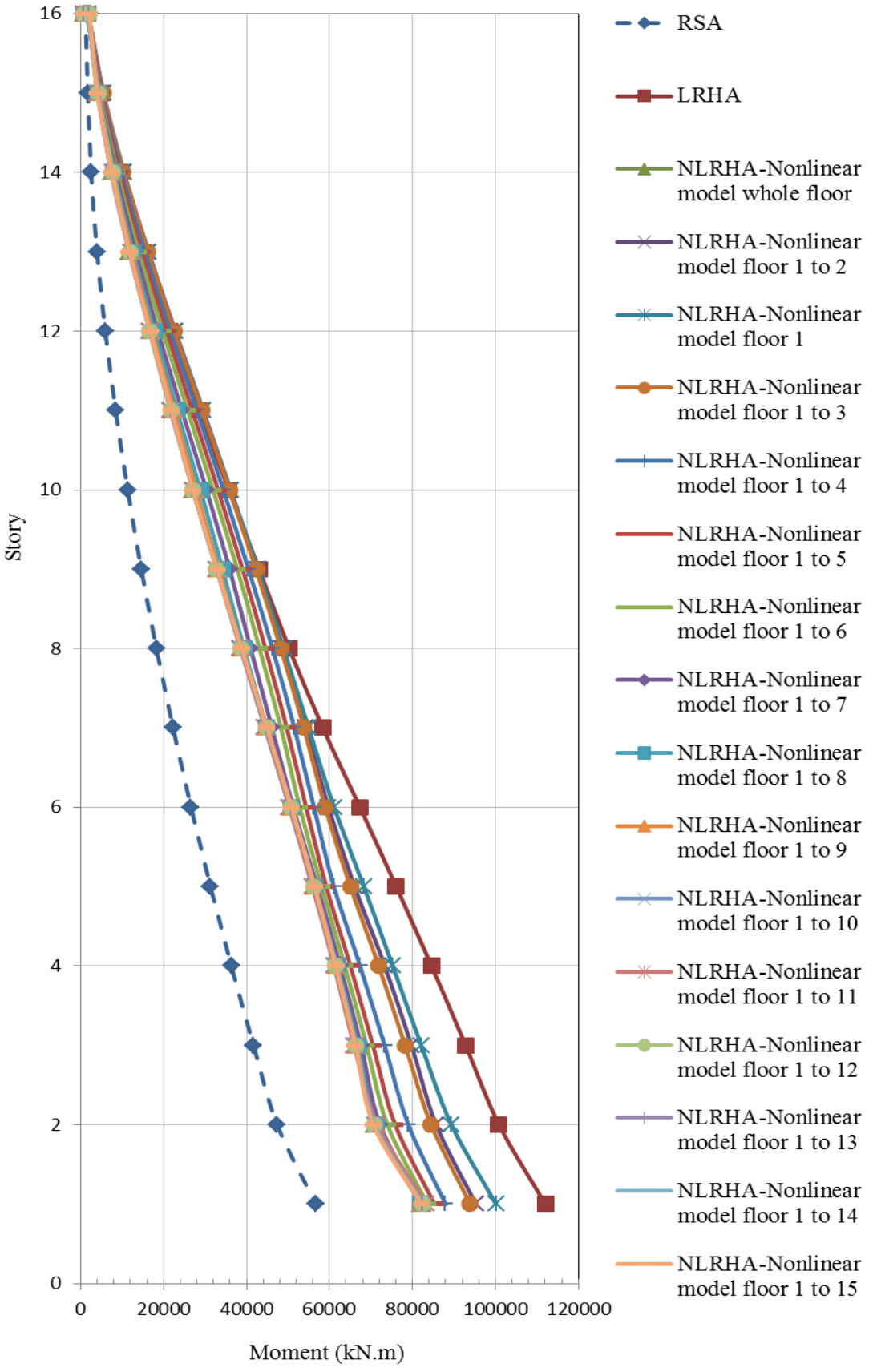

Figure D.5 Bending moment of W2 due to MCE5 – about E-W direction

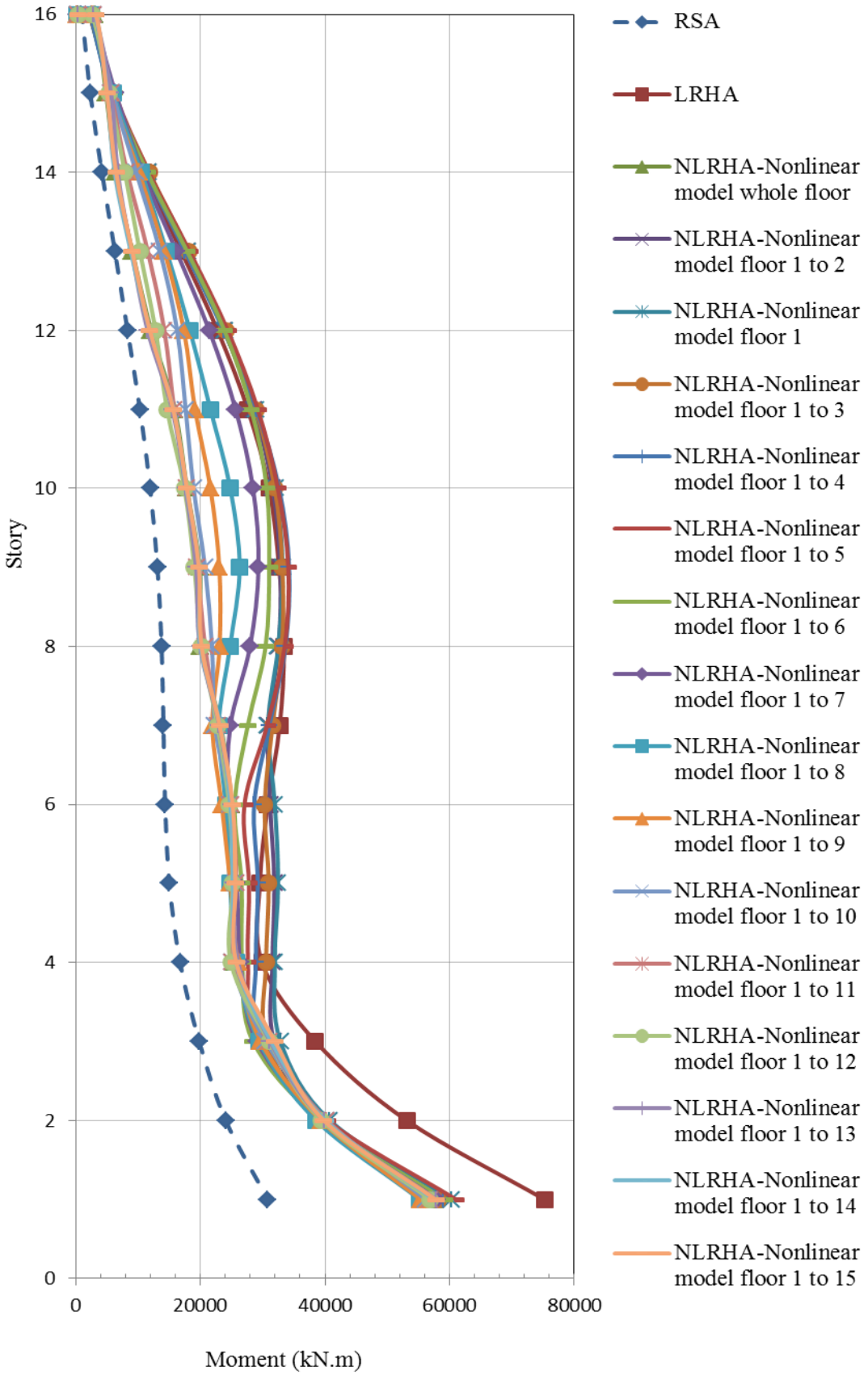

Figure D.6 Bending moment of W2 due to MCE5 – about N-S direction

APPENDIX E

Modified RSA procedure including modification in bending moment

When modified RSA procedure includes modification in bending moment of the walls, then the flexural strength of the structure needed to be redesigned based on the new demand in bending moment of the walls. To do this, the response spectrum for modified RSA procedure shown in Figure E.1 is used as input in ETABS to analyze the structure based on this new modified RSA procedure. The demands from this new approach are used to redesign the flexural strength of the walls.

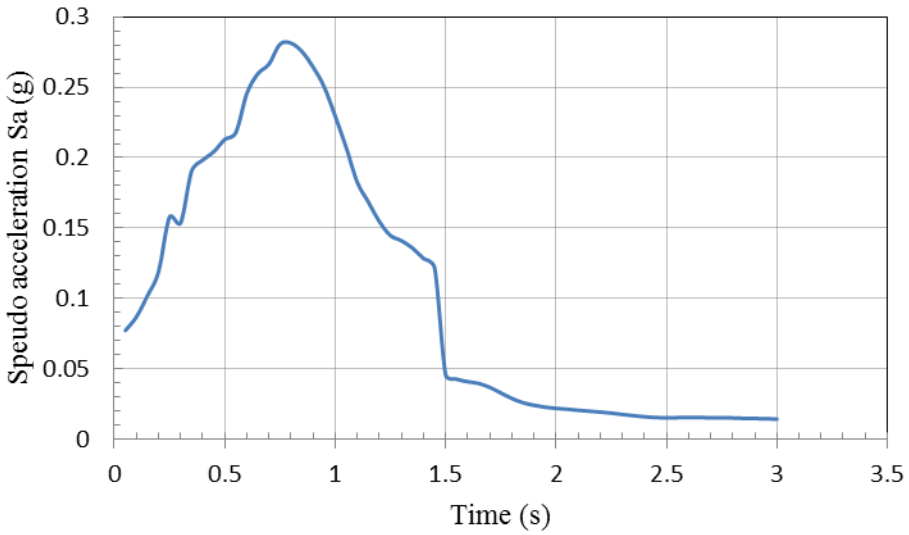

Figure E.1 Response spectrum for modified RSA procedure, damping ratio = 5%

E.1 Design of shear walls

Based on the P-M diagram of the walls illustrated in Figure 4.16 through Figure 4.23 of Chapter IV and the demands obtained from modified RSA procedure mentioned earlier, the vertical reinforcements of the walls can be computed and shown in Table E.1 of this section.

Table E.1 Vertical reinforcement of the walls in modified RSA procedure

	Wall 1 (W1)	Wall 2 (W2) = Wall 3 (W3)
Story	ρ (%)	ρ (%)
1	2.85	2.95
2	1.2	2.2
3	0.6	1.8
4	0.6	1.8
5	0.6	1.5
6	0.6	1.5
7	0.6	1.5
8	0.6	1.5
9	0.6	1.2
10	0.6	1.2
11	0.6	0.97
12	0.45	0.75
13	0.45	0.55
14	0.3	0.3
15	0.3	0.26
16	0.3	0.15

Note: ρ = area of vertical reinforcement over the area of the cross section of the wall

E.2 Nonlinear response history analysis

The building designed by the modified RSA procedure is then run through the rigorous NLRHA using the DBE ground motions in PERFORM-3D software. The seismic demands (shear force and bending moment) in the walls (W1, W2 and W3) due to the seven DBE ground motions are shown in Figure E.2 through Figure E.11. The mean values of these demands in NLRHA are then compared with the corresponding demands from modified RSA procedure and illustrated in Figure E.12 through Figure E.21. The results show that this modified RSA procedure gives a good estimation of seismic demands (shear and moment) for the core walls (W1, W2 and W3) which approaches the best estimated seismic demands evaluated from NLRHA. Furthermore, the demands from both analyses, modified RSA and NLRHA, have similar distribution pattern over entire height of the walls. Attention should be paid to the shear force of W2 and W3 in N-S direction depicted in Figure E.14 and Figure E.18, respectively, in which the modified RSA overestimates the demand - about 1.3 times the corresponding demands from NLRHA procedure.

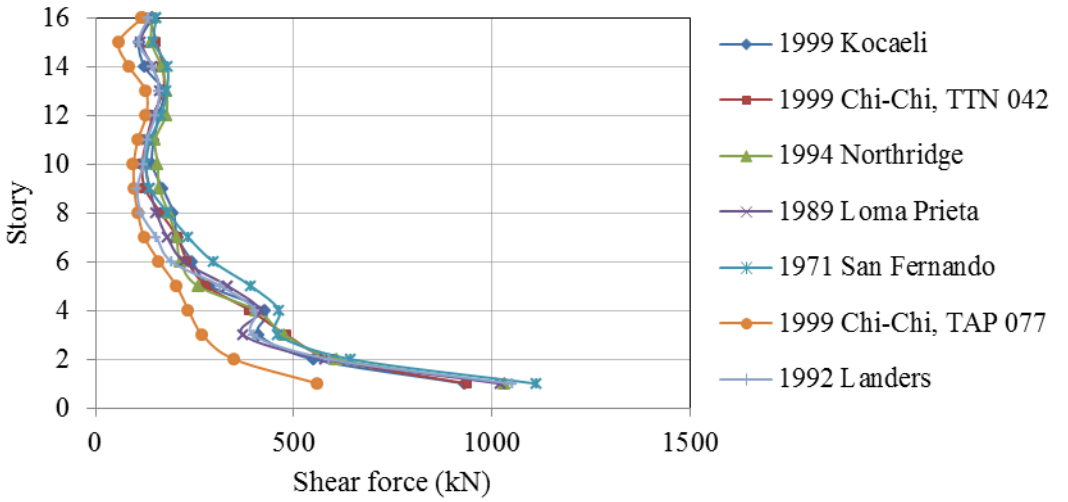

Figure E.2 Shear force in wall1 (W1) – NLRHA due to DBE

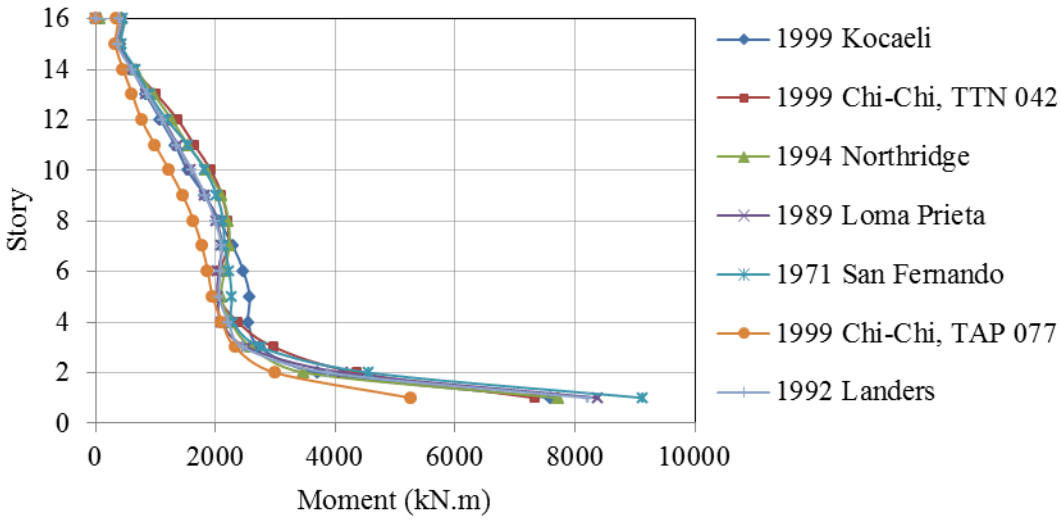

Figure E.3 Bending moment in wall1 (W1) – NLRHA due to DBE

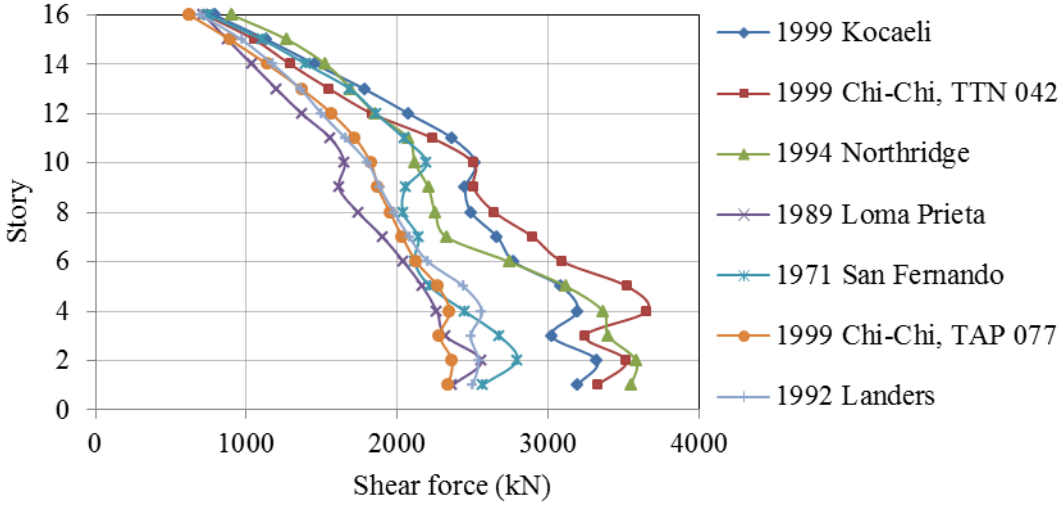

Figure E.4 Shear forces in wall2 (W2) in N-S direction – NLRHA due to DBE

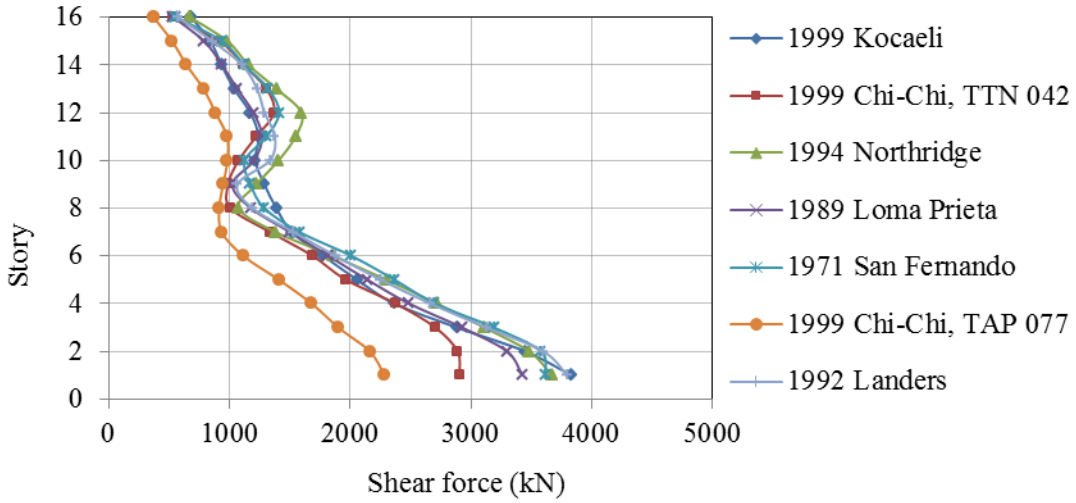

Figure E.5 Shear forces in wall2 (W2) in E-W direction – NLRHA due to DBE

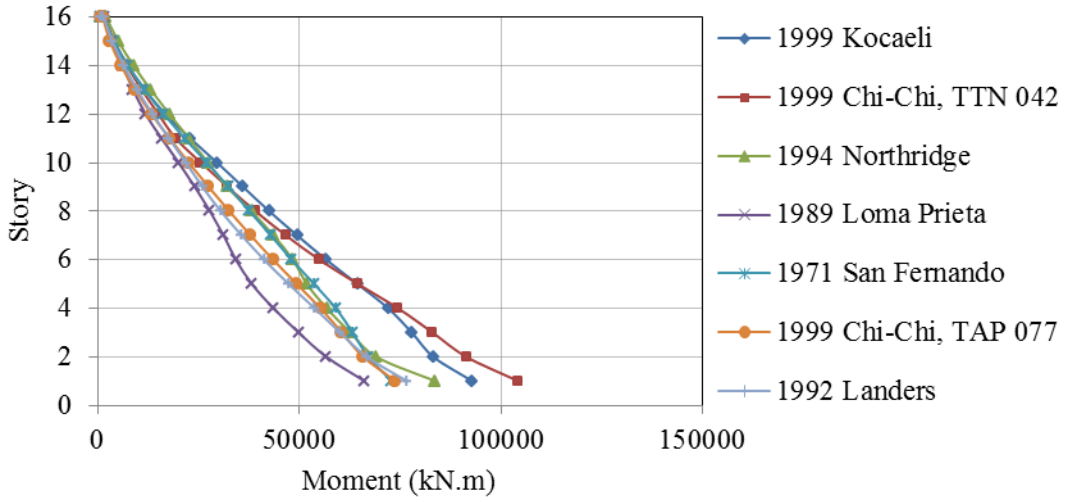

Figure E.6 Bending moment in wall2 (W2) about E-W direction – NLRHA due to DBE

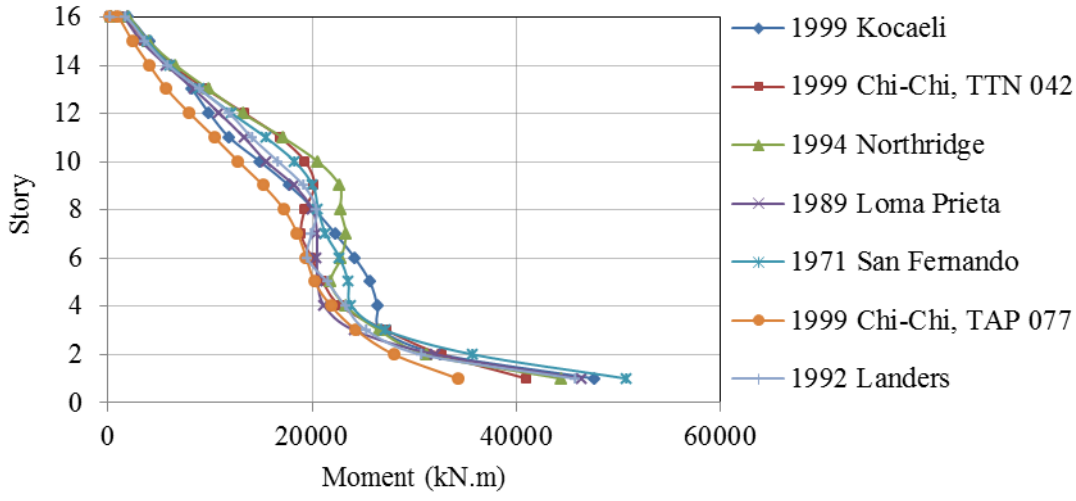

Figure E.7 Bending moment in wall2 (W2) about N-S direction – NLRHA due to DBE

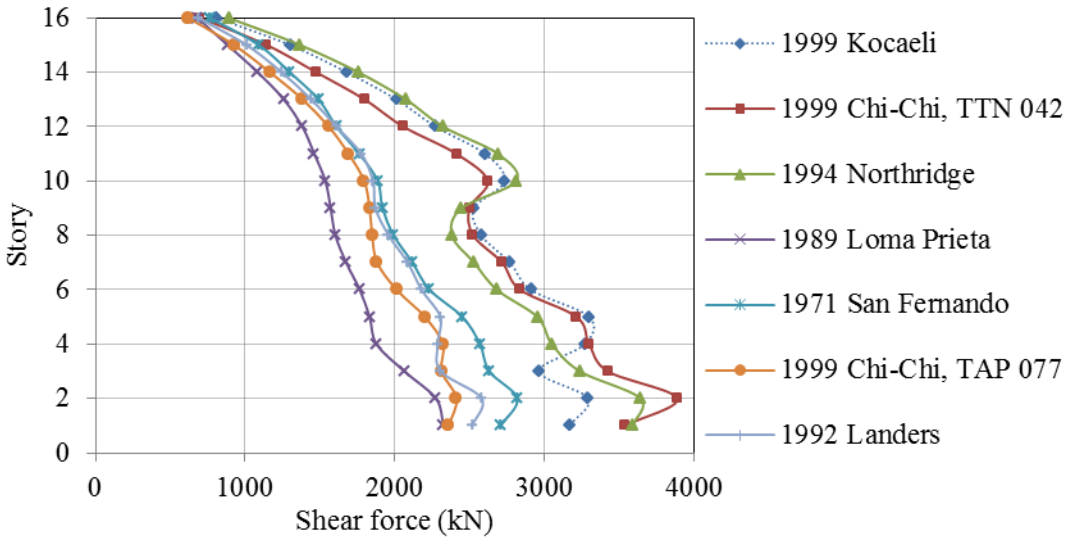

Figure E.8 Shear force in wall3 (W3) in N-S direction – NLRHA due to DBE

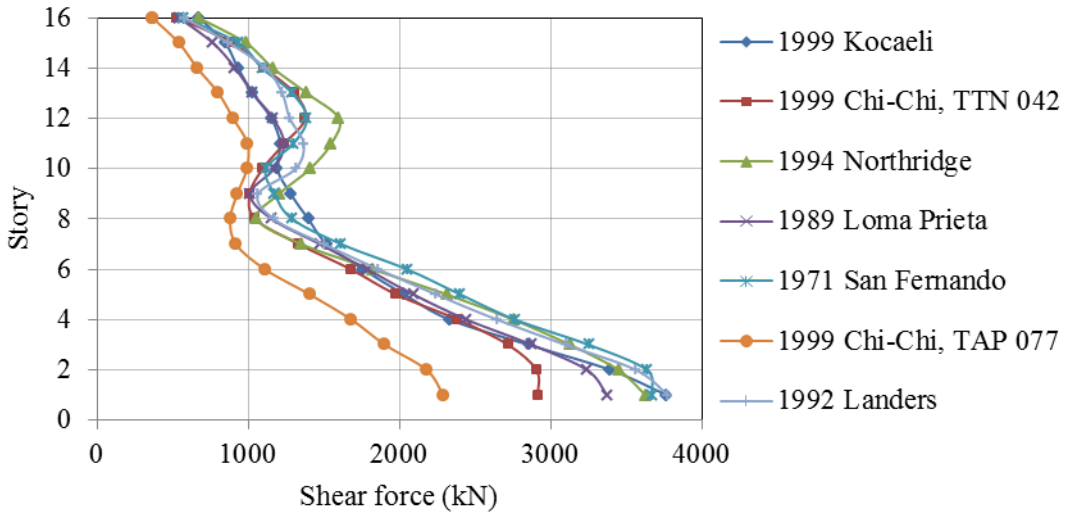

Figure E.9 Shear force in wall3 (W3) in E-W direction – NLRHA due to DBE

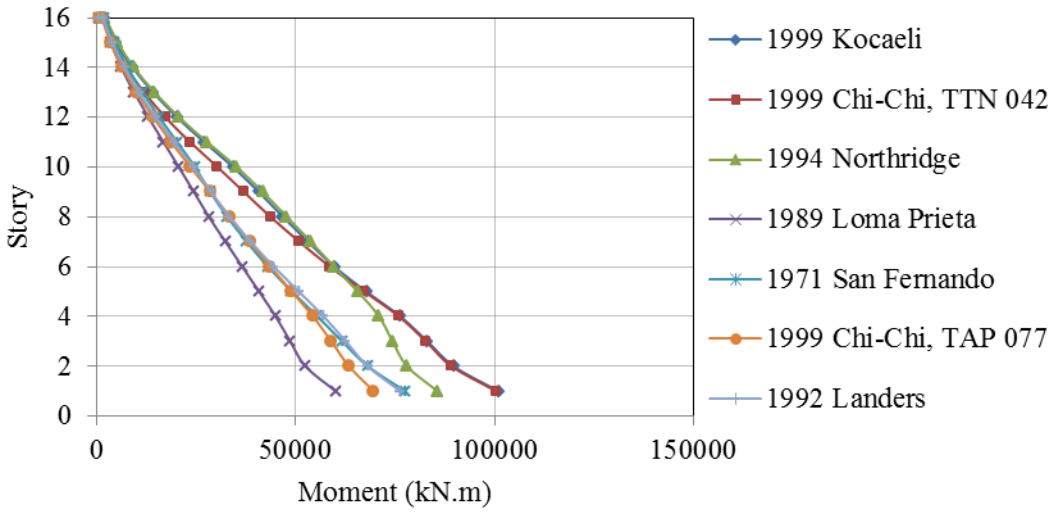

Figure E.10 Bending moment in wall3 (W3) about E-W direction – NLRHA due to DBE

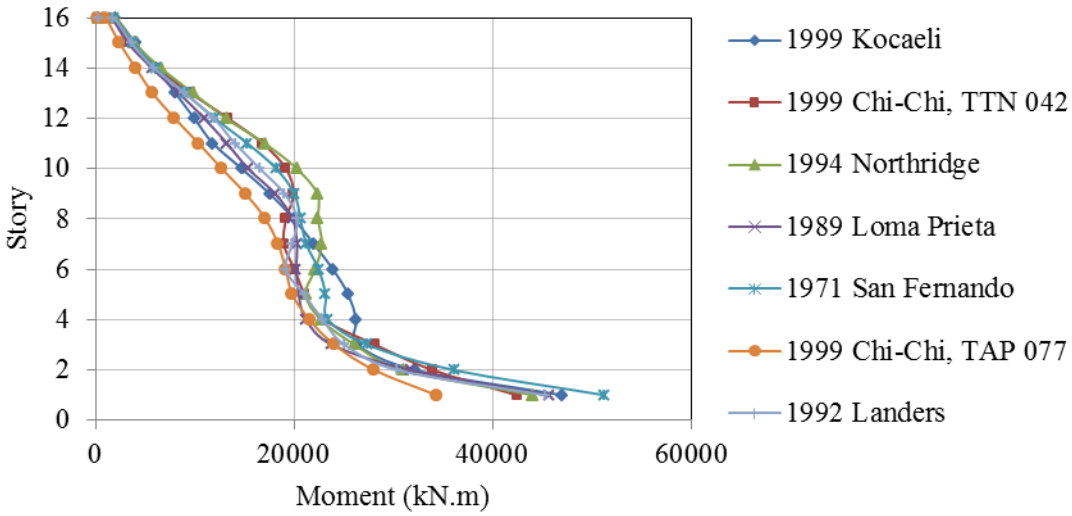

Figure E.11 Bending moment in wall3 (W3) about N-S direction – NLRHA due to DBE

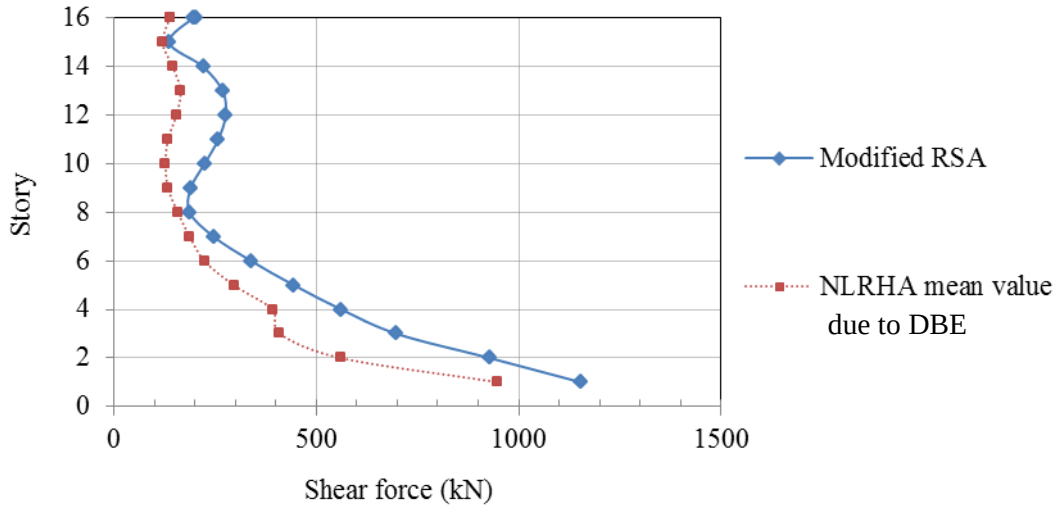

Figure E.12 Comparison of seismic shear demand in wall1 (W1) – Modified RSA versus NLRHA

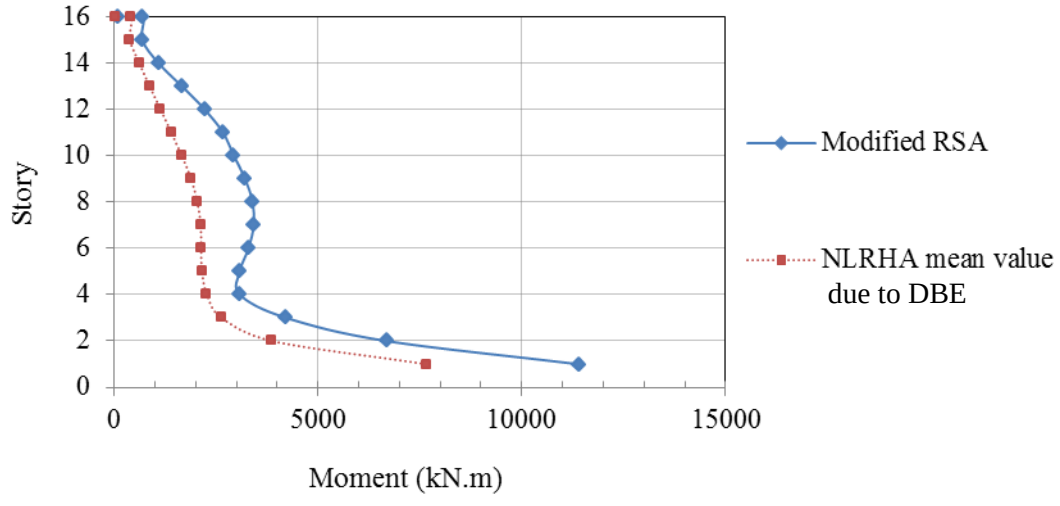

Figure E.13 Comparison of bending moment in wall1 (W1) – Modified RSA versus NLRHA

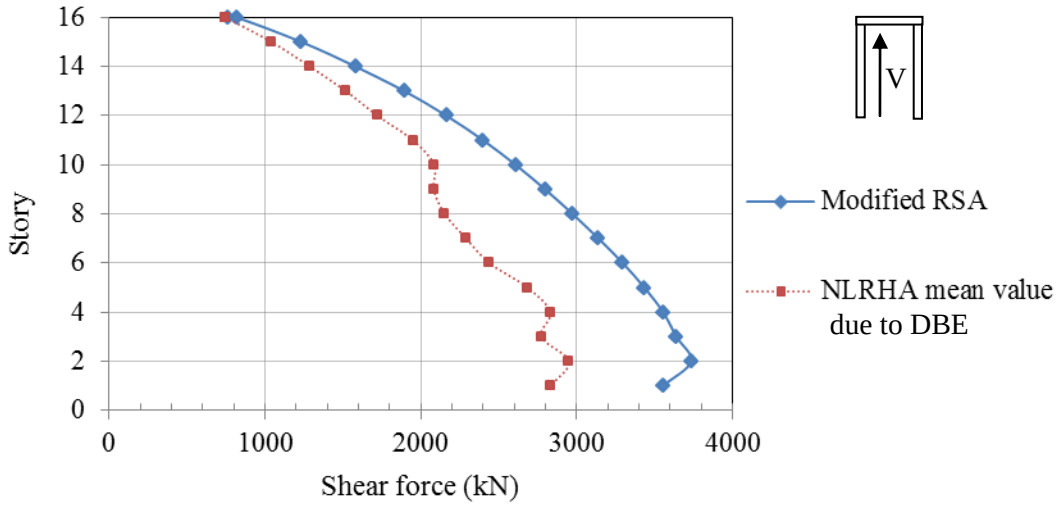

Figure E.14 Comparison of seismic shear demand in wall2 (W2) in N-S direction – Modified RSA versus NLRHA

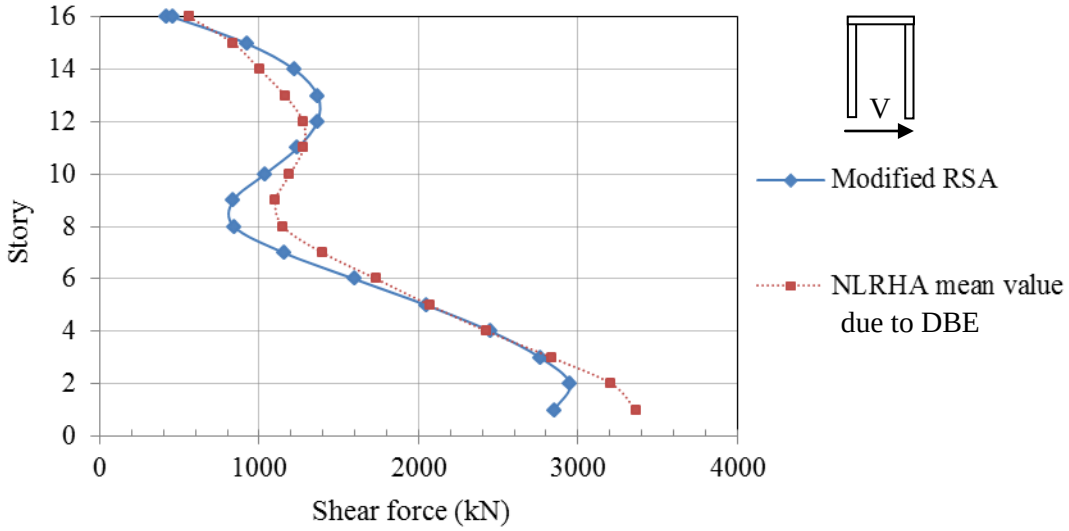

Figure E.15 Comparison of seismic shear demand in wall2 (W2) in E-W direction – Modified RSA versus NLRHA

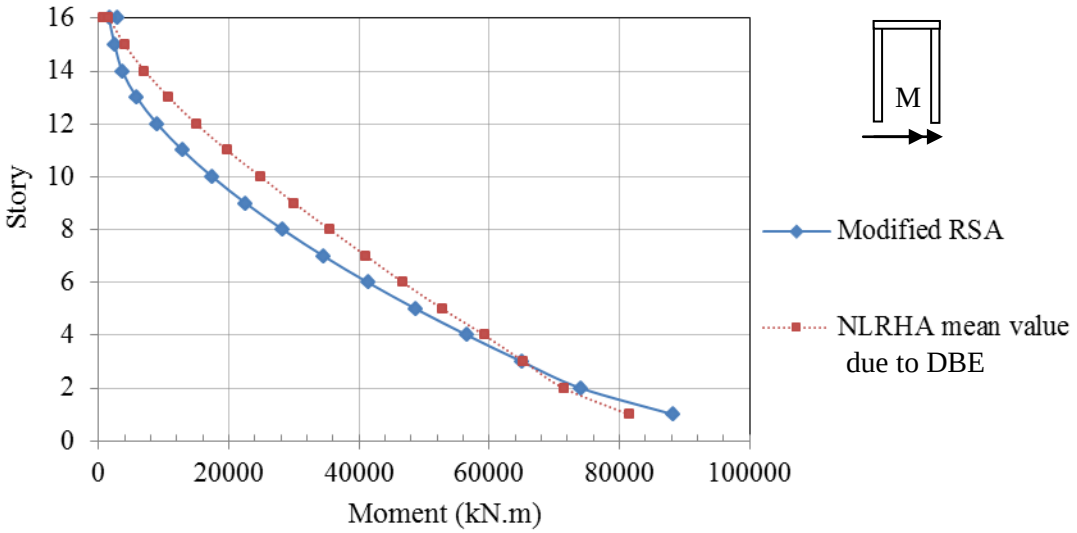

Figure E.16 Comparison of bending moment in wall2 (W2) about E-W direction – Modified RSA versus NLRHA

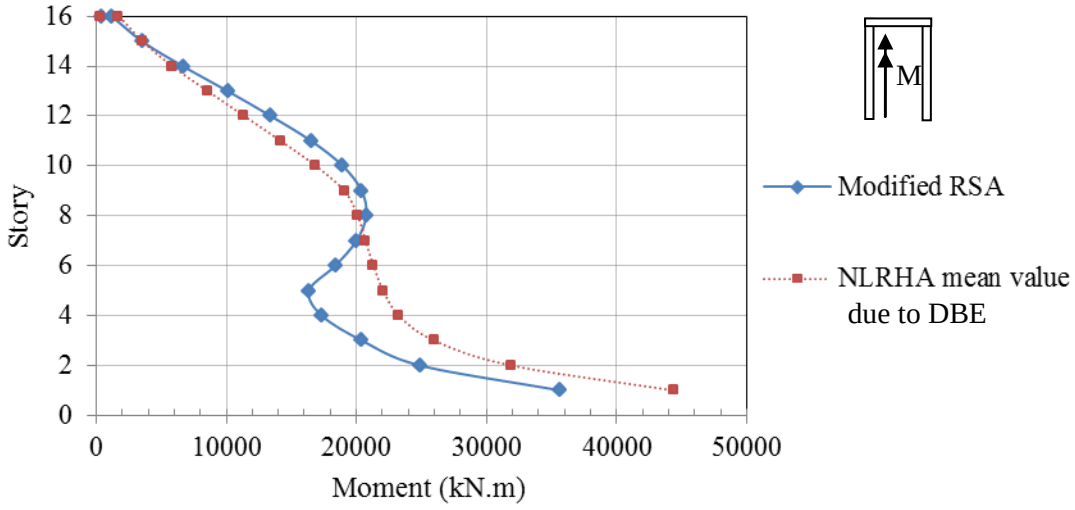

Figure E.17 Comparison of bending moment in wall2 (W2) about N-S direction – Modified RSA versus NLRHA

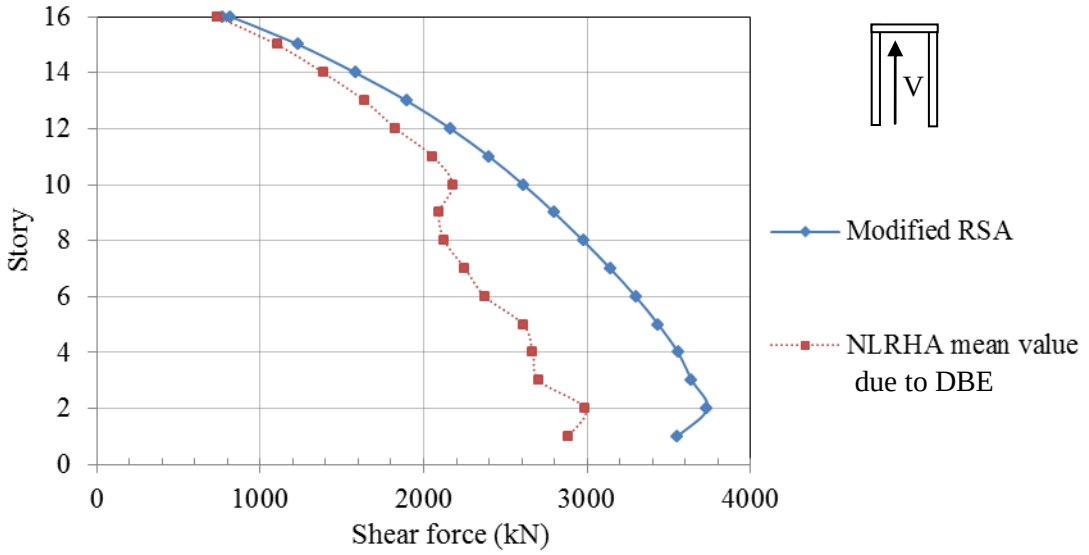

Figure E.18 Comparison of seismic shear demand in wall3 (W3) in N-S direction – Modified RSA versus NLRHA

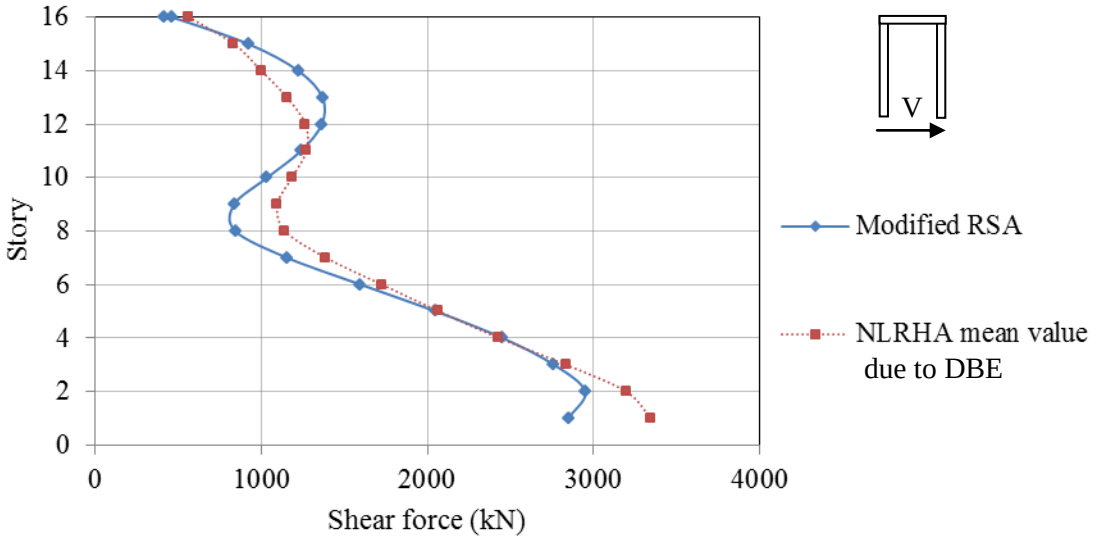

Figure E.19 Comparison of seismic shear demand in wall3 (W3) in E-W direction – Modified RSA versus NLRHA

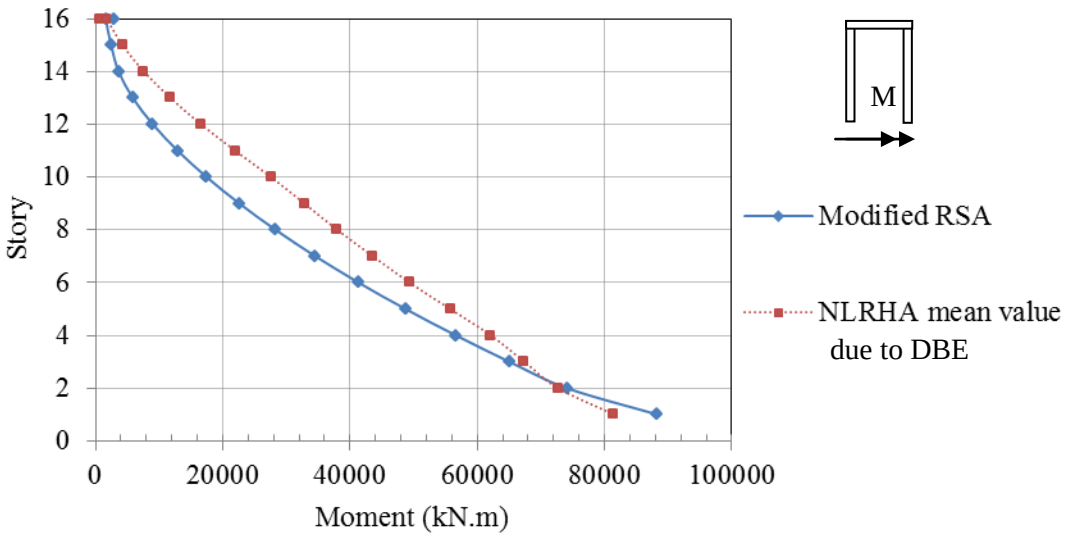

Figure E.20 Comparison of bending moment in wall3 (W3) about E-W direction – Modified RSA versus NLRHA

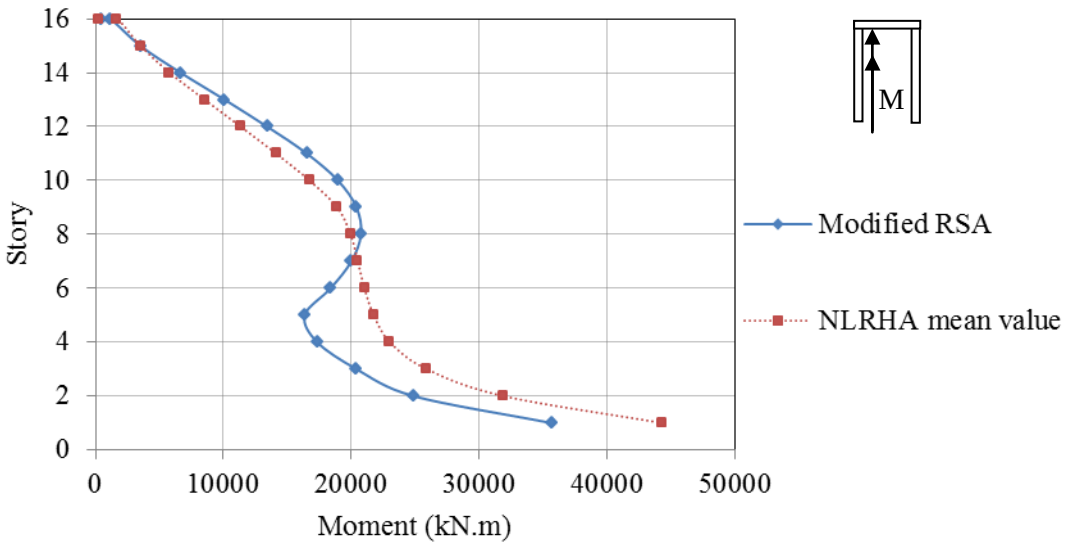

Figure E.21 Comparison of bending moment in wall3 (W3) about N-S direction – Modified RSA versus NLRHA

APPENDIX F

Comparison of PERFORM-3D and ETABS models in RSA procedure

There are three models shown in Figure F.2 through Figure F.9. Two of them are modeled in ETABS with and without torsional effect, and the other one is modeled in PERFORM-3D without torsional effect. Next, we will compare the responses in RSA procedure of the models in ETABS and PERFORM-3D with no torsional effect. The seismic responses (story drift ratio, shear demand and bending moment in wall elements) of both models in RSA procedure are reasonably close in all the cases except the seismic shear demand in wall2 of N-S direction. This is caused by the different period of both models in mode 3 as shown in Table F.1. This difference in period makes the spectra acceleration different by around 20% in both models as depicted in Figure F.1.

Table F.1 The first three mode periods of the models

Modes	Periods (sec)	
	PERFORM-3D	ETABS
1	2.973	2.92
2	2.898	2.86
3	1.467	1.3

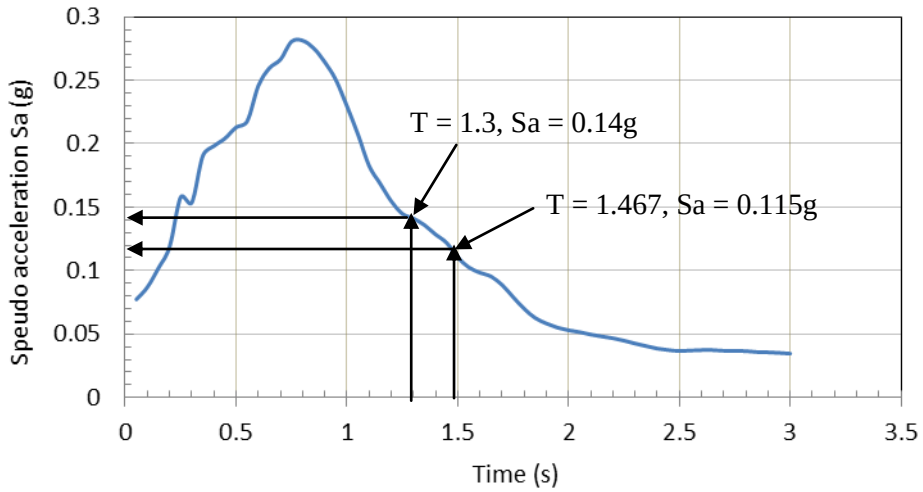

Figure F.1 Average response spectrum, damping ratio = 5%

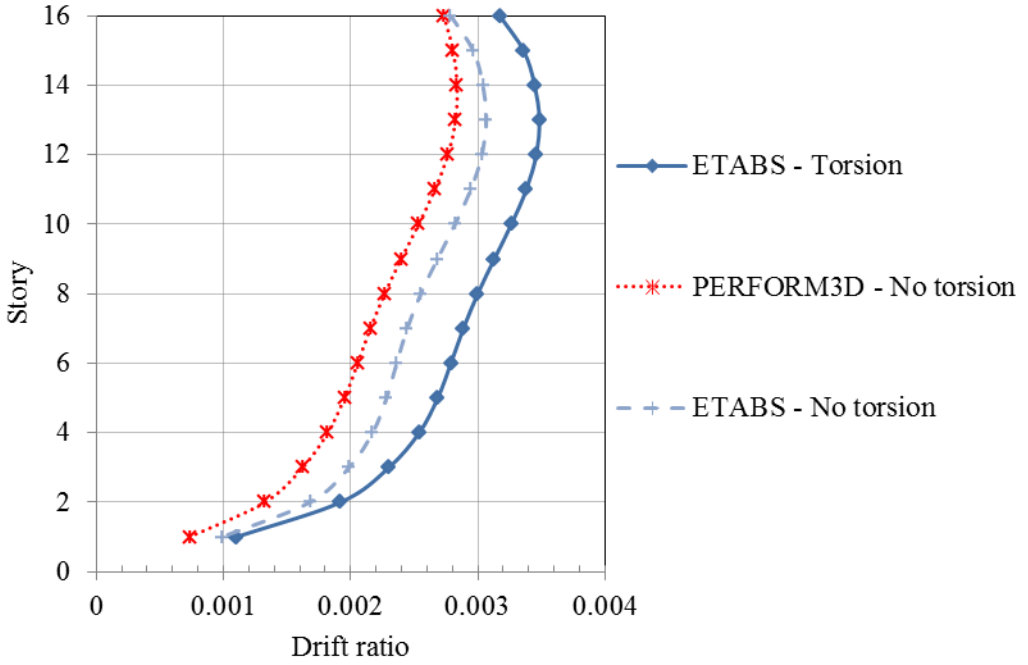

Figure F.2 Maximum story drift ratio in E-W direction

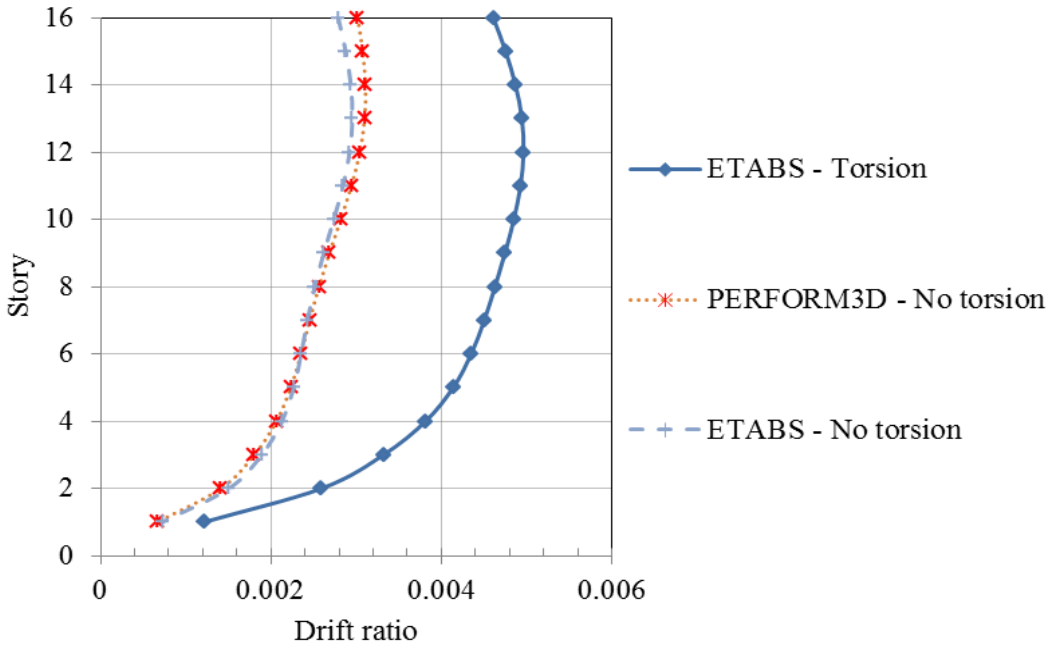

Figure F.3 Maximum story drift ratios in N-S direction

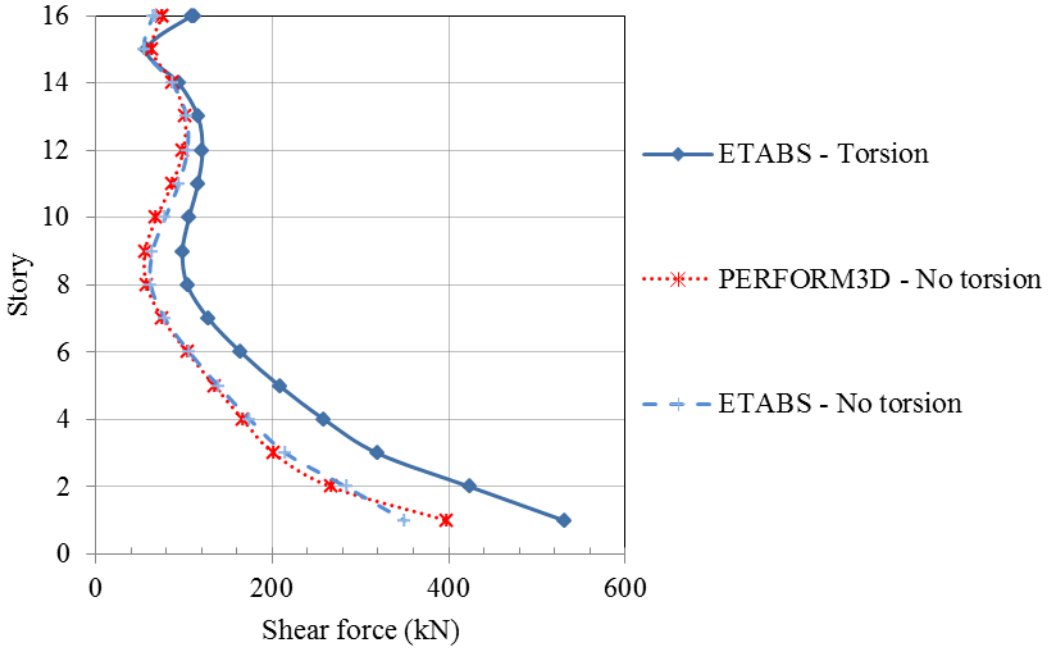

Figure F.4 Shear force in wall1

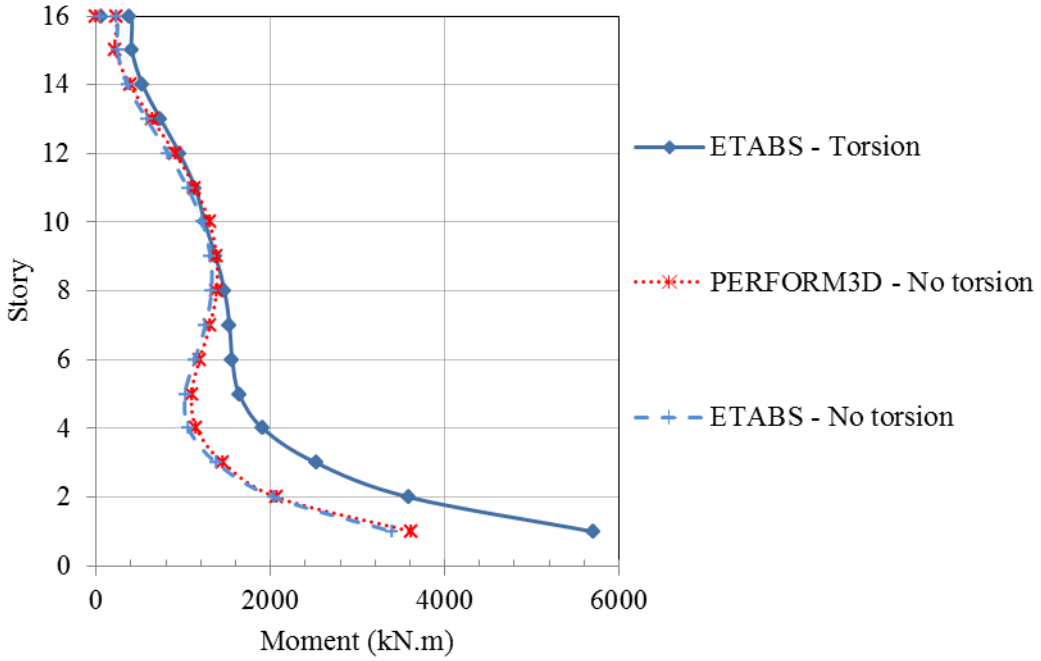

Figure F.5 Moment in wall1

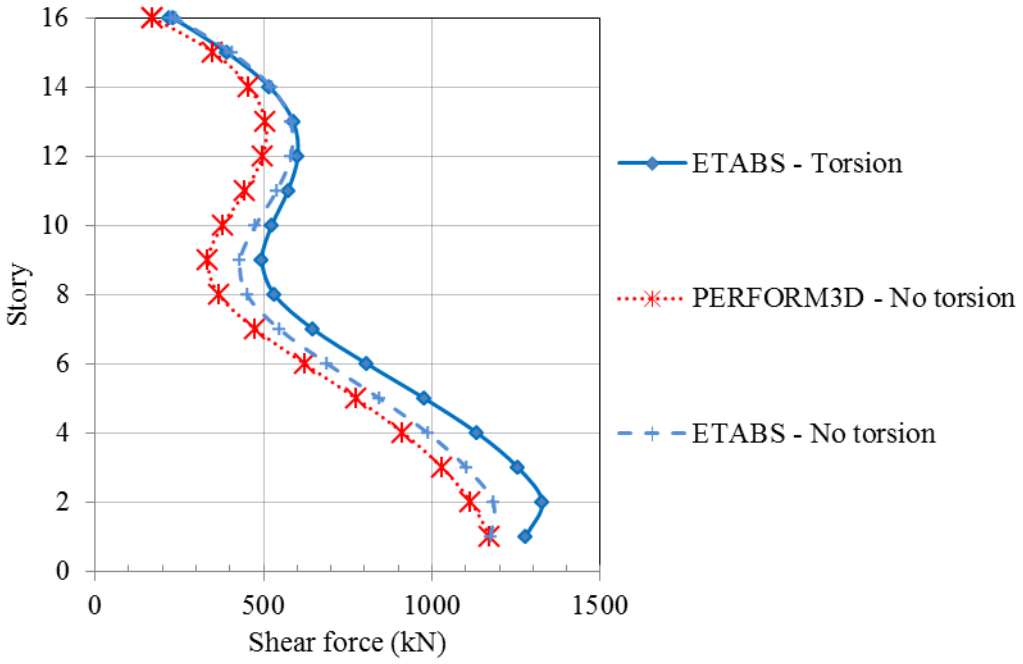

Figure F.6 Shear force in wall 2 – E-W direction

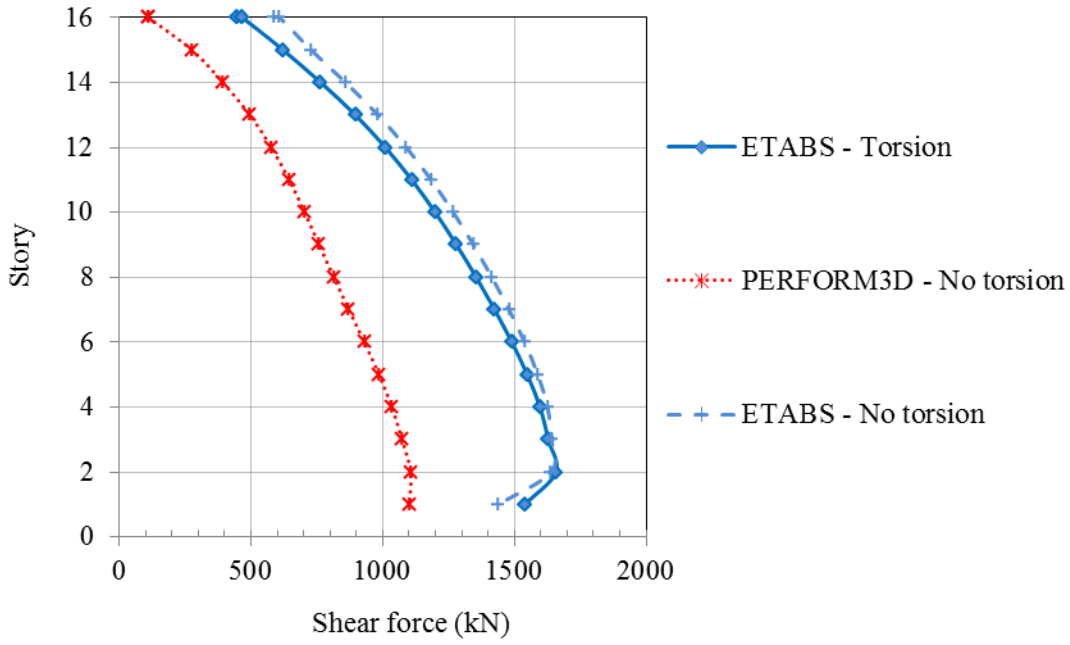

Figure F.7 Shear force in wall 2 – N-S direction

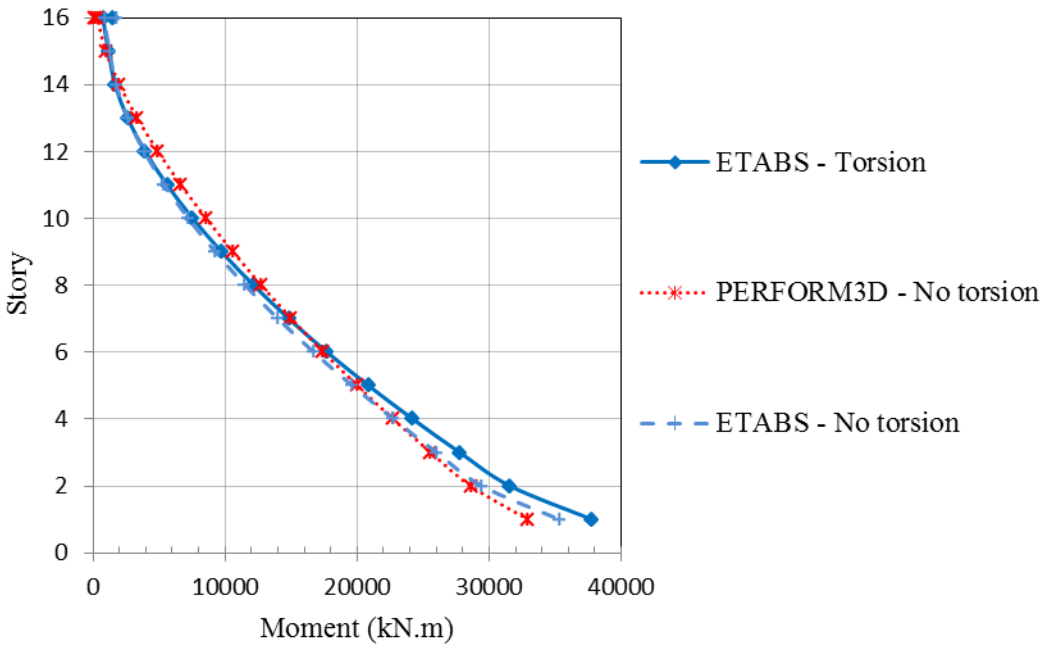

Figure F.8 Moment in wall 2 – about E-W direction

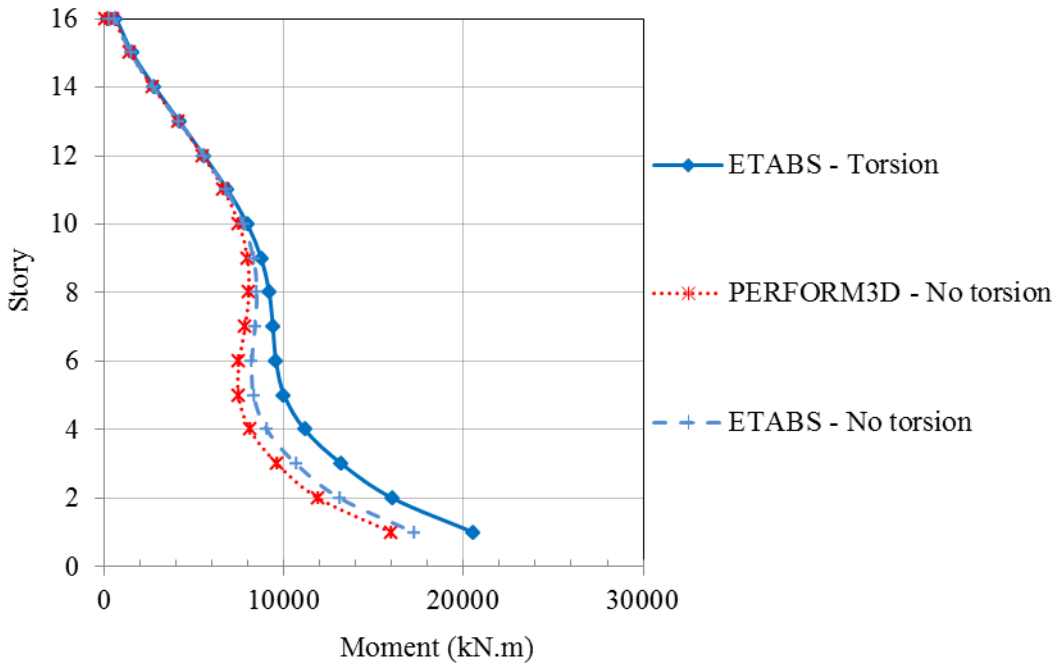

Figure F.9 Moment in wall 2 – about N-S direction

APPENDIX G

Designing process of the wall2

The envelop case of the load combination considers the maximum demand of each load cases, and the walls are designed to resist this maximum demand from RSA procedure. Table G.1 and Table G.2 show the seismic demands at the base of wall2 from RSA procedure in N-S and E-W direction, respectively.

Table G.1 Seismic demands at the base of wall2 from RSA procedure – N-S direction

Pmin (kN)	Pmax (kN)	Mmax (kN.m)
5964	13945	38524

Table G.1 Seismic demands at the base of wall2 from RSA procedure – E-W direction

Pmin (kN)	Pmax (kN)	Mmax (kN.m)
5964	13945	20960

The wall2 is first designed to resist the demands in both, N-S and E-W directions separately and then the most critical case will be chosen to design the wall2. As shown in Table G.3 and Table G.4, The most critical case is to design the wall2 to resist the demand (Pmin = 5964 kN, Mmax = 20960 kN.m) in E-W direction, which results in ro = 0.6%.

Table G.3 Design of wall2 in N-S direction

Mcapa at Pmin (kN.m)	Mcapa at Pmax (kN.m)
40000	53000 (ro min)
ro = 0.4%	ro = ro_{min} = 0.15%

ro: area of reinforcement divided by the area of the concrete cross-section

Table G.4 Design of wall2 in E-W direction

Mcapa at Pmin (kN.m)	Mcapa at Pmax (kN.m)
21000	21000 (ro min)
ro = 0.6%	ro = ro_{min} = 0.15%

ro: area of reinforcement divided by the area of the concrete cross-section

The wall2 is designed considering biaxial loading or M2-M3 interaction also, the linear M2-M3 interaction relationship is assumed. As illustrated in Figure G.1, the amount of reinforcement ro = 0.6 % cannot resist the demand in N-S and E-W directions simultaneously, so the strength, amount of reinforcement, needs to be increase such that it can resist the biaxial demand. To resist this biaxial demand, the reinforcement needs to be increased from ro = 0.6% to ro = 1.5% as shown in Figure G.2. This increase corresponds to increasing the capacity of the walls by almost 2 times in each direction.

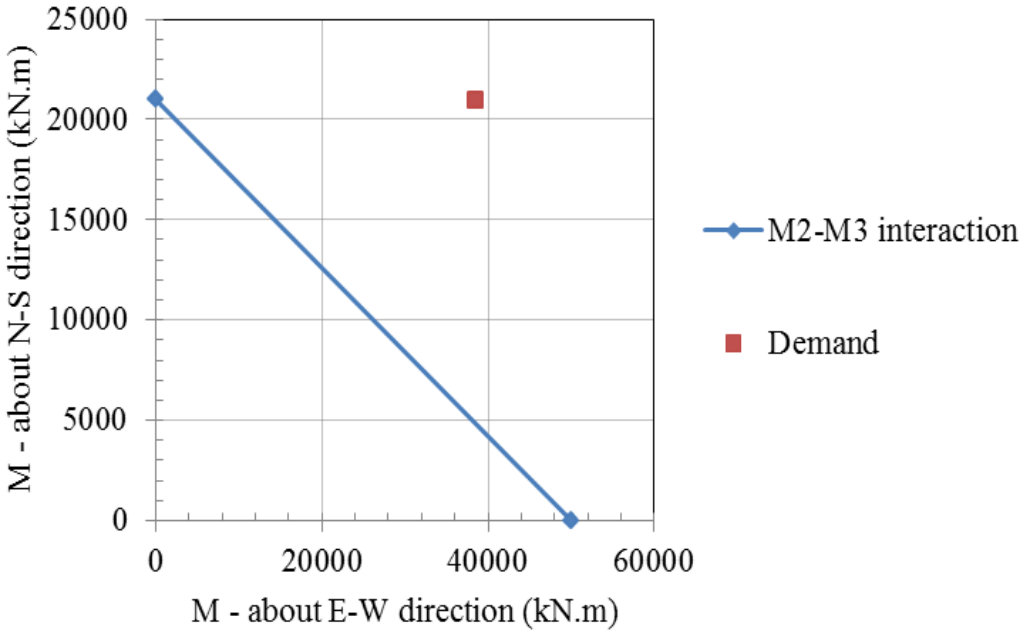

Figure G.1 Biaxial moment interaction diagram of wall2 for ro = 0.6%

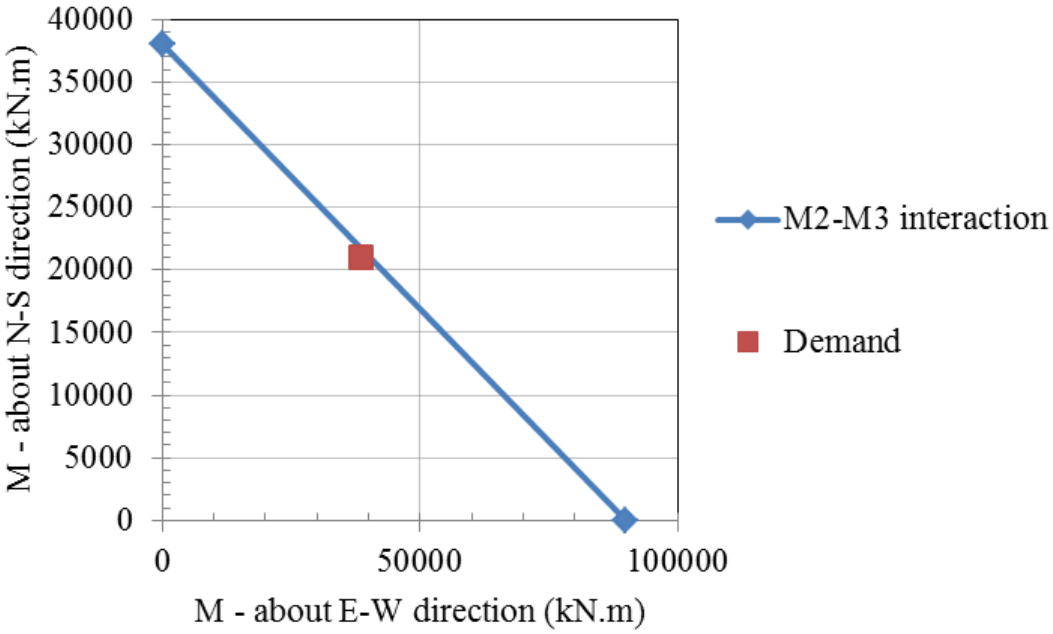

Figure G.2 Biaxial moment interaction diagram of wall2 for ro = 1.5 %

BIOGRAPHY

Leng Ky was born in 1986 in Phnom Penh, the capital city of Cambodia. He went to Santhomok high school located in Phnom Penh and graduated in 2005. He then successfully passed the entrance examination to study at Institute of Technology of Cambodia (ITC), Phnom Penh, where he spent 5 years to finish his bachelor degree in Civil Engineering in 2010. In the same year as he graduated from ITC, he was awarded a scholarship sponsored by JICA under AUN/SEED-Net program to pursue his master of Civil Engineering in the field of Structural Engineering at Chulalongkorn University, Thailand.